2015

Influences of target surface roughness on impingement jet array heat transfer

Warren Buzzard

INFLUENCES OF TARGET SURFACE ROUGHNESS ON IMPINGEMENT JET ARRAY HEAT TRANSFER

by

WARREN BUZZARD

A THESIS

Submitted in partial fulfillment of the requirements for the degree of Master of Science in Aerospace Systems Engineering
in
The Department of Mechanical and Aerospace Engineering
to
The school of Graduate Studies
of
The University of Alabama in Huntsville

HUNTSVILLE, ALABAMA

2015

In presenting this thesis in partial fulfillment of the requirements for a master's degree from The University of Alabama in Huntsville, I agree that the Library of this University shall make it freely available for inspection. I further agree that permission for extensive copying for scholarly purposes may be granted by my advisor or, in his/her absence, by the Chair of the Department or the Dean of the School of Graduate Studies. It is also understood that due recognition shall be given to me and to The University of Alabama in Huntsville in any scholarly use which may be made of any material in this thesis.

Warren Buggard
(student signature)

9-30-2015
(date)

THESIS APPROVAL FORM

Submitted by Warren Buzzard in partial fulfillment of the requirements for the degree of Master of Science in Aerospace Systems Engineering and accepted on behalf of the Faculty of the School of Graduate Studies by the thesis committee.

We, the undersigned members of the Graduate Faculty of The University of Alabama in Huntsville, certify that we have advised and/or supervised the candidate on the work described in this thesis. We further certify that we have reviewed the thesis manuscript and approve it in partial fulfillment of the requirements for the degree of Master of Science in Aerospace Systems Engineering.

09/30/2015
Committee Chair
(Date)

10/01/2015

10/1/2015
Department Chair

College Dean

11/12/15
Graduate Dean

ABSTRACT
The School of Graduate Studies
The University of Alabama in Huntsville

Degree Master of Science Program Aerospace Systems Engineering

Name of Candidate Warren C. Buzzard

Title Influences of Target Surface Roughness on Impingement Jet Array Heat Transfer

The present investigation involves testing the addition of special surface roughness patterns to an impingement surface to improve the effectiveness of impingement cooling. This investigation utilizes various sizes, distributions, shapes, and patterns of surface roughness elements for impingement cooling augmentation. Surface roughness shapes include rectangles, triangles, and cylinders. Combinations of small roughness and large pins are considered. Tests are performed at Reynolds numbers of 900, 1500, 5000, and 11000. In general, plates with small roughness alone perform better than plates with a combination of small roughness and large pins at Reynolds numbers of 900 and 1500. Combinations of small rectangle roughness and large pins give better heat transfer results than the small rectangle roughness alone at Reynolds numbers of 5000 and 11000, while the triangle roughness and cylinder roughness configurations with large pins show little improvement over small roughness alone. All triangle roughness configurations perform better than the rectangle configurations.

09/30/2015

Abstract Approval: Committee Chair

Department Chair

Graduate Dean

ACKNOWLEDGEMENTS

I would like to thank my professor, Dr. Phil Ligrani, for providing the continuous support and encouragement that I needed to complete this thesis. I would also like to thank Mr. Zhong Ren for all the help and guidance in performing the lab work. I would like to thank Mr. Tony Hall for helping set up the lab and for helping with troubleshooting when help was required. Finally, I would like to thank my parents for providing the means and support for me to finish both of my degrees.

TABLE OF CONTENTS

Page

LIST OF FIGURES

Figure Page

LIST OF TABLES

LIST OF SYMBOLS

A	=	impingement hole area
A_{ht}	=	heat transfer area on the target plate
D	=	diameter of an individual impingement hole
H	=	height of roughness element
k	=	ratio of specific heats
L	=	length of roughness element
$\dot{m}$	=	impingement air mass flow rate
M_a	=	impingement air flow Mach number
M_i	=	impingement air flow ideal Mach number
N	=	number of impingement holes
Nu	=	local Nusselt number
$\overline{Nu}$	=	line-averaged Nusselt number
$\overline{\overline{Nu}}$	=	spatially-averaged Nusselt number
P_a	=	impingement air static pressure
Q	=	total power provided to the thermofoil heater
q_{cb}	=	convection heat flux from back side of the target plate
q_{cf}	=	convection heat flux from front side (or impingement side) of the target plate
q_{rf}	=	radiation heat flux from front side (or impingement side) of the target plate
R	=	ideal gas constant
Re_j	=	impingement air flow Reynolds number
T_b	=	local temperature on the back surface of the polystyrene target plate
T_i	=	impingement air ideal static temperature
T_j	=	impingement air static temperature
T_{oj}	=	impingement air stagnation temperature
T_{tc}	=	local thermocouple temperature between the heater and the polystyrene target plate

T_W	=	local target surface temperature on the surface of the heater adjacent impingement air
u_a	=	impingement air velocity
W	=	width of roughness element
x	=	streamwise coordinate
y	=	spanwise coordinate
z	=	normal coordinate
X	=	streamwise distance between centerlines of adjacent impingement holes
Y	=	spanwise distance between centerlines of adjacent impingement holes
Z	=	distance between target plate and impingement hole plate
α	=	air thermal conductivity
ρ_a	=	impingement air static density
μ	=	dynamic viscosity

CHAPTER 1

INTRODUCTION

Impingement cooling plays an important role in the operation of a jet engine. The better the engine components are cooled down, the more efficient and the more powerful the engine is. If the effectiveness of impingement cooling is increased, the engine can be run at higher temperatures. Impingement cooling is used for jet engine components such as the leading edge of turbine blades, combustion chamber liners, transition pieces, and splash plates. One method of impingement cooling enhancement that shows promise is the addition of surface treatments on the impingement surface. These surface treatments may include the use of small surface roughness elements of various sizes and shapes arranged in certain patterns. These surface roughness elements can be used in combination with ramps, ribs, bumps, or dips to enhance heat transfer on the impingement surface. The present investigation involves testing the addition of these special surface roughness patterns to the impingement surface to improve the effectiveness of impingement cooling. This investigation utilizes various sizes, distributions, shapes, and patterns of surface roughness elements for impingement cooling augmentation.

A recent example of research in this area is Xing and Weigand [1]. This paper is a study in staggered impingement heat transfer on a rib roughened plate with different crossflow schemes. The impingement jet array considered is a nine-by-nine staggered configuration at Reynolds numbers of 15,000 to 35,000. The distance between the impingement jets and the target plate is set at 3, 4, and 5 jet diameters. Tests are completed with a flat plate and a rib roughened plate at three jet-induced crossflow schemes. The rib turbulators on the plate are 1 jet diameter in height and width and 6 jet diameters in length. The

impingement jets impact the plate in the space between the rib turbulators. The results show that both the flat plate and the rib-roughened plate give the best heat transfer with the minimum jet-to-plate distance and the minimum crossflow. Additionally, the plate with the rib-turbulators gives higher heat transfer coefficients than the flat plate for maximum and minimum crossflow. When crossflow is increased, the crossflow reduces the interferences between the individual jets. The rib-roughened plate gives 7.5% higher heat transfer coefficients than the flat plate, but this value is in the measurement uncertainty of 9%. The rib turbulator edges are believed to be making the boundary layer thinner and increasing the crossflow velocity.

Another example of research in this area is Xing et al. [2]. This research investigates impingement heat transfer on a flat and micro-rib roughened plate with different crossflow schemes. This investigation also uses a nine-by-nine impingement jet array. The spacing between the impingement jets is 5 jet diameters. The jet-to-plate distances considered are 3, 4, and 5 jet diameters. Jet Reynolds numbers considered include 15,000, 25,000, and 35,000. The micro-ribs on the plate are 1 mm in height and width and are the same length as the target plate. The ribs are spaced 5 mm apart. The results show that a jet-to-plate spacing of 3 diameters gives the highest heat transfer coefficients for both the flat plate and the micro-rib roughened plate. When the jet-to-plate spacing is changed, the channel cross-sectional area changes, which causes a different crossflow velocity. In addition, the minimum crossflow case results in the highest heat transfer for the micro-rib roughened plate. When compared to the flat plate, the micro-rib roughened plate gives higher maximum heat transfer values, but also gives the lowest minimum heat transfer values between the impingement jets. This is thought to be due to the micro-ribs reducing the influence of crossflow and increasing heat transfer performance. The jets impinge onto the ribs, which thin the boundary layer and enhance heat transfer. The experimental results in this investigation are compared with CFD analysis, which gives similar results.

Xing and Weigand [3] provides a study in impingement heat transfer on a flat and dimpled plate with different crossflow schemes. This study considers a nine-by-nine jet array at Reynolds numbers of 15,000 to 35,000 with jet-to-plate distances of 3, 4, and 5 jet diameters. The jet-to-jet spacing is 5 diameters. Three crossflow arrangements, minimum, medium, and maximum, are considered. The dimpled plate has dimples that have a diameter of 1.8 jet diameters and a depth of 0.15 jet diameters. The spacing between the dimples in the same row is 5 jet diameters. The rows of dimples are 2.5 jet diameters apart and are in a

staggered pattern. The results show that the minimum crossflow with a jet-to-plate spacing of 3 diameters gives the highest heat transfer for both the flat plate and the dimpled plate. When compared to the flat plate, the dimpled plate gives higher heat transfer coefficients for the maximum and minimum crossflow cases. The dimples are believed to be making the boundary layer thinner and increasing the crossflow velocity. When the jets impinge on a dimple, it is thought to have a coupled effect of jet impingement and channel flow caused by the spent air.

Nakamata et al. [4] provides a study of the effect of roughened elements and cooling hole shape on impingement cooling effectiveness. The tests are completed with a mainflow heating air at Reynolds numbers of 260,000 to 470,000. The cooling air is at Reynolds numbers of 1,200 to 13,000. Five different target plate designs are considered and compared to a plain plate. The configurations considered include a plate with ribs, a plate with dips, a plate with dimples, a plate with bumps, and a plate with a combination of bumps and race tracks. The results show that the plate with a combination of bumps and race tracks gives the highest impingement cooling effectiveness. Additionally, the dips and dimples perform better than the ribs and bumps. The authors conclude that the concave structures (ribs and bumps) increase the heat transfer coefficient mainly through surface area enhancement. The dimples perform better, due to the fact that they cause a smaller pressure loss than the concave shapes.

This thesis is organized into three main sections. Chapter 2 describes the experimental setup, the target plate configurations, the measurement techniques, and the method for determining the Nusselt number on the surface of the target plates. Both experimental setups, polystyrene and ProtoCAM, are explained. Chapter 3 describes the numerical conduction analysis that is used for determining factors and verifying experimental results. Chapter 4 provides and compares the experimental results for all test cases. Additionally, Chapter 4 provides a discussion of physical phenomena responsible for the observed data trends. Chapter 5 gives a summary and conclusions. Within the Appendices, presented are a data file directory, software directory, and an uncertainty analysis.

CHAPTER 2

EXPERIMENTAL APPARATUS AND PROCEDURES

Chapter 2 presents a description of the impingement flow facility, the experimental setup and configurations, the measurement devices, and the methods for gathering and analyzing the data. Multiple test setups are shown, including a polystyrene test plate configuration and multiple ProtoCAM test plate configurations.

A. Impingement Flow Facility and Impingement Plate

Parts of the experimental apparatus and procedures are described by Lee et al. [5]. Materials from this reference are also included here so that all approach and apparatus details are discussed completely and thoroughly.

Schematic diagrams of the laboratory facility used for heat transfer measurements are presented in Figures 2.1 and 2.2. Figure 2.3 displays a photo of the facility, including the infrared camera and power supply and measurement devices. The facility is constructed of 6.1 mm thick ASTM A38 steel plates, and A53 Grade B ARW steel piping. The air stream through the plenums and channel is drawn from the laboratory atmosphere. To achieve the Reynolds number of the present study, a New York Blower Co. 7.5 HP, size 1808 pressure blower is employed. The air mass flow rate provided to the test section is measured using an ASME standard orifice plate, flow-mounted calibrated copper-constantan thermocouples, and Validyne DP15-20 and DP15-22 pressure transducers (with diaphragms rated at 0.86 and 1.40 kPa, respectively) connected to Validyne Model CD15 Carrier Demodulators. Each of the thermocouples

measures recovery temperature, which is used with local velocity magnitude to determine gas static temperature. The blower exits into a series of two plenums arranged in series, where the upstream plenum is 0.63 m in length along each side, and the downstream plenum dimensions are 0.63 m long, 0.77 m tall, and 0.77 m wide. A Bonneville cross-flow heat exchanger is located within each plenum. As the air exits the heat exchanger, and the second plenum, the air passes into a 0.22 m outer diameter pipe, which contains the ASME Standard orifice plate employed to measure the air mass flow rate. This pipe then connects to the 0.635 m by 0.635 m side of a plenum.

Upon entering this plenum, the air first encounters a flow baffle to distribute the flow, and a honeycomb and screens to improve flow spatial uniformity. These are followed by the upper plenum, located below the honeycomb and flow straightening devices (as shown in Figure 2.2), with top dimensions of 0.635 m and 0.635 m, and height of 0.40 m. Individual plates with holes used to produce the impingement jets are located at the bottom of this plenum, as shown in Figure 2.2. The plenum is thus designed so that different impingement plates can be installed at this location. The present investigation uses two different impingement plates. One plate is used for the purpose of gathering data for the sponsor of the project and the other is used for gaining additional data. The impingement plate that is used for the sponsor's data is called plate 1 and the plate for additional data is called plate 2.

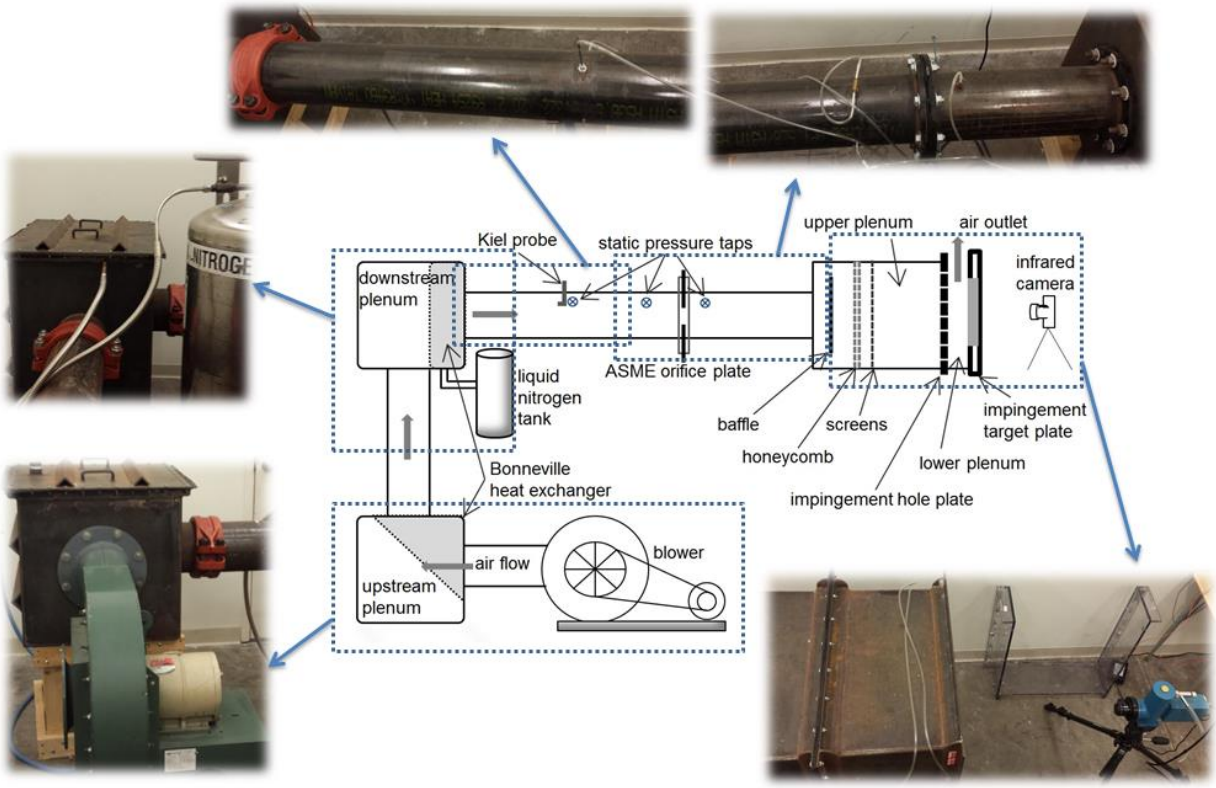

Figure 2.1: Impingement flow facility

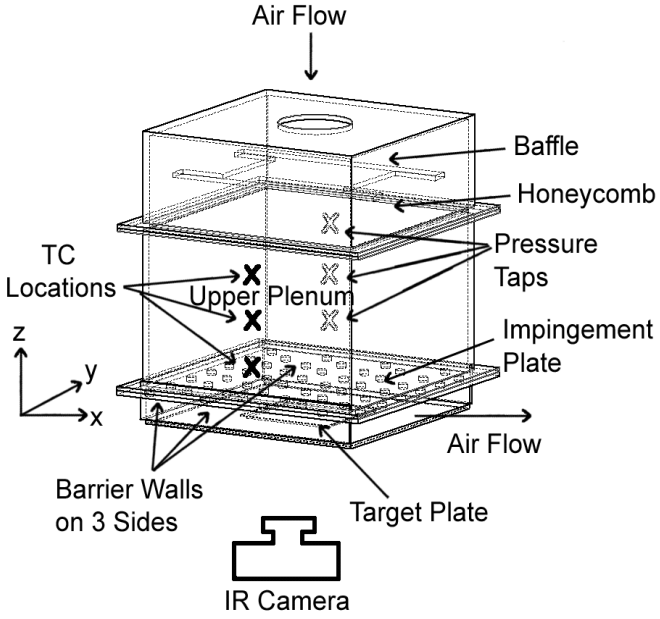

Figure 2.2: Impingement flow facility test section, including impingement plenum, and impingement channel.

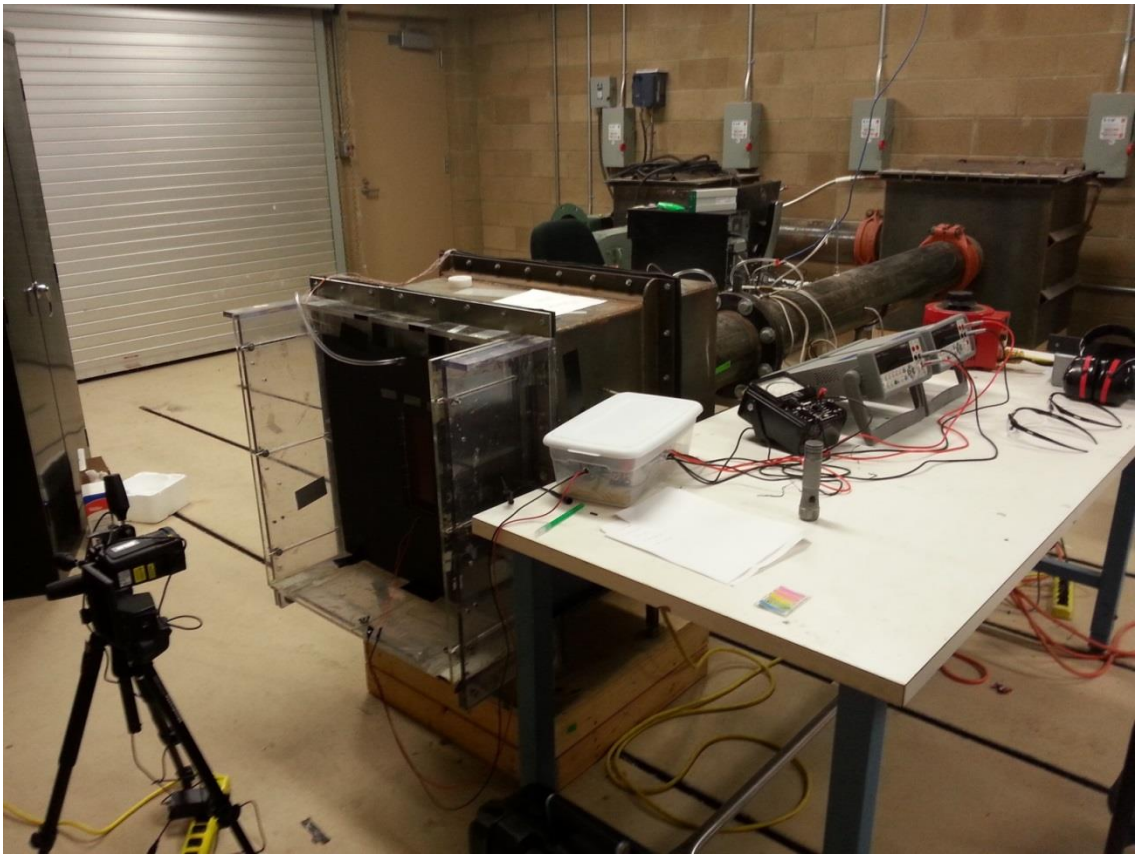

Figure 2.3: Picture of impingement flow facility

Figures 2.4 and 2.5 show that the impingement plates consist of 8 to 9 rows of holes in the streamwise direction. Plate 1 is arranged so that all holes are in line with each other, while plate 2 is arranged so that holes in adjacent rows are staggered with respect to each other. With these arrangements, 3 to 6 holes are located in each streamwise row. On plate 1, the spacing between holes in the streamwise direction X is 10D and the spacing between holes in the spanwise direction Y is 2.7D. The thickness of plate 1 is 1.4D. On plate 2, the spacing between holes in the streamwise direction X is 5D and the spacing between holes in the spanwise direction Y is 5D. The thickness of plate 2 is 1.6D. For both impingement plates, the spacing between the hole exit planes and the target plate is denoted Z/D, with a value employed in the present investigation of 2.5D.

The impingement cooling flow which issues from these holes is contained within the channel formed by the impingement jet plate and the target surface, and is constrained to exit in a single direction, which here, is denoted as the x-direction. This channel is called the lower plenum or impingement plenum. The

impingement plenum channel is made up of a volume of air between the target and jet impingement plate, with 7.4*D* spanwise margins on each side of the plate 1 test configurations and 2.5D spanwise margins on each side of the plate 2 test configurations. In the present study, the hole diameter size, *D*, blower, mass flow rate, and pressure level are employed so that the Mach number ranges from 0.01 to 0.2 and the Reynolds number is between 900 and 11,000. This range of Mach numbers are selected because previous investigations show that local and spatially-averaged Nusselt numbers show no dependence on Mach number, when values are less than approximately 0.25 [5]. Diagrams of the impingement channels for both test configurations are shown in Figures 2.6 and 2.7.

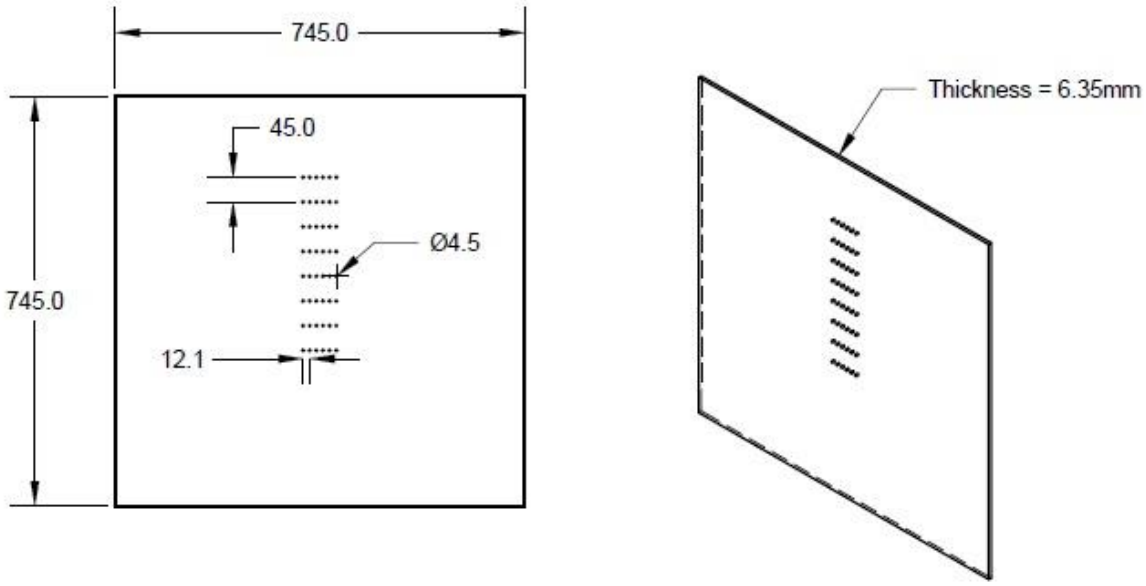

Impingement holes	Non-Dimensional Value	Dimensional Value(mm)
Hole Diameter		4.5
Streamwise Spacing	x/D=10	x=45
Spanwise Spacing	y/D=2.7	y=12.15

Impingement Plate	Non-Dimensional Value	Dimensional Value(mm)
Thickness	t/D=1.411	t=6.35

Figure 2.4: Diagram of impingement plate 1 with hole dimensions and layout. All dimensions in millimeters.

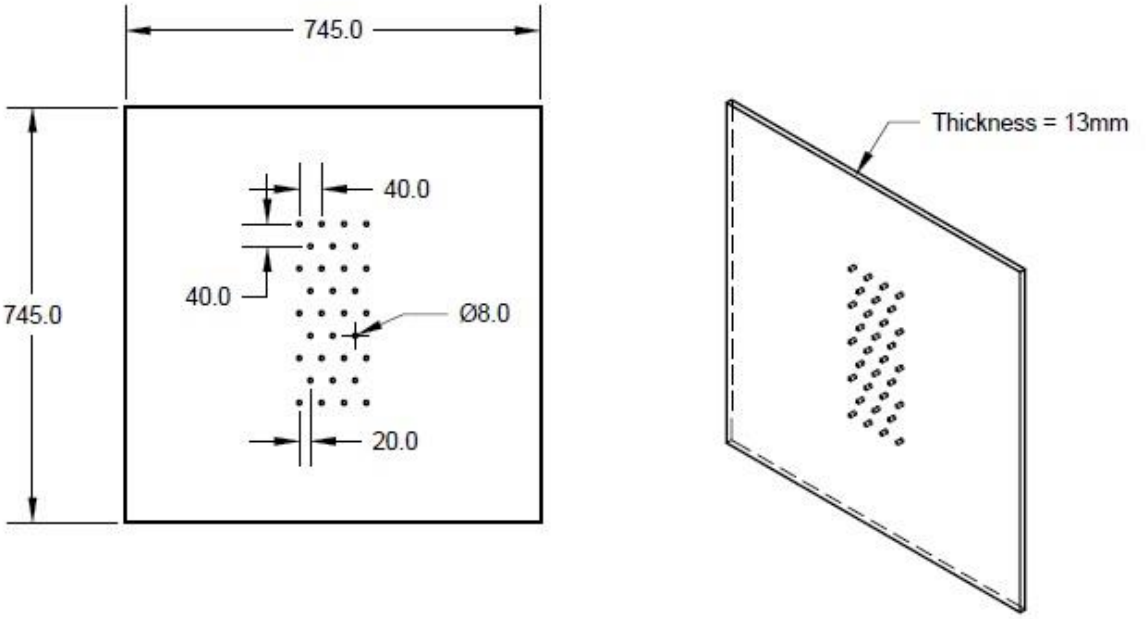

Impingement holes	Non-Dimensional Value	Dimensional Value(mm)		Impingement Plate	Non-Dimensional Value	Dimensional Value(mm)
Hole Diameter		8		**Thickness**	t/D=1.625	t=13
Streamwise Spacing	x/D=5	x=40				
Spanwise Spacing	y/D=5	y=40				

Figure 2.5: Diagram of impingement plate 2 with hole dimensions and layout. All dimensions in millimeters.

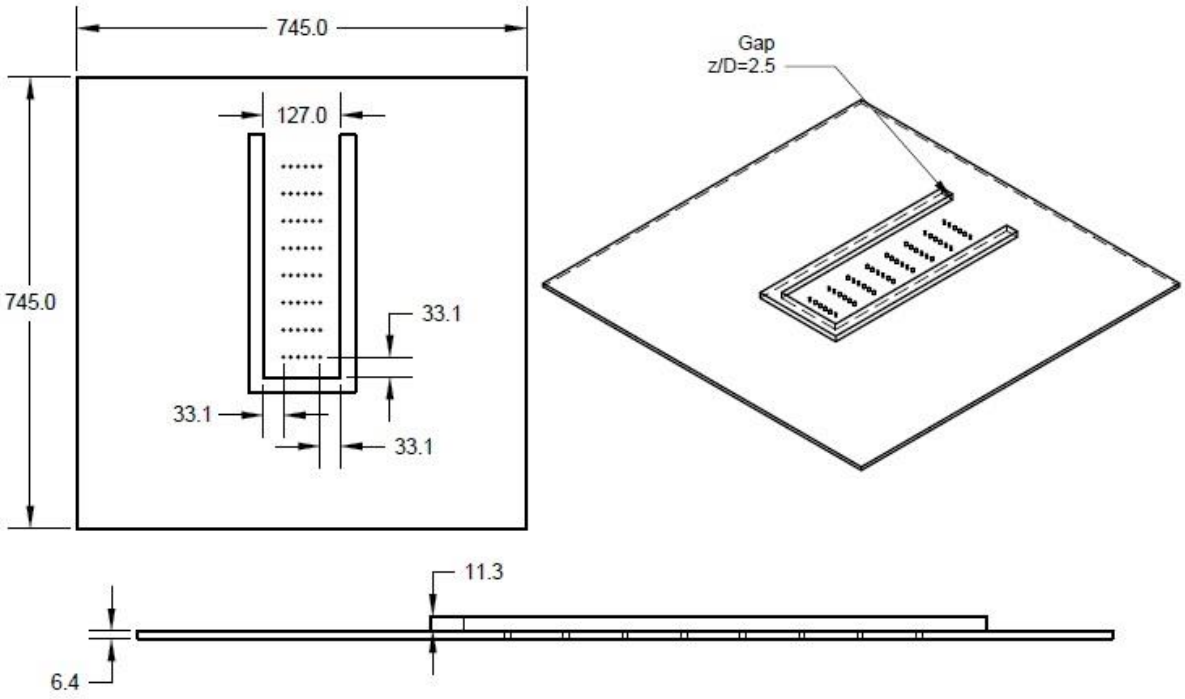

Impingement Passage	Non-Dimensional Value	Dimensional Value(mm)
Gap	z/D=2.5	z=11.25

Figure 2.6: Diagram of impingement passage with impingement plate 1. All dimensions in millimeters.

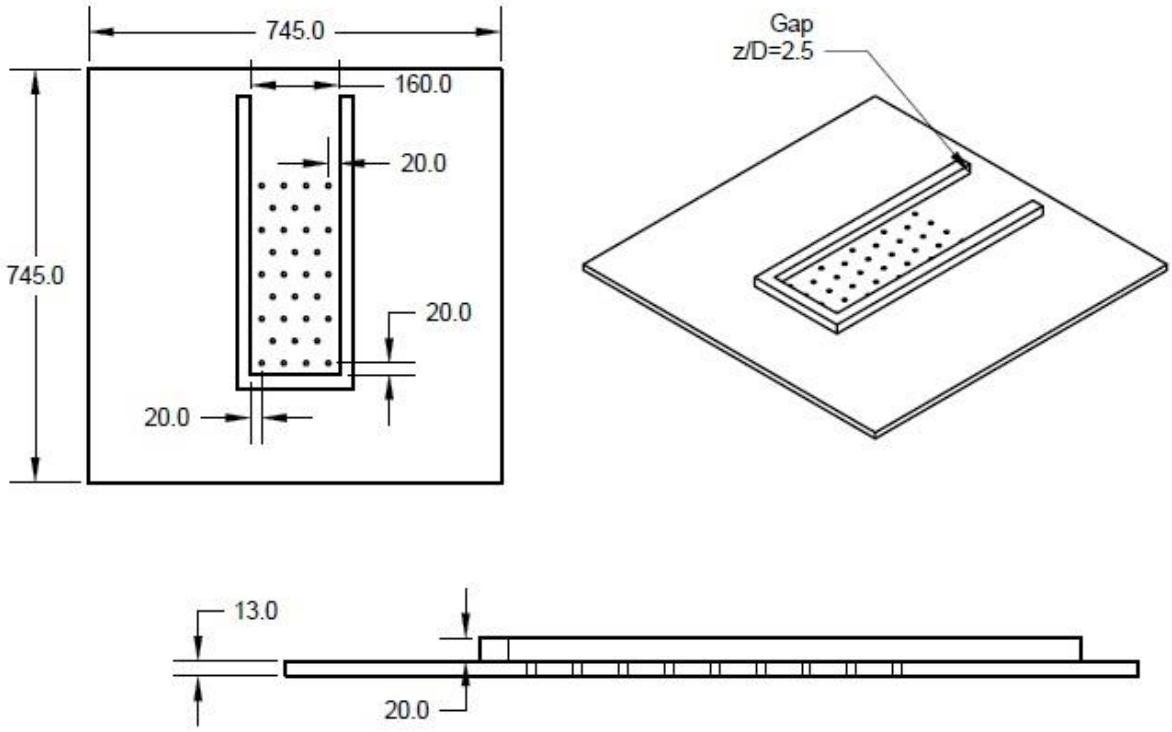

Impingement Passage	Non-Dimensional Value	Dimensional Value(mm)
Gap	z/D=2.5	z=20

Figure 2.7: Diagram of impingement passage with impingement plate 2. All dimensions in millimeters.

B. Polystyrene Target Plate Test Surfaces for Measurements of Surface Nusselt Numbers

For the polystyrene test configuration, local surface Nusselt numbers are measured on a heated target plate, which is comprised of a polystyrene layer, which is 1.31 mm thick, and an attached heater, which is approximately 0.29 mm thick, giving a total target plate thickness of 1.60 mm. The size of the target plate is 127 mm by 255 mm. This configuration has the heater located adjacent to the air stream with impinging air jets, while the polystyrene layer is viewed by the infrared camera as spatially-resolved measurements of surface temperature are obtained. Figure 2.8 displays the polystyrene test configuration.

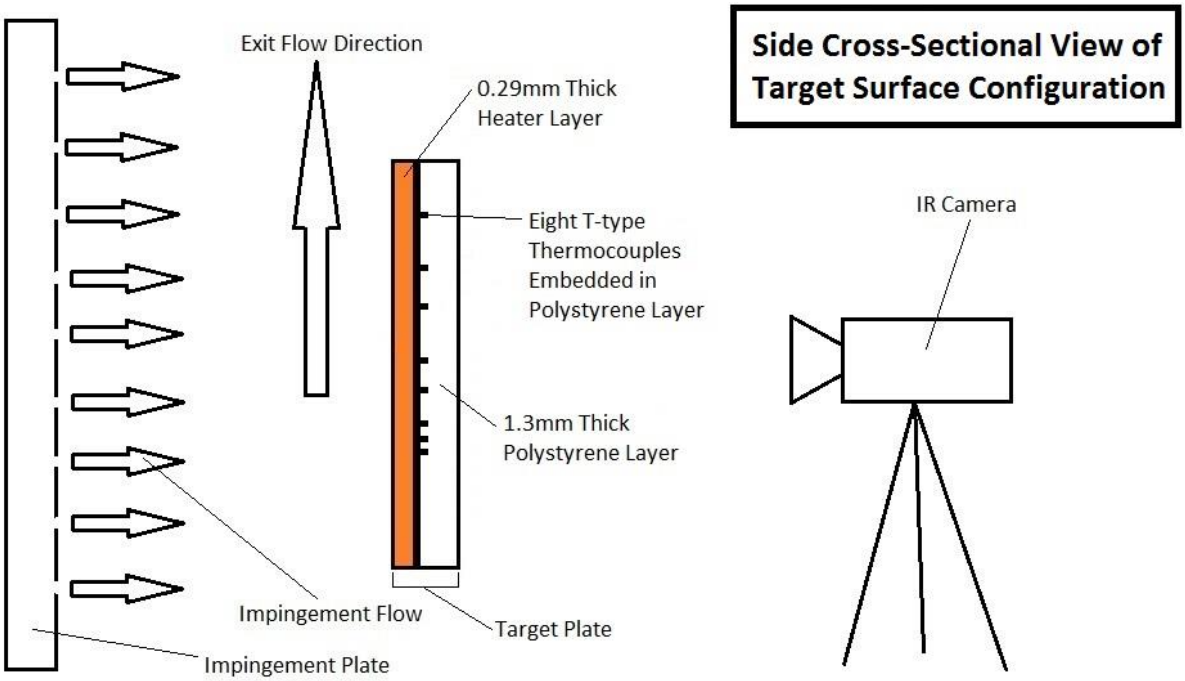

Figure 2.8: Diagram of polystyrene test configuration

The target plate is mounted on the bottom surface of the impingement plenum. Eight Omega T-type copper-constantan thermocouples are placed at different streamwise and spanwise locations within the polystyrene target plate so that each senses a different temperature as data are acquired. These provide measurements of local surface temperatures, after correction for thermal contact resistance and temperature variations through the 1.3 mm layer of polystyrene and the 0.29 mm heater layer. Thermocouple lead wires are placed in grooves along the polystyrene plate, and bonded into place with Loctite 1365736 heavy duty epoxy having approximately the same thermal conductivity as polystyrene, to minimize thermal disturbances resulting from their presence. The custom-made HK5184R26 thermo-foil heaters are manufactured by Minco Products Inc. Each heater is encased between two layers of DuPont Kapton polyimide film. This heater provides a constant surface heat flux boundary condition adjacent to the impingement air stream. Each target plate assembly is mounted within a frame to minimize distortion and shape variations which may occur as heat transfer tests are underway. Each target plate is also replaced after 3 or 4 test sequences with a new plate, because of shape changes which occur within the plates when they are utilized for more than this number of repeated test sequences.

C. ProtoCAM Target Plate Test Surfaces for Measurements of Surface Nusselt Numbers

For the ProtoCAM test configuration, local surface Nusselt numbers are measured on a heated target plate, which is comprised of a layer of Accura 25 plastic layer (manufactured by ProtoCAM), which is 1.31 mm thick, and an attached heater, which is approximately 0.29 mm thick, giving a total target plate thickness of 1.60 mm. The Accura 25 plastic layer contains roughness elements of varying sizes for testing. The size of the target plate is 127 mm by 255 mm. In the ProtoCAM test configuration, the Accura 25 plastic layer is located adjacent to the air stream with impinging air jets with the surface roughness facing the jets directly. The heater is located on the ambient air side of the target plate and is viewed by the infrared camera as spatially-resolved measurements of surface temperature are obtained. The reason that the heater is on the opposite side of the polystyrene configuration is that the roughness could not be manufactured on the heater layer. The heater for the ProtoCAM configuration needs to be placed on the ambient side so that the air can impinge on the rough surface. Figure 2.9 displays the ProtoCAM test configuration.

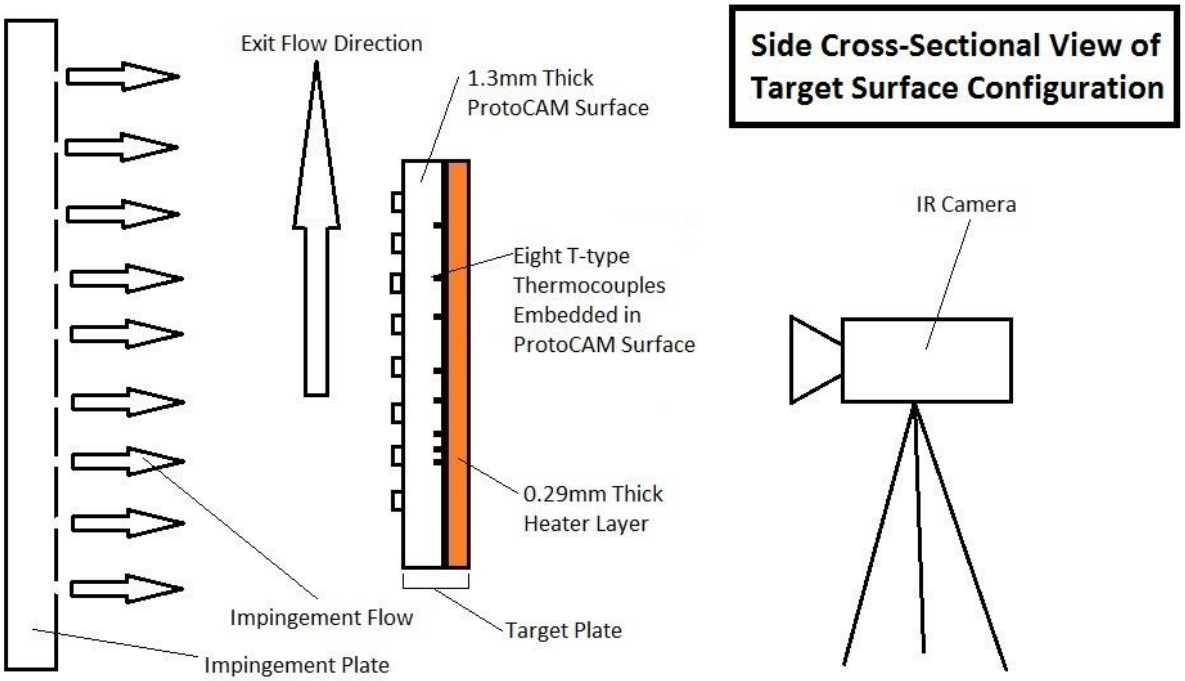

Figure 2.9: Diagram of ProtoCAM test configuration

The target plate is mounted on the bottom surface of the impingement plenum. Eight type-T copper-constantan thermocouples are placed at different streamwise and spanwise locations within the ProtoCAM target plate so that each senses a different temperature as data are acquired. These provide measurements of

local surface temperatures, after correction for thermal contact resistance and temperature variations through the target plate. Thermocouple lead wires are placed in grooves along the ProtoCAM plate, and bonded into place with Loctite 1365736 heavy duty epoxy having approximately the same thermal conductivity as polystyrene, to minimize thermal disturbances resulting from their presence. The custom-made HK5184R26 thermo-foil heaters are manufactured by Minco Products Inc. Each heater is encased between two layers of DuPont Kapton polyimide film. This heater provides an approximately constant surface heat flux boundary condition adjacent to the impingement air stream. Each target plate assembly is mounted within a frame to minimize distortion and shape variations which may occur as heat transfer tests are underway. Each target plate is also replaced after 3 or 4 test sequences with a new plate, because of shape changes which occur within the plates when they are utilized for more than this number of repeated test sequences.

The present investigation involves testing 19 different surface roughness configurations and one smooth plate. As stated previously, all plates consist of Accura 25 plastic and are manufactured by ProtoCAM. Figures 2.10 through 2.17 show diagrams of all target plates. Configurations considered include a smooth plate, a plate with large pins only, plates with small roughness, and plates with a combination of small roughness and large pins. Three different small roughness shapes are considered: rectangle, triangle, and cylinder. A listing of all roughness configurations considered is shown in Table 2.1. All three of these small roughness configurations are laid out in a grid with streamwise and spanwise spacings of 2 mm each. Three heights of small roughness are also considered: 1 mm, 1.5 mm, and 2 mm. The rectangle, triangle, and cylinder small roughness plates are displayed in Figures 2.12, 2.14, and 2.16, respectively.

The plate with large pins only and the rectangle and triangle combination plates all have the same sizing and spacing of large pins. The streamwise and spanwise spacing of the large pins is 5D and 2.7D, respectively. The length, width, and height of the large pins are 1.7D, 0.6D, and 1.48D, respectively. The large rectangle roughness plate is shown in Figure 2.11. Figures 2.13 and 2.15 show the rectangle and triangle combination plates, respectively.

The large pins on the cylinder roughness plates are cylinders with a streamwise spacing of 5D and a spanwise spacing of 2.7D. The diameter of the large cylinder pins is 0.7D. The combination cylinder plates also include a set of medium sized cylinder pins. The medium pins have a streamwise spacing of 2.5D, a

spanwise spacing of 1.35D, and a diameter of 0.35D. The small, medium, and large cylinder combination plate is shown in Figure 2.17.

Table 2.1: Target surface roughness configurations.

Plate Number	Description
1	Baseline – SMOOTH
2	Large RECTANGLE Roughness
3	Small RECTANGLE Roughness – Height = 1.0 mm
4	Small RECTANGLE Roughness – Height = 1.5 mm
5	Small RECTANGLE Roughness – Height = 2.0 mm
6	Large RECTANGLE + Small RECTANGLE Roughness – Height = 1.0 mm
7	Large RECTANGLE + Small RECTANGLE Roughness – Height = 1.5 mm
8	Large RECTANGLE + Small RECTANGLE Roughness – Height = 2.0 mm
9	Small TRIANGLE Roughness – Height = 1.0 mm
10	Small TRIANGLE Roughness – Height = 1.5 mm
11	Small TRIANGLE Roughness – Height = 2.0 mm
12	Large RECTANGLE + Small TRIANGLE Roughness – Height = 1.0 mm
13	Large RECTANGLE + Small TRIANGLE Roughness – Height = 1.5 mm
14	Large RECTANGLE + Small TRIANGLE Roughness – Height = 2.0 mm
15	Small CYLINDER Roughness – Height = 1.0 mm
16	Small CYLINDER Roughness – Height = 1.5 mm
17	Small CYLINDER Roughness – Height = 2.0 mm
18	Large CYLINDER + Medium CYLINDER + Small CYLINDER Roughness – Height = 1.0 mm
19	Large CYLINDER + Medium CYLINDER + Small CYLINDER Roughness – Height = 1.5 mm
20	Large CYLINDER + Medium CYLINDER + Small CYLINDER Roughness – Height = 2.0 mm

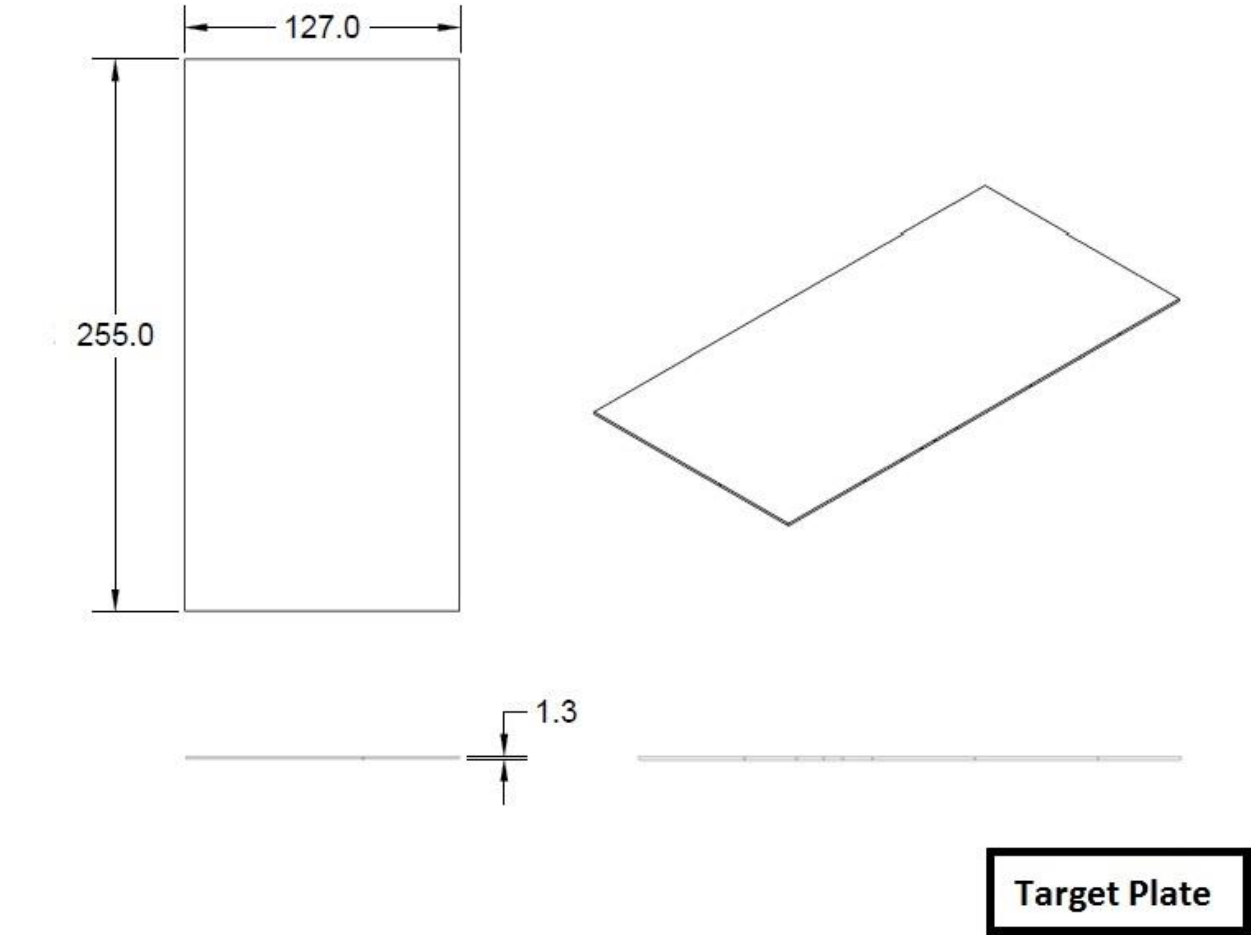

Figure 2.10: Smooth target plate. All dimensions in millimeters.

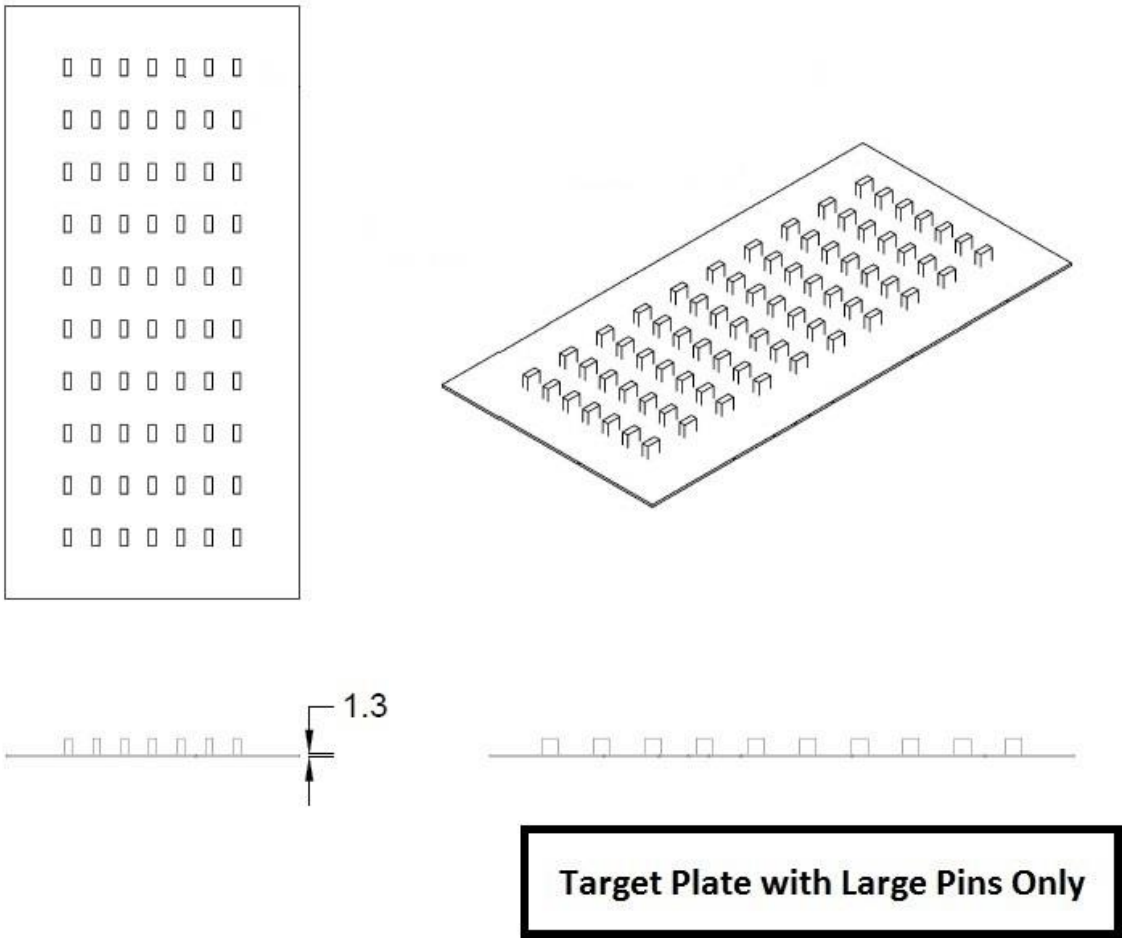

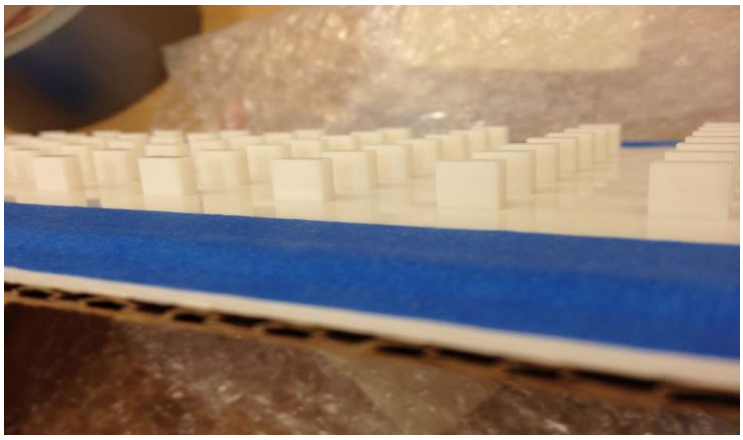

Figure 2.11: Target plate with large pins only. All dimensions in millimeters.

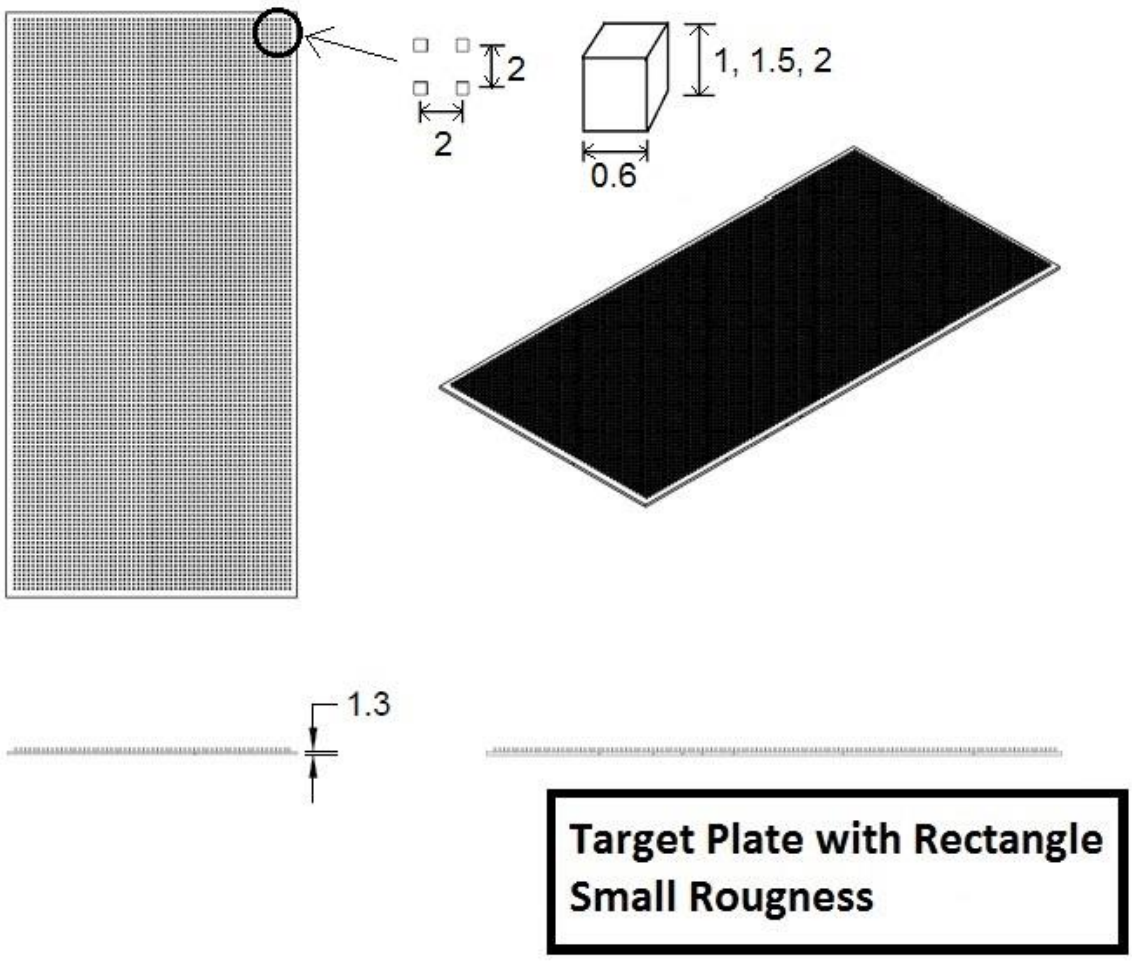

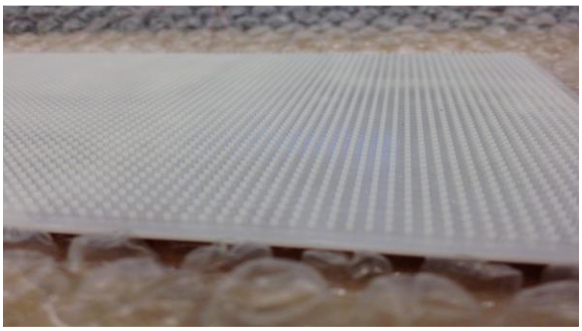

Figure 2.12: Small rectangle roughness target plate. All dimensions in millimeters.

Table 2.2: Sizing and spacing of small rectangle roughness

Small Rectangle Roughness	Non-Dimensional Value	Dimensional Value (mm)
Streamwise Spacing	x/D=0.444	x=2
Spanwise Spacing	y/D=0.444	y=2
Length	L/D=0.133	L=0.6
Width	W/D=0.133	W=0.6
Height	H/D=0.222, H/D=0.333, H/D=0.444	H=1, H=1.5, H=2
Hole Diameter		D=4.5

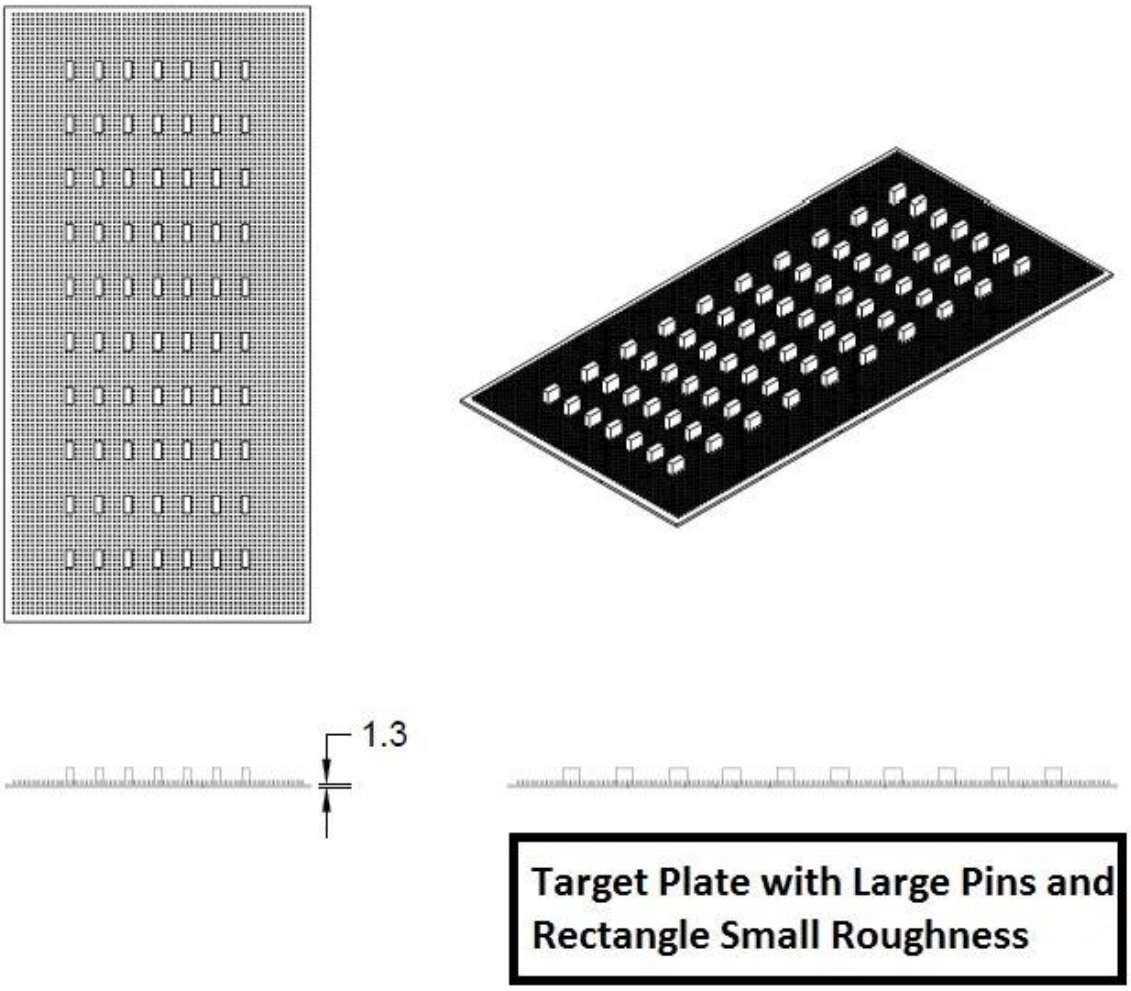

Figure 2.13: Small rectangle roughness with large pins. All dimensions in millimeters.

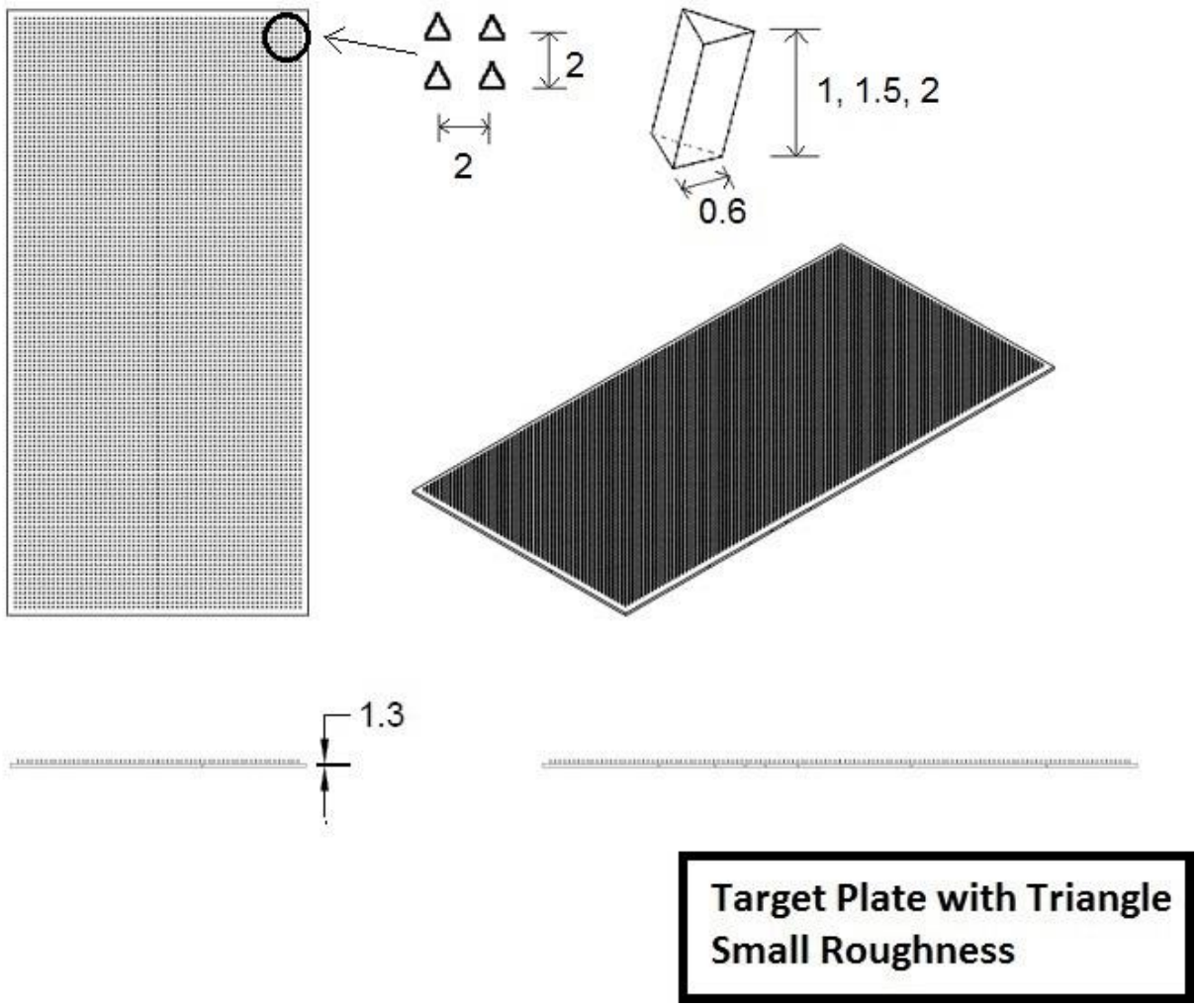

Table 2.3: Sizing and spacing of small triangle roughness

Small Triangle Roughness	Non-Dimensional Value	Dimensional Value (mm)
Streamwise Spacing	x/D=0.444	x=2
Spanwise Spacing	y/D=0.444	y=2
Side length	W/D=0.133	W=0.6
Height	H/D=0.222, H/D=0.333, H/D=0.444	H=1, H=1.5, H=2
Hole Diameter		D=4.5

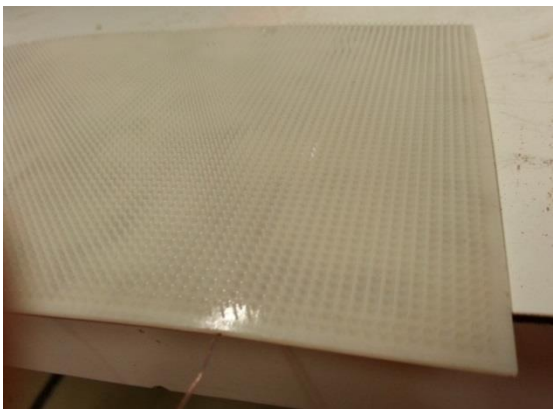

Figure 2.14: Small triangle roughness target plate. All dimensions in millimeters.

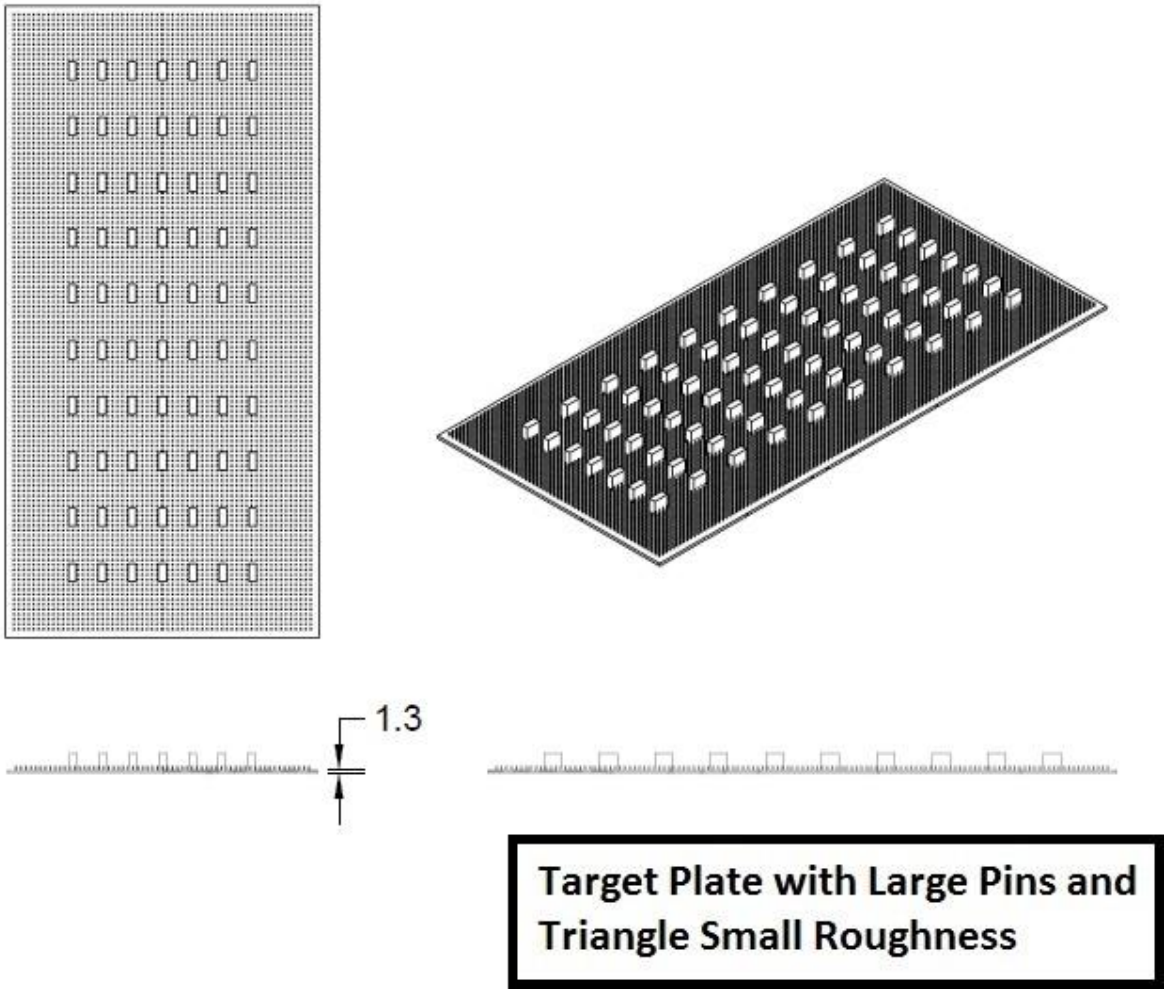

Figure 2.15: Small triangle roughness with large pins. All dimensions in millimeters.

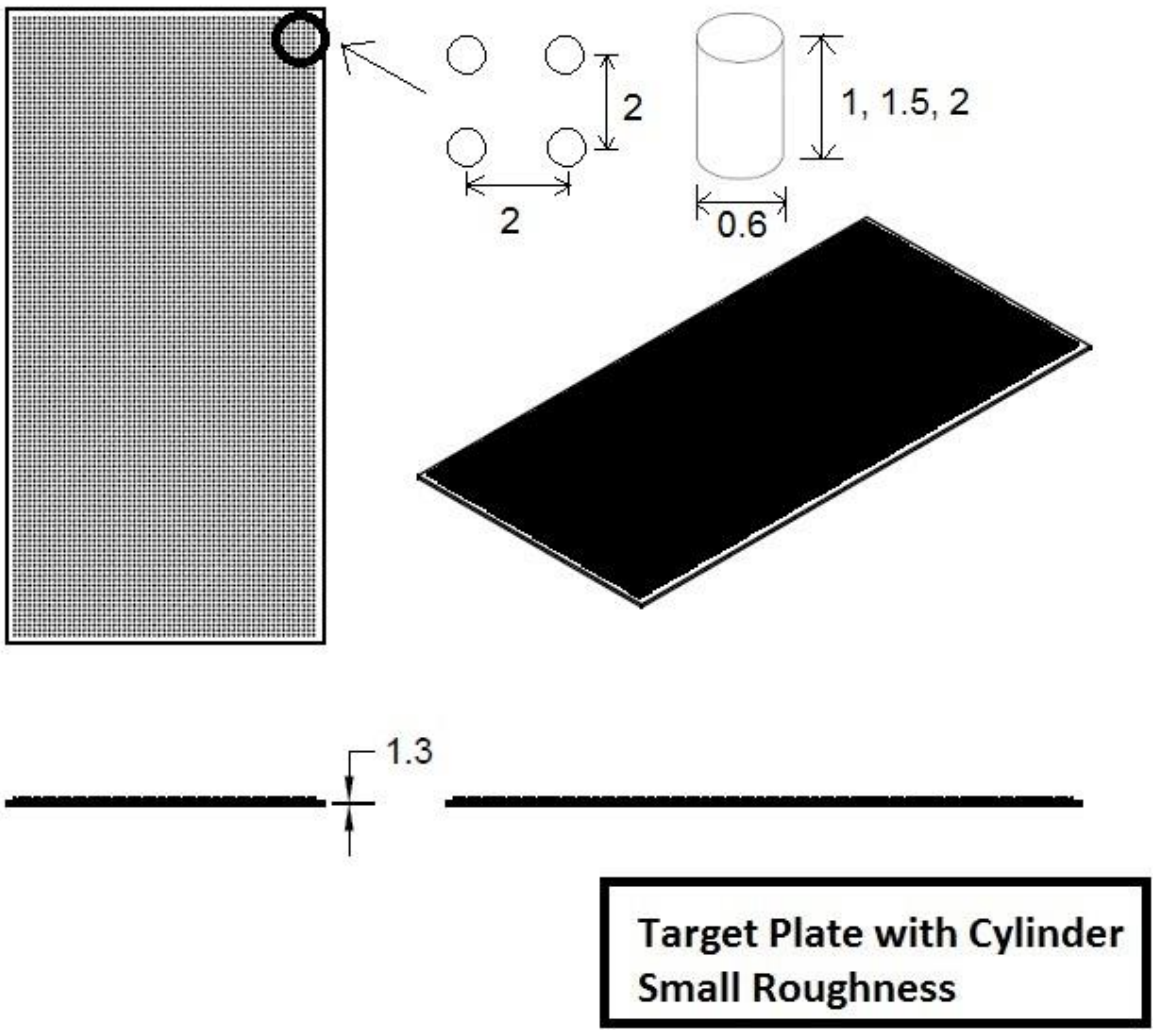

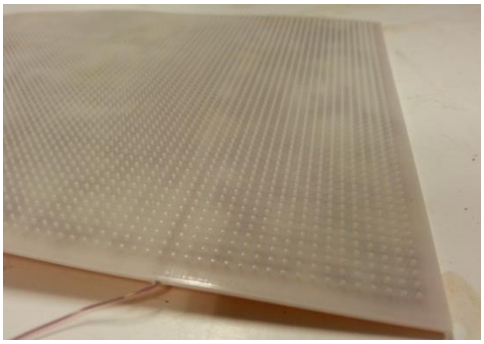

Figure 2.16: Small cylinder roughness target plate. All dimensions in millimeters.

Table 2.4: Sizing and spacing of small cylinder roughness

Small Cylinder Roughness	Non-Dimensional Value	Dimensional Value (mm)
Streamwise Spacing	x/D=0.25	x=2
Spanwise Spacing	y/D=0.25	y=2
Diameter	d/D=0.075	d=0.6
Height	H/D=0.125, H/D=0.1875, H/D=0.25	H=1, H=1.5, H=2
Hole Diameter		D=8

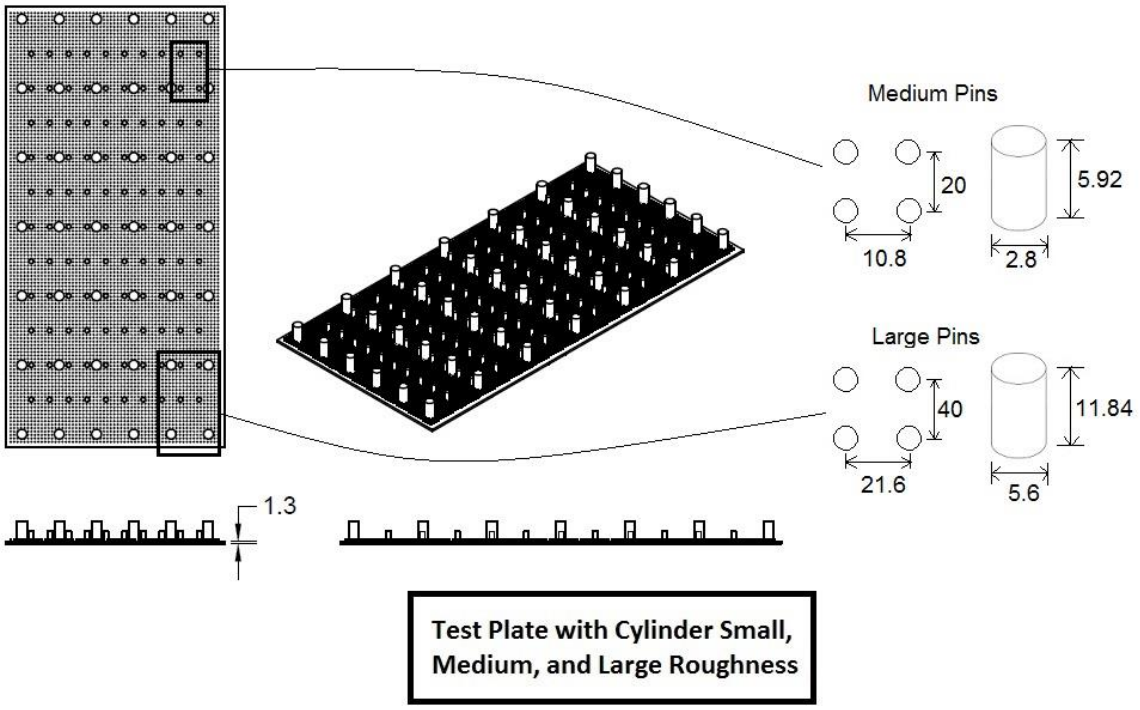

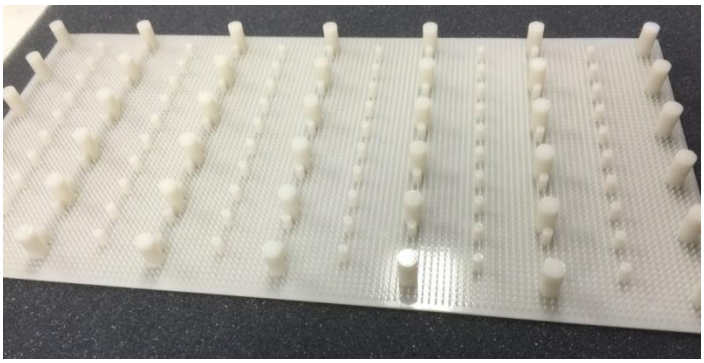

Figure 2.17: Small cylinder roughness with large pins. All dimensions in millimeters.

Table 2.5: Sizing and spacing of cylinder roughness

	Small Pins		**Medium Pins**		**Large Pins**	
	Non-Dimensional Value	Dimensional Value (mm)	Non-Dimensional Value	Dimensional Value (mm)	Non-Dimensional Value	Dimensional Value (mm)
Streamwise Spacing	x/D=0.25	x=2	x/D=2.5	x=20	x/D=5	x=40
Spanwise Spacing	y/D=0.25	y=2	y/D=1.35	y=10.8	y/D=2.7	y=21.6
Diameter	d/D=0.075	d=0.6	d/D=0.35	d=2.8	d/D=0.7	d=5.6
Height	H/D=0.125, H/D=0.1875, H/D= 0.25	H=1, H=1.5, H=2	H/D=0.74	H=5.92	H/D=1.48	H=11.84
Hole Diameter		D=8		D=8		D=8

D. Measurement Procedures – Velocities, Temperatures, and Mass Flow Rates

As shown in Figure 2.18, multiple wall static pressure taps are located on the surface of the test plenum and along the pipe leading to the plenum. As tests are conducted, calibrated Validyne Model DP15-20 and DP15-22 pressure transducers driven by Validyne Model CD15 Carrier Demodulators are used to sense pressures from these static pressure taps. The total pressure is measured upstream of the orifice plate with a United Sensor KRF-12 Kiel probe. The Kiel probe is connected to the positive side of a Validyne Model DP15-20 pressure transducer, driven by a Validyne Model CD15 Carrier Demodulator. The negative side of the pressure transducer is connected to a static pressure tap at the same location as the Kiel probe. The difference between the total pressure and the static pressure gives the dynamic pressure upstream of the orifice plate. This allows the calculation of the airflow velocity. Voltages from the carrier demodulators are read sequentially using National Instruments NI-USB 6210 Data Acquisition terminals. The terminals relay the information to a Dell Precision T1700 computer. The voltage outputs from this unit are acquired by the computer through its USB port, using LABVIEW 11.0 software.

Air temperature measurements were made using four Omega T-type copper-constantan thermocouples. Local airflow recovery temperatures are measured using two thermocouples located in the central part of the lower plenum. Additionally, one thermocouple is located at the orifice plate and one is located in the ambient air. Voltages the thermocouples employed in the study are read sequentially using National Instruments NI-USB 9162 Data Acquisition terminals. These terminals relay the information to a Dell Precision T1700 computer. The voltage outputs from this unit are acquired by the computer through its USB port, using LABVIEW 11.0 software.

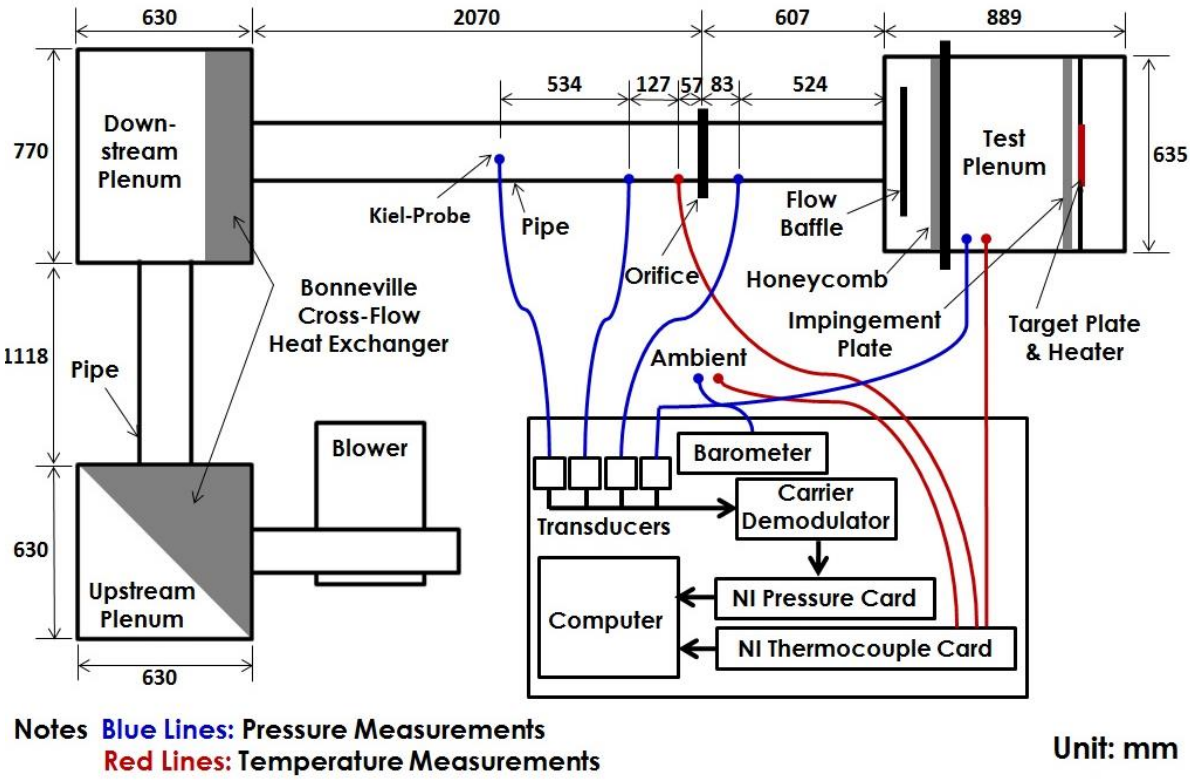

Figure 2.18: Diagram of measuring facilities

An iterative procedure is used to determine the impingement static temperature T_j, and the impingement flow Mach number Ma. With impingement static temperature T_j, impingement flow Mach number Ma, and other parameters known, the impingement Reynolds number is subsequently given by an equation of the form

$$\mathrm{Re}_j = \rho_a u_a D / \mu \tag{1}$$

Note that Re_j is equivalent to $4\dot{m}/\pi ND\mu$, where N is the total number of impingement holes, $\dot{m}$ is the total mass flow rate, D is the diameter of the impingement hole, and μ is the dynamic viscosity of the air.

A Kiel-type stagnation pressure probe is used to measure the total pressure in the pipe at a position which is located upstream of the orifice plate employed to measure mass flow rate. A wall pressure tap located on the surface of the pipe, and a calibrated copper-constantan thermocouple positioned within the air stream are used to sense static pressure and flow recovery temperature, respectively, at the same streamwise location. Pressures and temperatures measured using the thermocouple, probe, and tap are sensed and processed using the same types of instrumentation mentioned earlier. The velocities deduced from this arrangement are used

to provide a cross-check on the velocities deduced from mass flow rates, which are measured using the ASME standard orifice plate. A diagram of the orifice plate configuration with dimensions is shown in Figure 2.19.

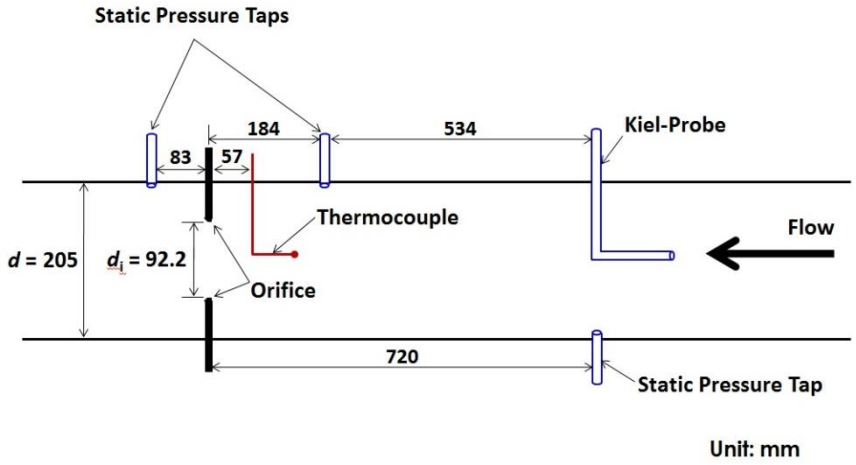

Figure 2.19: Diagram of orifice plate

E. Measurement Procedures – Heat Transfer Target Surface

As impingement heat transfer measurements are made, spatially-resolved distributions of the target test surface temperature, T_W , are determined using infrared imaging in conjunction with thermocouples, energy balances, digital image processing, and *in situ* calibration procedures. These are then used to determine spatially-resolved surface Nusselt numbers. To accomplish this, the infrared radiation emitted by the polystyrene or heater surface of the impingement test plate is captured using a FLIR T650sc 640x480 infrared camera, which operates at infrared wavelengths from 7.5 μm to14 μm. Temperatures, measured using the calibrated, copper-constantan thermocouples distributed along the test surface adjacent to the flow, are used to perform the *in situ* calibrations simultaneously as the radiation contours from surface temperature variations are recorded.

This is accomplished as the camera views the heater from behind, as shown in Figure 2.20. In general, all eight thermocouple junction locations are present in the infrared field viewed by the camera. The exact spatial locations and pixel locations of these thermocouple junctions and the coordinates of the field of view are known from calibration maps obtained prior to measurements. During this procedure, the camera is focused, and rigidly mounted and oriented relative to the test surface in the same way as when radiation

contours are recorded. Voltages from the thermocouples are acquired using the apparatus mentioned earlier. An example of typical thermocouple calibration data is shown in Figure 2.20.

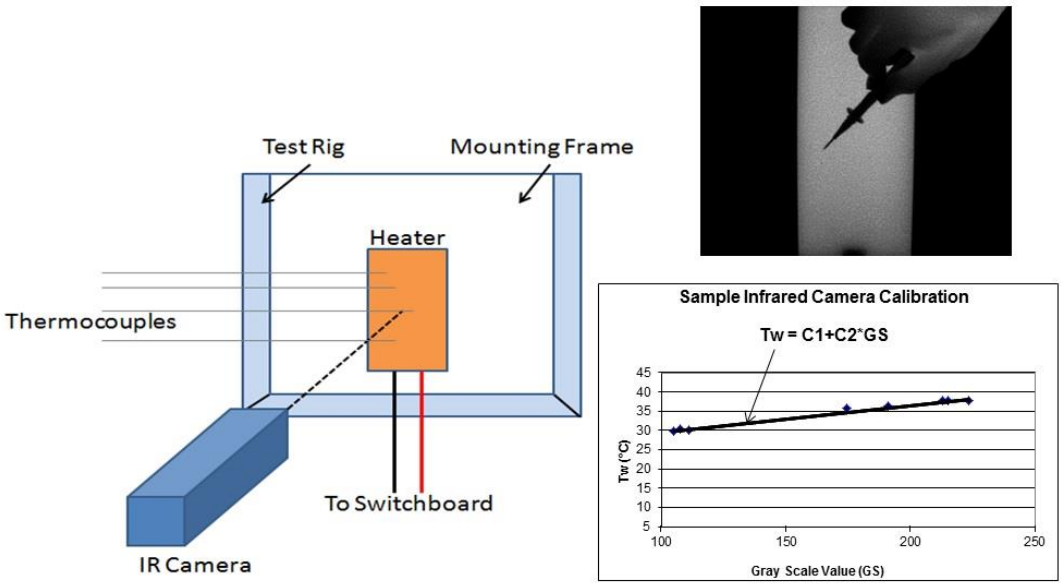

Figure 2.20: IR camera calibration method

Images from the infrared camera are recorded as 16-bit gray scale directly into the memory of a Dell Precision T1700 computer using Flir ResearchIR MAX 4 software. One set of 50 frames is taken at a rate of 30 Hz for 1.7 seconds. All of the resulting images are then ensemble averaged to obtain the final gray scale data image. This final data set is then imported into MATLAB software to convert each of 256 possible gray scale values to local Nusselt number at each pixel location using calibration data. Each individual image covers a 256 pixel by 192 pixel area.

F. Local Nusselt Number Measurements – Polystyrene Target Plate

The power to the thermo-foil heater, mounted on the polystyrene target plate, is controlled and regulated using an alternating current to direct current TDK Lambda Z100-4-U transformer power supply. The power supply is directed by a covered switchboard where the voltage is read by an Agilent 34401A Digital Benchtop Multimeter, and the amperage is read by both a Simpson 260 Series 8P Ammeter and an Agilent 34401A Digital Benchtop Multimeter. Energy balances, and analysis to determine temperature values on the two surfaces of the target plate, then allow determination of the magnitude of the total convective

power (due to impingement cooling) for a particular test. To determine the surface heat flux (used to calculate heat transfer coefficients and local Nusselt numbers), the total convective power level, provided by the particular thermo-foil heater employed, is divided by the single surface area of this heater, denoted A_{ht} . This value is inserted into the following equation

$$q_{cf} = \frac{Q}{A_{ht}} - q_{rf} - q_{rb} - q_{cb} \tag{2}$$

where Q is the total power provided to the thermofoil heater, A_{ht} is the heat transfer area on the target plate, q_{rf} is the radiation heat flux from front side (or impingement side) of the target plate, q_{rb} and q_{cb} are the radiation heat flux and the convection heat flux from the back side of the target plate, respectively.

One step in this procedure utilizes a one-dimensional conduction analysis, which is applied between the surface *within* the target plate where the thermocouples are located (between the heater and the polystyrene target plate), and the ambient air environment behind the polystyrene layer. This is used to determine T_b , the local temperature on the surface of the polystyrene target plate, adjacent to the ambient air environment. From the conduction analysis, T_b is given by

$$T_b = \frac{\left(\frac{k_t T_{tc}}{h_{loss} d_t} + T_{amb} \right)}{\left(1 + \frac{k_t}{h_{loss} d_t} \right)} \tag{3}$$

where k_t is the thermal conductivity of polystyrene, h_{loss} is the heat transfer coefficient to account for convection and radiation loss from the back side of the target plate, d_t is the thickness of the polystyrene plate, and T_{amb} is the ambient temperature. h_{loss} is determined by an iterative procedure, described later in this section. Also required for this analysis is T_{tc} , the local temperature within the target plate between the heater and the polystyrene plate, which is determined from thermocouple measurements. With these temperatures known, the radiation heat flux and the convection heat flux from the back side of the target plate, q_{rb} and q_{cb} , respectively, are determined from the following equation.

$$q_b = q_{rb} + q_{cb} = h_{loss}\left(T_b - T_{amb}\right) = k_t \frac{\left(T_{tc} - T_b\right)}{d_t} \tag{4}$$

The radiation heat flux q_{rf} on the front (or impingement side) of the target plate is determined using the following equation

$$q_{\mathrm{rf}} = \frac{\sigma\left(T_{\mathrm{W}}^4 - T_{\mathrm{amb}}^4\right)}{\left(\frac{1}{\varepsilon_{\mathrm{inf}}} - \frac{1}{\varepsilon_{\mathrm{f}}} - 1\right)} \tag{5}$$

where σ is the Stefan-Boltzmann constant, $\varepsilon_{\mathrm{inf}}$ is the emissivity of a plate located opposite to the target plate, and ε_{f} is the emissivity of the front surface of the target plate. $\varepsilon_{\mathrm{inf}}$ and ε_{f} are assumed to be equal to 0.9 for all conditions investigated. These approximations work due to the fact that previous testing has shown that $q_{rf}A_{ht}$ is only 3-6 percent of the total heat input, Q [6].

From one-dimensional conduction analysis, a formula for the convection heat flux from the impingement side of the target plate is given by

$$q_{\mathrm{cf}} = k_{\mathrm{h}} \frac{\left(T_{\mathrm{tc}} - T_{\mathrm{W}}\right)}{d_{\mathrm{h}}} + q_{\mathrm{vol}}\left(\frac{d_{\mathrm{h}}}{2}\right) \tag{6}$$

where k_{h} is the thermal conductivity of the heater, d_{h} is the thickness of the heater, and q_{vol} is the volumetric heat generation within the heater. Equation 6 can be rearranged to get a formula for T_w, the local target surface temperature on the surface of the test plate adjacent to the impingement air.

$$T_{\mathrm{W}} = T_{\mathrm{tc}} - \frac{d_{\mathrm{h}}}{k_{\mathrm{h}}}\left[q_{\mathrm{cf}} - q_{\mathrm{vol}}\left(\frac{d_{\mathrm{h}}}{2}\right)\right] \tag{7}$$

Because of the inter-dependence of T_w, q_{rf}, and q_{cf} (the convection heat flux from the front side or impingement side of the target plate), an iterative procedure is required to determine these quantities. This procedure uses a one-dimensional conduction analytical model for the heater, which includes source generation of thermal energy, to provide a relation between T_w, T_{tc}, and q_{cf}. This one-dimensional conduction model is shown in Equation 6. Also included in the analysis is thermal contact resistance between the internal thermocouples and the adjacent heater. This one-dimensional conduction approach is employed since magnitudes of lateral conduction within the target plate are very small and mostly insignificant (from three-dimensional analyses), relative to impingement convective heat flux levels.

The iterative procedure begins by assuming an initial percentage of the input heat, Q, exits the back of the polystyrene plate into ambient air. This is denoted h_{loss}, as seen in Equations 3 and 4. This initial value is put into Equations 3 and 4, which sets a value for $q_{cb} + q_{rb}$ in Equation 2. Using Equations 2, 4, and 7, a solution is found for T_w, q_{cf}, and q_{rf}. The value of q_{cf} that is found from Equation 2 in the system of equations is compared to the value of q_{cf} from Equation 6. If these values match, then the value for h_{loss} is correct. If not, the value of h_{loss} is incrementally changed until the equations converge on a solution. Once q_{cf} has been found, the Nusselt number can be calculated with the following equation

$$\mathrm{Nu} = \frac{hD}{\alpha} = \frac{q_{\mathrm{cf}} D}{\left(T_{\mathrm{W}} - T_{0j}\right) k_a} \tag{8}$$

where *h* is the heat transfer coefficient, D is the diameter of an individual impingement hole, and k_a is the air thermal conductivity. A diagram of the polystyrene experimental setup and Nusselt number determination is shown in Figure 2.21.

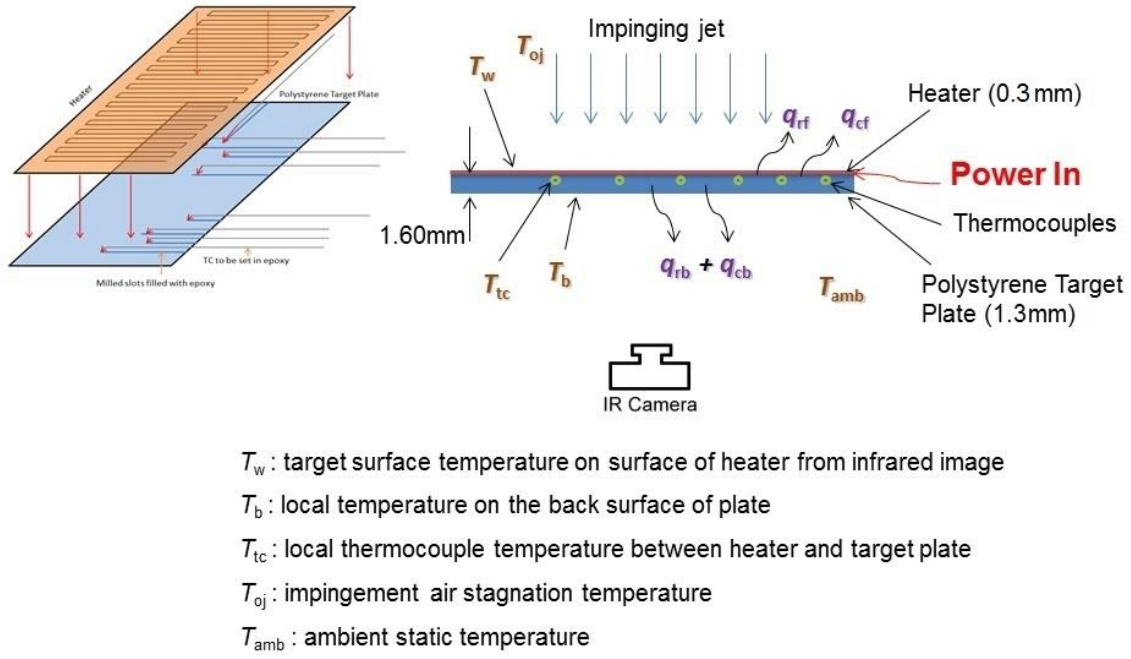

Figure 2.21: Nusselt number determination for polystyrene test configuration

G. Local Nusselt Number Measurements – ProtoCAM Target Plate

The power to the thermo-foil heater, mounted on the ProtoCAM target plate, is controlled and regulated using an alternating current to direct current TDK Lambda Z100-4-U transformer power supply. The power supply is directed by a covered switchboard where the voltage is read by an Agilent 34401A Digital Benchtop Multimeter, and the amperage is read by both a Simpson 260 Series 8P Ammeter and an Agilent 34401A Digital Benchtop Multimeter. Energy balances, and analysis to determine temperature values on the two surfaces of the target plate, then allow determination of the magnitude of the total convective power (due to impingement cooling) for a particular test. To determine the surface heat flux (used to calculate heat transfer coefficients and local Nusselt numbers), the total convective power level, provided by the particular thermo-foil heater employed, is divided by the single surface area of this heater, denoted A_{ht} . This value is inserted into the following equation

$$q_{\mathrm{cf}} = \frac{Q}{A_{\mathrm{ht}}} - q_{\mathrm{rf}} - q_{\mathrm{rb}} - q_{\mathrm{cb}} \tag{9}$$

where Q is the total power provided to the thermofoil heater, A_{ht} is the heat transfer area on the target plate, q_{rf} is the radiation heat flux from front side (or impingement side) of the target plate, q_{rb} and q_{cb} are the radiation heat flux and the convection heat flux from the back side of the target plate, respectively.

One step in this procedure utilizes a one-dimensional conduction analysis, which is applied between the surface *within* the target plate where the thermocouples are located (between the heater and the ProtoCAM target plate), and the ambient air environment behind the heater layer. This is used to determine T_b , the local temperature on the surface of the heater, adjacent to the ambient air environment. From the conduction analysis, T_b is given by

$$T_{\mathrm{b}} = \frac{\left(\frac{k_{\mathrm{h}} T_{\mathrm{tc}}}{h_{\mathrm{loss}} d_{\mathrm{h}}} + T_{\mathrm{amb}} + \frac{\left(q_{vol} \left(\frac{d_h}{2} \right) \right)}{h_{loss}} \right)}{\left(1 + \frac{k_{\mathrm{h}}}{h_{\mathrm{loss}} d_{\mathrm{h}}} \right)} \tag{10}$$

where k_h is the thermal conductivity of the heater , h_{loss} is the heat transfer coefficient to account for convection and radiation loss from the back side of the target plate, d_h is the thickness of the heater, T_{amb} is the ambient temperature, and q_{vol} is the volumetric heat flux within the heater. h_{loss} is determined by an iterative procedure, described later in this section. Also required for this analysis is T_{tc} , the local temperature within the target plate between the heater and the ProtoCAM plate, which is determined from thermocouple measurements. With these temperatures known, the radiation heat flux and the convection heat flux from the back side of the target plate, q_{rb} and q_{cb} , respectively, are determined from the following equation.

$$q_{\mathrm{b}} = q_{rb} + q_{cb} = h_{\mathrm{loss}}\left(T_{\mathrm{b}} - T_{\mathrm{amb}}\right) = k_{\mathrm{t}}\,\frac{\left(T_{\mathrm{tc}} - T_{\mathrm{b}}\right)}{d_{\mathrm{t}}} + q_{vol}\left(\frac{d_h}{2}\right) \tag{11}$$

The radiation heat flux q_{rf} on the front (or impingement side) of the target plate is determined using the following equation

$$q_{\mathrm{rf}} = \frac{\sigma\left(T_{\mathrm{W}}^4 - T_{\mathrm{amb}}^4\right)}{\left(\frac{1}{\varepsilon_{\mathrm{inf}}} - \frac{1}{\varepsilon_{\mathrm{f}}} - 1\right)} \tag{12}$$

where σ is the Stefan-Boltzmann constant, $\varepsilon_{\mathrm{inf}}$ is the emissivity of a plate located opposite to the target plate, and ε_{f} is the emissivity of the front surface of the target plate. $\varepsilon_{\mathrm{inf}}$ and ε_{f} are assumed to be equal to 0.9 for all conditions investigated. These approximations work due to the fact that previous testing has shown that $q_{rf}A_{ht}$ is only 3-6 percent of the total heat input, Q.

From one-dimensional conduction analysis, a formula for the convection heat flux from the impingement side of the target plate is given by

$$q_{\mathrm{cf}} = k_{\mathrm{t}}\,\frac{\left(T_{\mathrm{tc}} - T_{\mathrm{W}}\right)}{d_{\mathrm{t}}} \tag{13}$$

where k_{h} is the thermal conductivity of the ProtoCAM layer and d_{h} is the thickness of the ProtoCAM layer. Equation 13 can be rearranged to get a formula for T_w, the local target surface temperature on the surface of the test plate adjacent to the impingement air.

$$T_{\mathrm{W}} = T_{\mathrm{tc}} - \frac{d_{\mathrm{h}}}{k_{\mathrm{h}}}\left[q_{\mathrm{cf}}\right] \tag{14}$$

Because of the inter-dependence of T_W, q_{rf}, and q_{cf} (the convection heat flux from the front side or impingement side of the target plate), an iterative procedure is required to determine these quantities. This procedure uses a one-dimensional conduction analytical model for the ProtoCAM plate to provide a relation between T_W, T_{tc}, and q_{cf}. This one-dimensional conduction model is shown in Equation 13. Also included in the analysis is thermal contact resistance between the internal thermocouples and the adjacent heater. This one-dimensional conduction approach is employed since magnitudes of lateral conduction within the target plate are very small and mostly insignificant (from three-dimensional analyses), relative to impingement convective heat flux levels.

The iterative procedure begins by assuming an initial percentage of the input heat, Q, exits the back of the ProtoCAM plate into ambient air. This is denoted h_{loss}, as seen in Equations 10 and 11. This initial value is put into Equations 3 and 4, which sets a value for $q_{cb} + q_{rb}$ in Equation 9. Using Equations 9, 11, and 14, a solution is found for T_w, q_{cf}, and q_{rf}. The value of q_{cf} that is found from Equation 9 in the system of equations is compared to the value of q_{cf} from Equation 13. If these values match, then the value for h_{loss} is correct. If not, the value of h_{loss} is incrementally changed until the equations converge on a solution. Once q_{cf} has been found, the Nusselt number can be calculated with the following equation

$$\mathrm{Nu} = \frac{hD}{\alpha} = \frac{q_{cf} D}{(T_W - T_{0j}) k_a} \tag{15}$$

where *h* is the heat transfer coefficient, D is the diameter of an individual impingement hole, and k_a is the air thermal conductivity. A diagram of the ProtoCAM experimental setup and Nusselt number determination is shown in Figure 2.22.

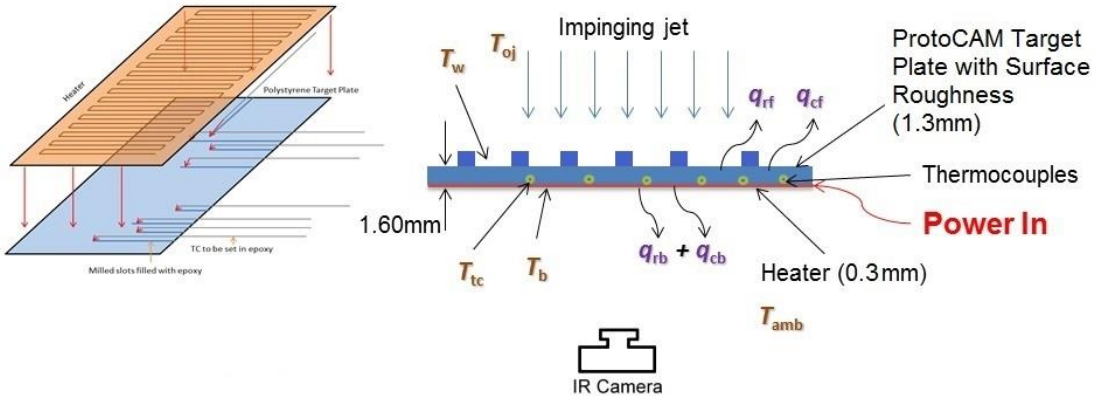

T_w : target surface temperature on surface of plate from infrared image

T_b : local temperature on the back surface of heater

T_{tc} : local thermocouple temperature between heater and target plate

T_{oj} : impingement air stagnation temperature

T_{amb} : ambient static temperature

Figure 2.22: Nusselt number determination for ProtoCAM test configuration

The iterative procedure is only required for the baseline ProtoCAM configuration. Previous studies have shown that the heat lost out the back of the target plate only varies with Reynolds number. After the iterative procedure is completed for the initial test, the assumption is made that a constant percentage of the heat exits the heater on the ambient air side for all plates considered. The constant heat flux factor that is used is called the conduction factor. In addition to the conduction factor, a temperature factor is used to correct small variations of local adiabatic surface temperature due to conduction within the test surface. These two factors are determined by CFD simulations, as described in the next chapter. Table 2.6 displays the temperature and conduction factors used for the present investigation.

Table 2.6: Nusselt number determination for ProtoCAM test configuration

	CF	TF
Re=900	0.6143	0.8
Re=1500	0.6143	0.8
Re=5000	0.8778	0.87
Re=11000	0.8679	0.69

The corrected convection heat flux from the front side (or impingement side) of the target plate is then given by

$$q_{\mathrm{cf}} = \frac{Q}{A_{\mathrm{ht}}} - q_{\mathrm{rf}} - q_{\mathrm{rb}} - q_{\mathrm{cb}} = \frac{Q}{A_{\mathrm{ht}}} - q_{\mathrm{rf}} - \frac{Q}{A_{\mathrm{ht}}} * CF \tag{16}$$

The local Nusselt number is then given as

$$\mathrm{Nu} = \frac{hD}{k} = \frac{q_{\mathrm{cf}} D}{\left(T_{\mathrm{W}} - T_{0\,j}\right) * TF * k_a} \tag{17}$$

The conduction and temperature factors are CF and TF, respectively.

CHAPTER 3

NUMERICAL CONDUCTION ANALYSIS

Chapter 3 presents a description of the numerical analysis procedure for simulations of physical tests. This chapter includes a description of the software inputs, assumptions, and a discussion of selected results. Numerical analysis software simulations are used to determine variations of temperature and heat flux throughout the target surface. From these results, magnitudes of TF and CF are determined. In addition, the assumption of one-dimensional target surface conduction is verified. The software that is used for this purpose is SC/Tetra Version 11. SC/Tetra is a general purpose thermo-fluid simulation software that uses a hybrid mesh. These numerical predictions are completed for the polystyrene plate and for ProtoCAM plate numbers 1 through 8 (as listed in Table 2.1) at a Reynolds number of 5000.

A. Numerical Analysis - Polystyrene Configuration

The following section presents the numerical analysis used with the polystyrene configuration. To verify the physical test results, SC/Tetra outputs the polystyrene surface temperature map and the heat flux, which allows for the calculation of surface Nusselt numbers. The temperature that SC/Tetra gives for the impingement surface is put into Equation 8, giving the surface Nusselt number. If the Nusselt numbers from these numerical predictions agree with Nusselt numbers from experimental measurements, the TF factor is sufficient. SC/Tetra also outputs the heat flux vector out of the target plate on the impingement side, which is used to determine CF factors. In addition, SC/Tetra outputs the heat flux in the streamwise and spanwise directions. If these heat flux values are close to zero, the assumption of one-dimensional conduction is verified. The polystyrene test configuration places the heater layer on the impingement jet

side and the polystyrene layer on the infrared camera viewing side. A diagram of the test plate arrangement used for the numerical predictions is shown in Figure 3.1.

Assumptions for this analysis include a constant thermal conductivity through all materials, uniform heat distribution throughout the heater, constant ambient air temperature of 22.6°C, and a static pressure of 1 atm. Table 3.1 gives the material properties used for these predictions. The boundary conditions for the simulations include adiabatic edges and a constant surface heat flux on the back of the polystyrene layer (adjacent to ambient air). The temperature variations on the front of the polystyrene plate are from experimental measurements.

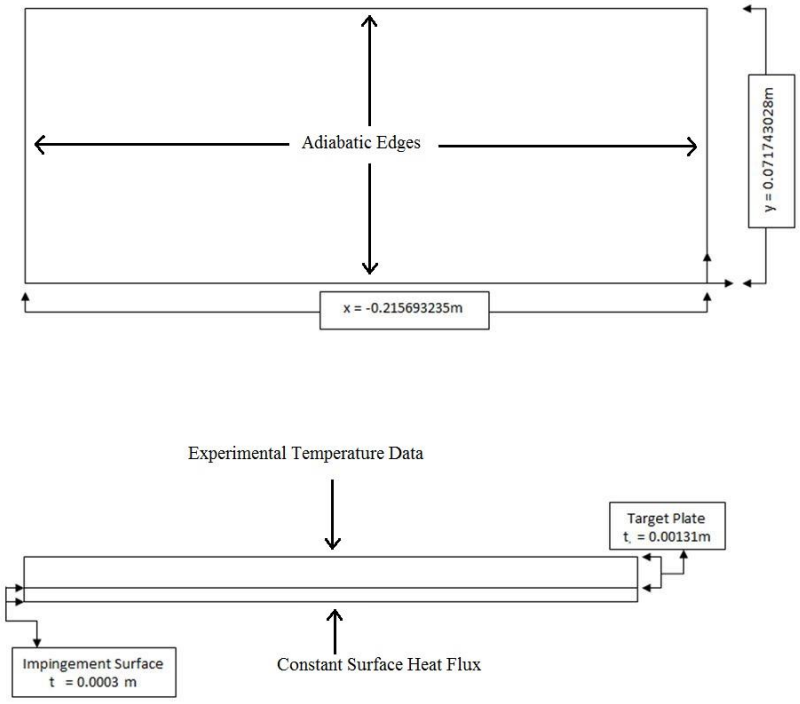

Figure 3.1: Test Plate Geometry

Table 3.1: Material Property Inputs for Polystyrene Numerical Predictions

Material	Density (kg/m^3)	Specific Heat (J/kgK)	Thermal Conductivity (W/mK)
Polystyrene	1060	1300	0.09
Polycarbonate (heater)	1200	1300	0.2

The temperature results used to obtain the data in Figures 3.2 through 3.6 are taken with values of x/D=10, y/D=2.7, D=4.5 mm, z=2.5D, Ma=0.058, and a Reynolds number of 5000. The results from this simulation are shown in Figures 3.2 through 3.6. Figure 3.2 shows temperature variations for the impingement surface. Figures 3.3 and 3.4 show heat flux variations in the x-direction and y-direction, respectively. The average values of heat flux for the x and y-directions are very low and are less than 0.6 W/m^2. When compared to the average value of heat flux in the z-direction, as shown in Figure 3.5, these values are minimal. This confirms the assumption of one-dimensional conduction analysis that is employed for experiments. Additionally, Figure 3.6 shows that local experimentally measured and numerically predicted Nusselt number values are in excellent agreement, which verifies numerically predicted temperature and heat flux variations, as well as the associated values of CF and TF.

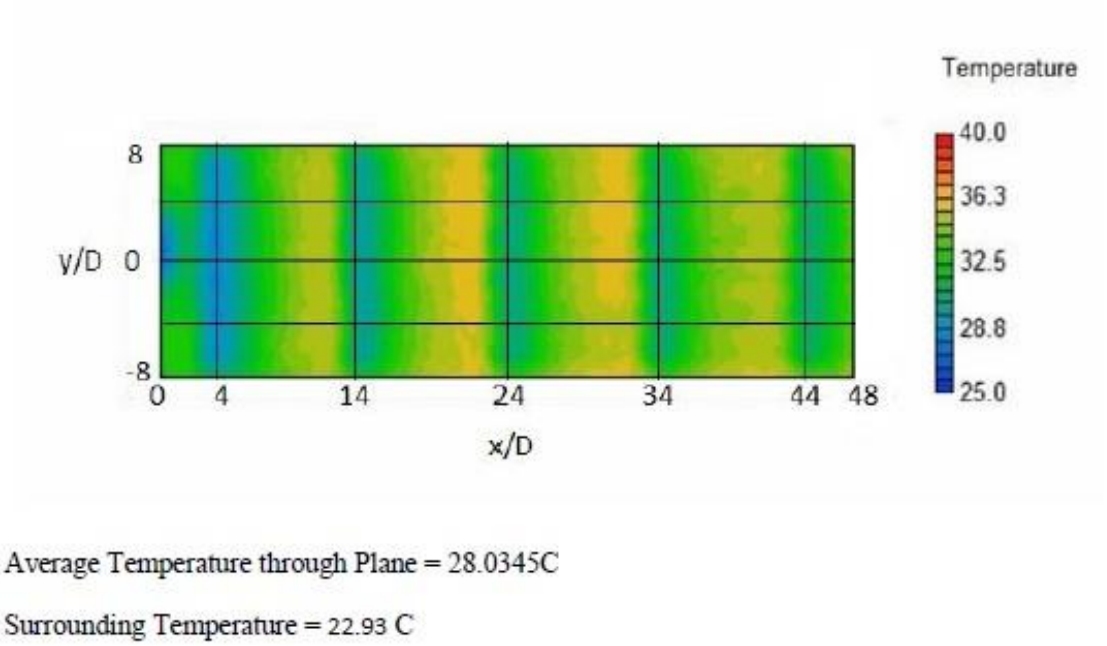

Figure 3.2: Temperature map on impingement surface

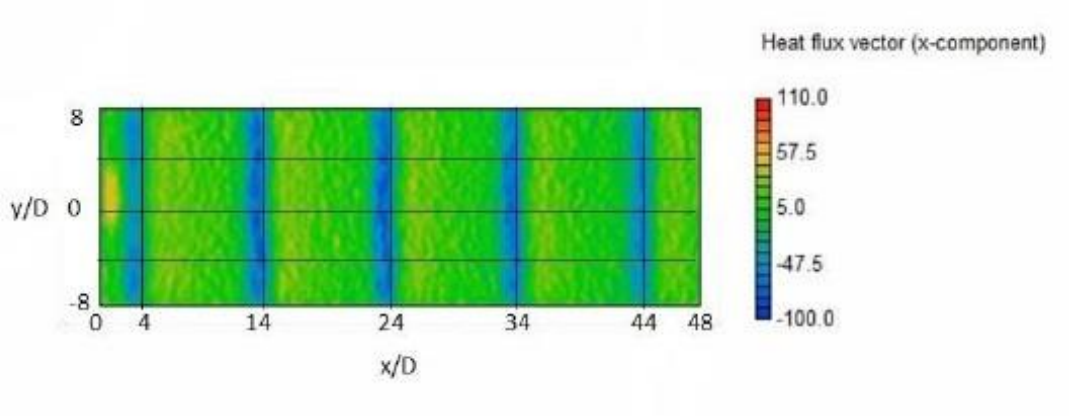

Average Heat Flux Vector (X-Component through the target plate = 0.583256W/m^2)

Figure 3.3: Heat flux vector in x-direction on impingement surface

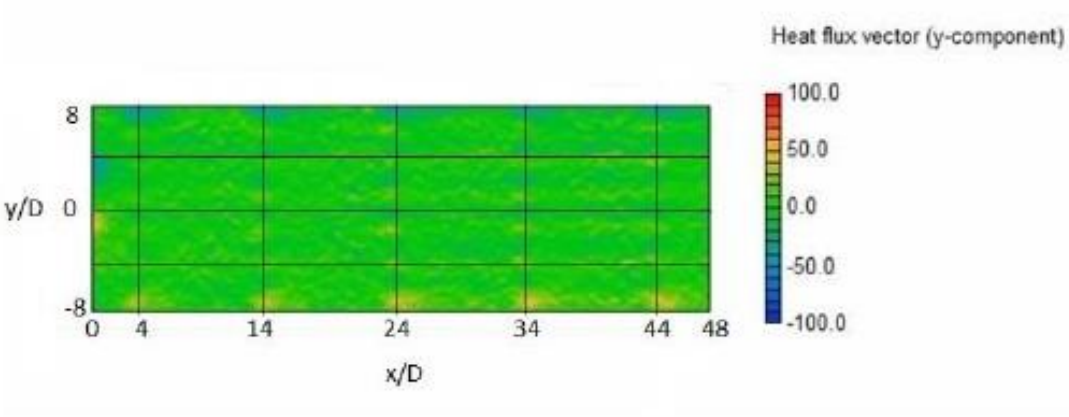

Average Heat Flux Vector (Y-Component through the target plate = 0.308724W/m^2)

Figure 3.4: Heat flux vector in y-direction on impingement surface

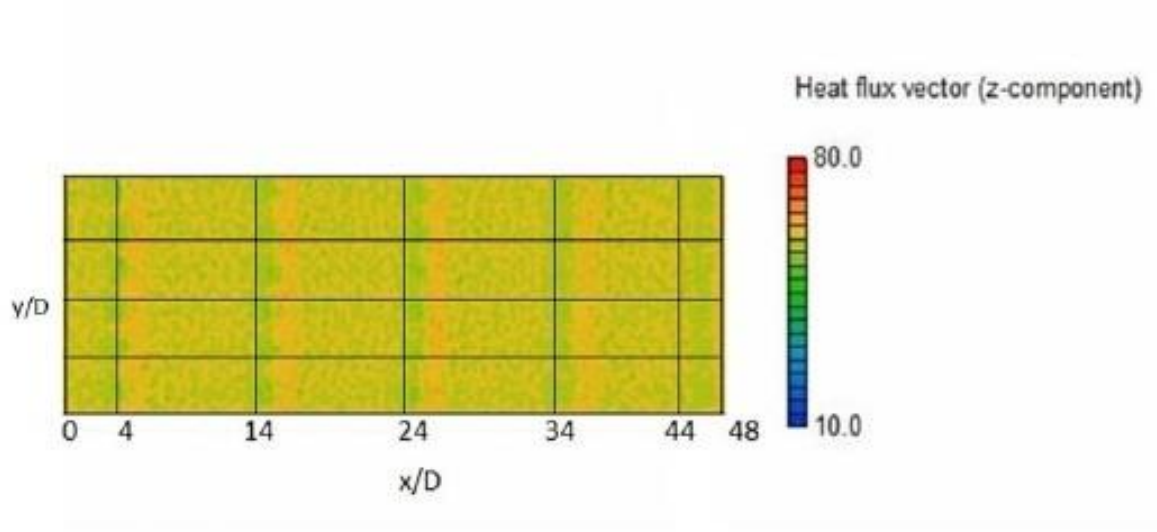

Average Heat Flux Vector (Z-Component through the target plate = 59.1213W/m^2)

Figure 3.5: Heat flux vector in z-direction on impingement surface

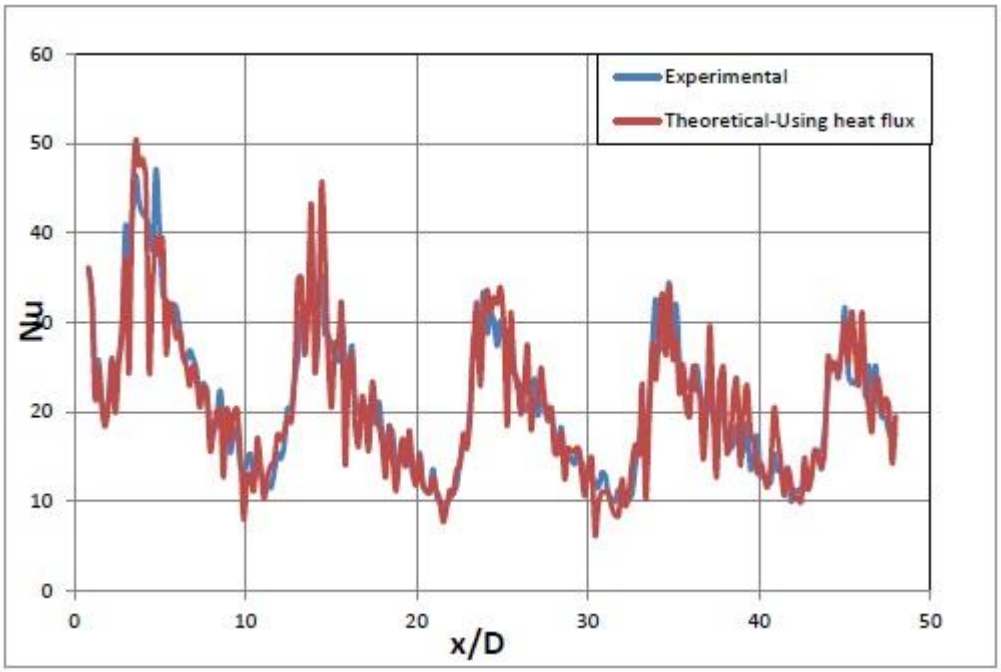

Figure 3.6: Comparison of experimental and numerical Nusselt numbers at y/D=0

B. Numerical Analysis - ProtoCAM Configuration

The following section presents the numerical analysis with the ProtoCAM configuration. To verify the physical test results, SC/Tetra outputs the impingement surface temperature map and the heat flux, which allows for the calculation of surface Nusselt numbers. The temperature that SC/Tetra gives for the impingement surface is put into Equation 17, giving the surface Nusselt number. If the Nusselt numbers from these numerical predictions agree with Nusselt numbers from experimental measurements, the TF factor is sufficient. SC/Tetra also outputs the heat flux vector out of the target plate on the impingement side, which is used determine the CF factors. In addition, SC/Tetra outputs the heat flux in the streamwise and spanwise directions. If these heat flux values are close to zero, the assumption of one-dimensional conduction is verified. The ProtoCAM test configuration places the ProtoCAM layer on the impingement jet side and the heater layer on the infrared camera viewing side. A diagram of the test plate arrangement used for the numerical predictions is shown in Figure 3.7.

Assumptions for this analysis include a constant thermal conductivity through all materials, uniform heat distribution throughout the heater, constant ambient air temperature of 22.6°C, and a static pressure of 1 atm. Table 3.2 gives the material properties used for these predictions. The boundary conditions for the ProtoCAM simulations include adiabatic edges and a constant surface heat flux on the surface between the heater and the polystyrene layer. The temperature variation on the front of the back of the heater layer is from experimental measurements.

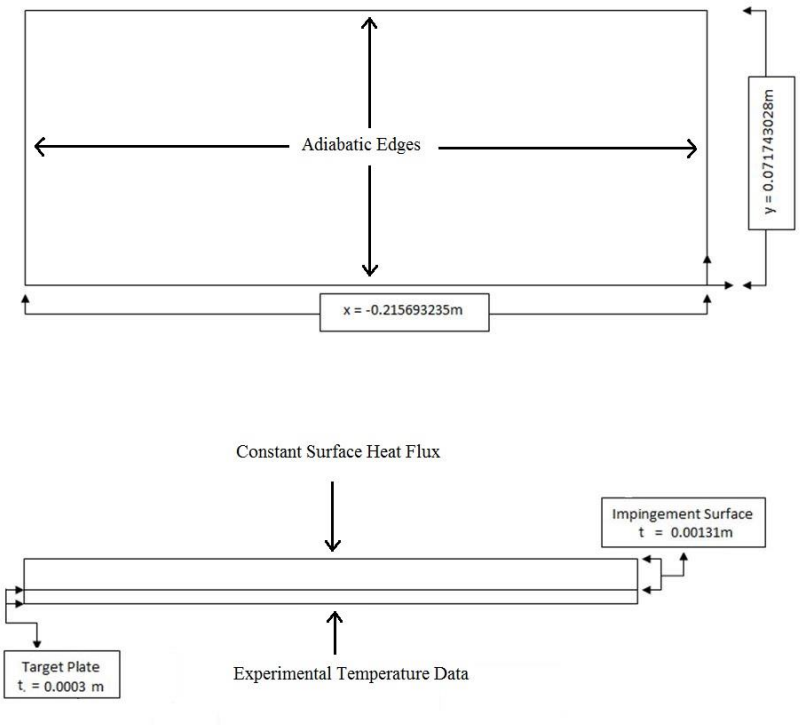

Figure 3.7: Test Plate Geometry

Table 3.2: Material Property Inputs for ProtoCAM Numerical Predictions

Material	Density (kg/m^3)	Specific Heat (J/kgK)	Thermal Conductivity (W/mK)
ProtoCAM	1190	1300	0.173
Polycarbonate (heater)	1200	1300	0.2

The temperature results are taken with values of x/D=10, y/D=2.7, D=4.5 mm, z=2.5D, Ma=0.058, and a Reynolds number of 5000. The boundary condition on the impingement surface on the front of the target plate is a constant heat flux. The simulation uses the conductive factor for the portion of heat flux that enters the ProtoCAM plate from the heater. The results from two simulations are shown in Figures 3.8 through 3.17. Figures 3.8 through 3.12 show the results from simulations of the ProtoCAM baseline plate. The heat flux variations, as shown in Figures 3.9 through 3.11, show that the heat flux in the x and y direction are extremely small in comparison to the heat flux in the z-direction. The values of heat flux in the x and y direction are both under 2 W/m^2, while the heat flux in the z-direction is 1003.77 W/m^2. This confirms the

assumption of one-dimensional analysis that is employed for experiments. Additionally, Figure 3.12 shows that local experimentally measured and numerically predicted Nusselt number values are in excellent agreement, which verifies the numerically predicted temperature and heat flux variations, as well as the associated values of CF and TF.

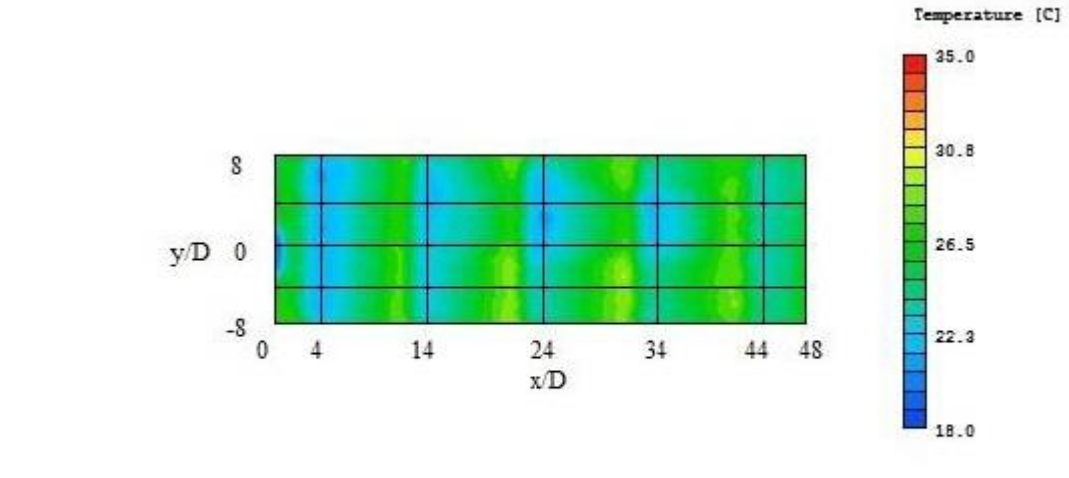

Figure 3.8: Temperature map on impingement surface of ProtoCAM Baseline

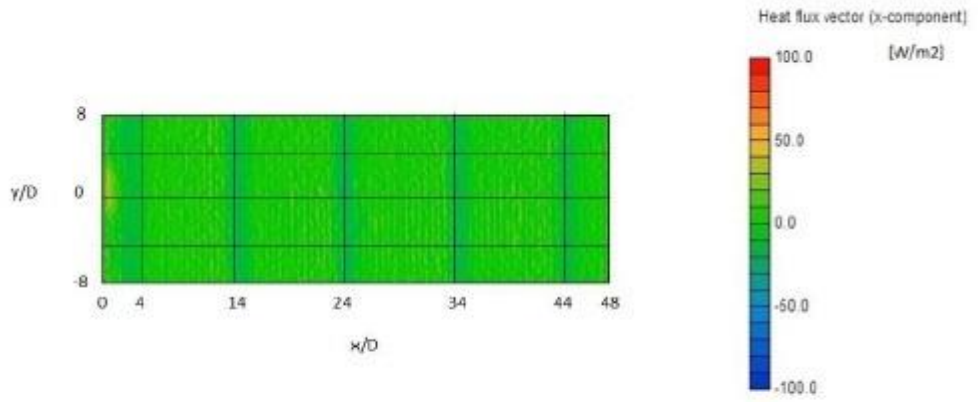

Average Heat Flux Vector (X-Component through the target plate = 0.711842 W/m^2)

Figure 3.9: Heat flux vector in x-direction on impingement surface of ProtoCAM baseline plate

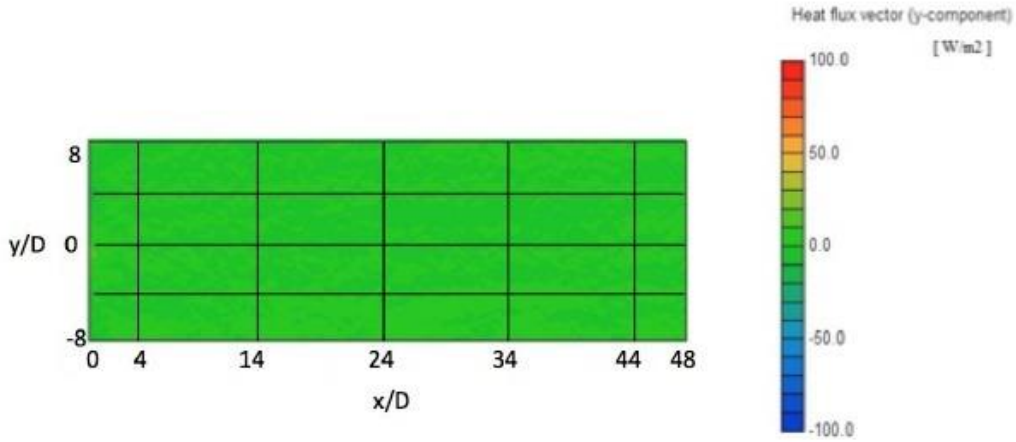

Average Heat Flux Vector (Y-Component through the target plate = 1.86469W/m^2)

Figure 3.10: Heat flux vector in y-direction on impingement surface of ProtoCAM baseline plate

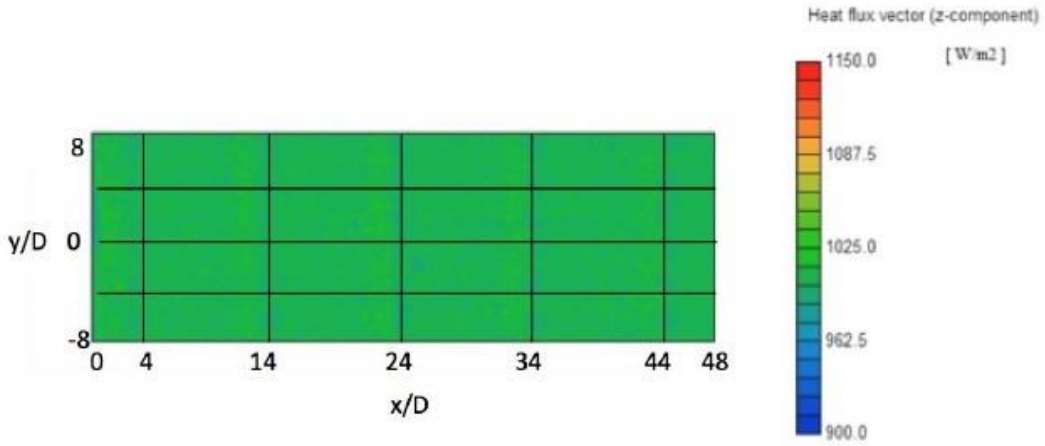

Average Heat Flux Vector (Z-Component through the target plate = 1003.77 W/m^2)

Figure 3.11: Heat flux vector in z-direction on impingement surface of ProtoCAM baseline plate

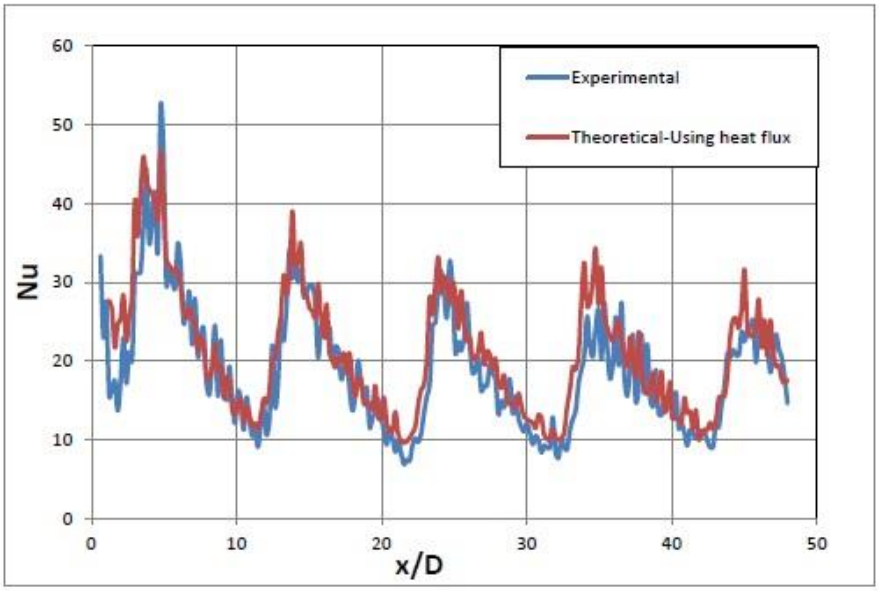

Figure 3.12: Comparison of experimental and numerical Nusselt numbers at y/D=0 on ProtoCAM baseline plate

Another example of numerical results from SC/Tetra is presented below. Figures 3.13 through 3.17 show the results from numerical analysis of the 1 mm small rectangle roughness plates. The results from this prediction are also very close to what is observed in experimental measurements. The heat flux variations as seen in Figures 3.14 through 3.16 show strong one-dimensional flow, with the heat flux in the x and y directions both under 0.5 W/m^2 and the heat flux in the z-direction at 1322 W/m^2. This confirms the assumption of one-dimensional conduction analysis employed for experiments. Additionally, the plot of experimental and numerical Nusselt numbers in Figure 3.17 shows strong agreement between local experimentally measured and numerically predicted Nusselt numbers. This also verifies numerically predicted temperature and heat flux variations and the associated values of CF and TF. Numerical data for all other experimental conditions show similar quantitative and qualitative trends, with strong agreement between the experimentally measured and numerically predicted Nusselt numbers.

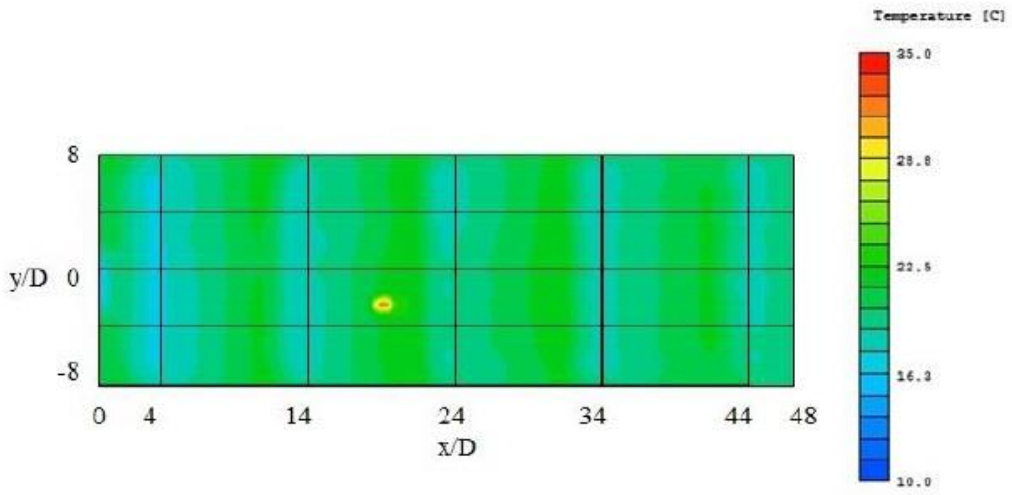

Average Temperature through Plane = 17.98 C

Surrounding Temperature = 11.43 C

Figure 3.13: Temperature map on impingement surface of 1 mm small rectangle roughness plate

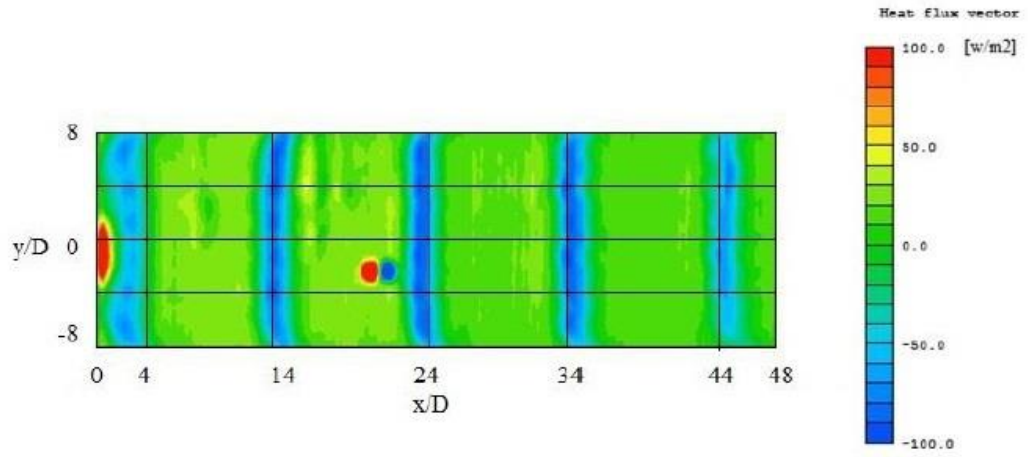

Average Heat Flux Vector (X-Component through the target plate = 0.422 W/m^2)

Figure 3.14: Heat flux vector in x-direction on impingement surface of 1 mm small rectangle roughness plate

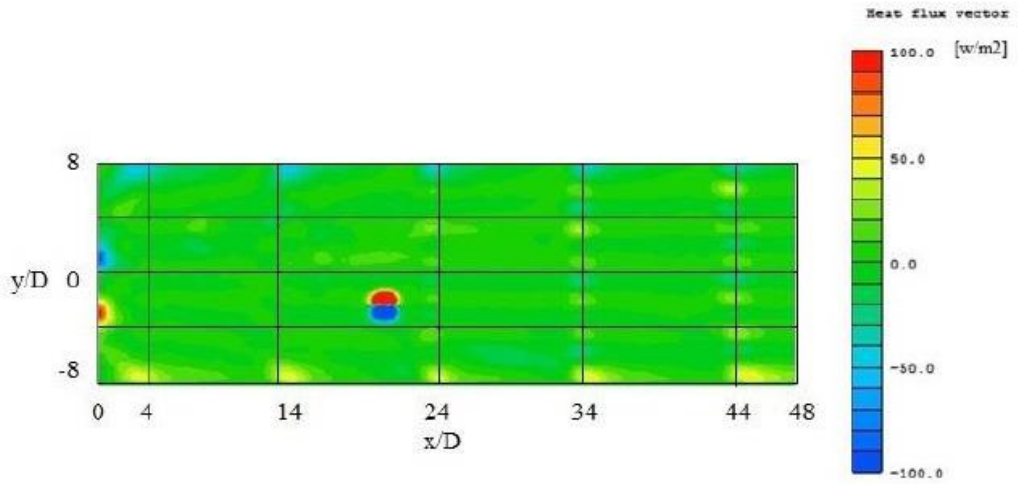

Average Heat Flux Vector (Y-Component through the target plate = 0.334W/m^2)

Figure 3.15: Heat flux vector in y-direction on impingement surface of 1 mm small rectangle roughness plate

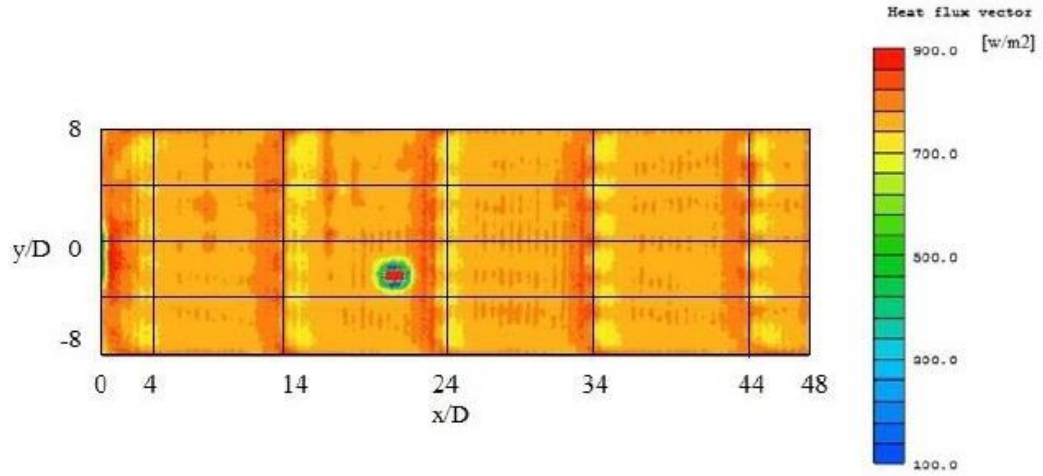

Average Heat Flux Vector (Z-Component through the target plate = 1322 W/m^2)

Figure 3.16: Heat flux vector in z-direction on impingement surface of 1 mm small rectangle roughness plate

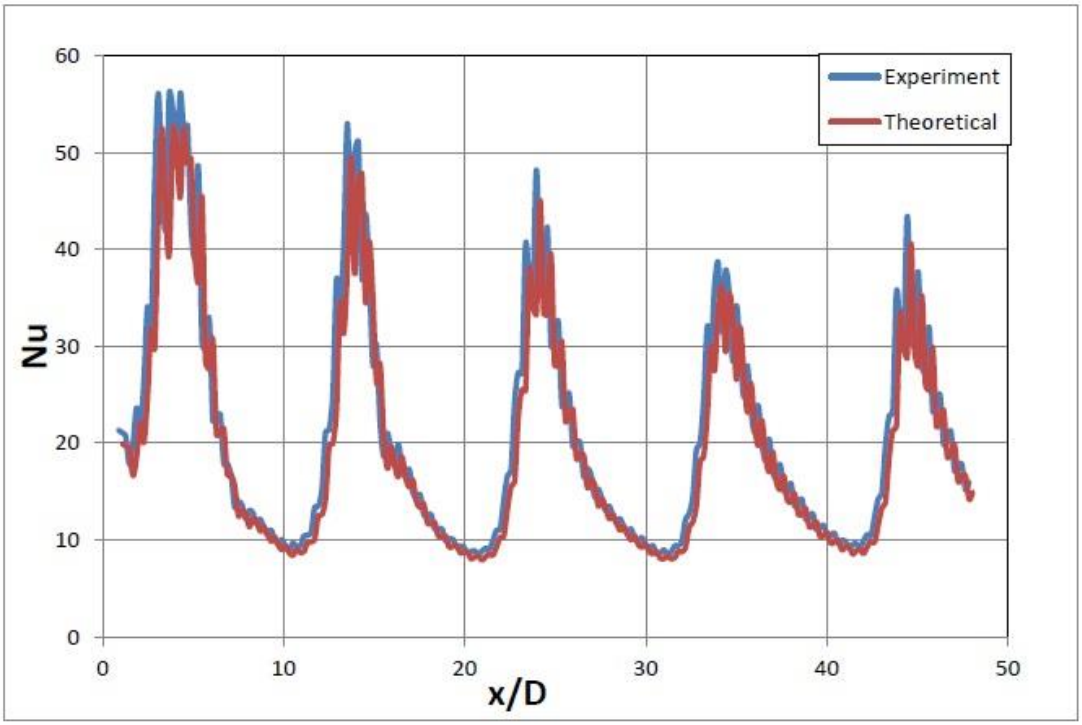

Figure 3.17: Comparison of experimental and numerical Nusselt numbers at y/D=0 on 1 mm small rectangle roughness plate

CHAPTER 4

EXPERIMENTAL RESULTS

Chapter 4 presents the Nusselt number results of all tests performed for the current investigation. The results from test plates 1 through 20 (as listed in Table 2.1) are included. Tests are generally performed at four Reynolds numbers: 900, 1500, 5000, and 11000. The flow which is present at Reynolds numbers of 900 and 1500 is believed to be laminar. The flow which is present at Reynolds numbers of 5000 and 11000 is believed to be turbulent. The data in figures 4.1 through 4.52 is line-averaged and spatially-averaged. These plots are generated after MATLAB outputs a grid of Nusselt numbers. For the line-averaged plots, an average value at each x/D value is calculated from all points between y/D=-5.4 and y/D=5.4 at that x/D value. The spatially-averaged data is calculated from the line-averaged data. To obtain the spatially-averaged data, averages are determined of the line-averaged data in four sections. The average is taken from x/D=2 to x/D=12, from x/D=12 to x/D=22, from x/D=22 to x/D=32, and from x/D=32 to x/D=42. Averages over these regions give four spatially-averaged data points.

A. Example of Local Nusselt Number Results

Figures 4.1 through 4.3 show examples of experimentally measured local Nusselt number data. These examples are associated with the ProtoCAM baseline case at a Reynolds number of 5000 and Mach number of 0.047. Figure 4.1 displays surface Nusselt number variations. The dark areas correspond to higher local Nusselt numbers. These maximum values are located where jets impinge onto the target plate. Local maximum Nusselt numbers for the impingement jets become lower as x/D increases due to the cross-flow air moving toward the exit of the test section. Figure 4.2 displays local Nusselt number data along the

line at y/D=0. The maximum values are located at x/D values where the impinging air jets impact the target plate. The minimum values are then present between each row of impingement holes. Figure 4.3 shows Local Nusselt numbers along the line at y/D=4. There is a row of impingement jets at x/D=4 which are shown by six local peaks from y/D=-8 to y/D=8. These peaks are less defined because of the close proximity of adjacent jets, and the increased mixing between adjacent jets.

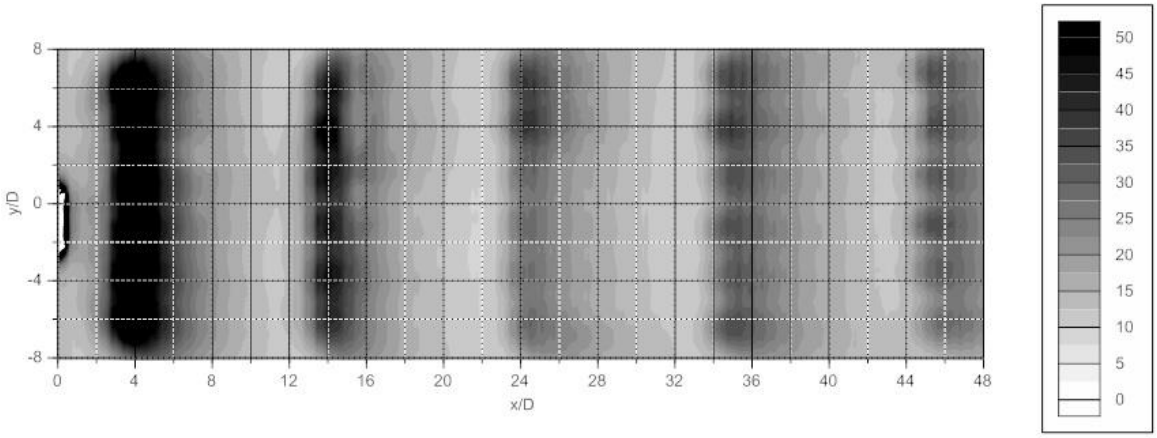

Figure 4.1: Local surface Nusselt number variations for the ProtoCAM baseline plate at Re=5000.

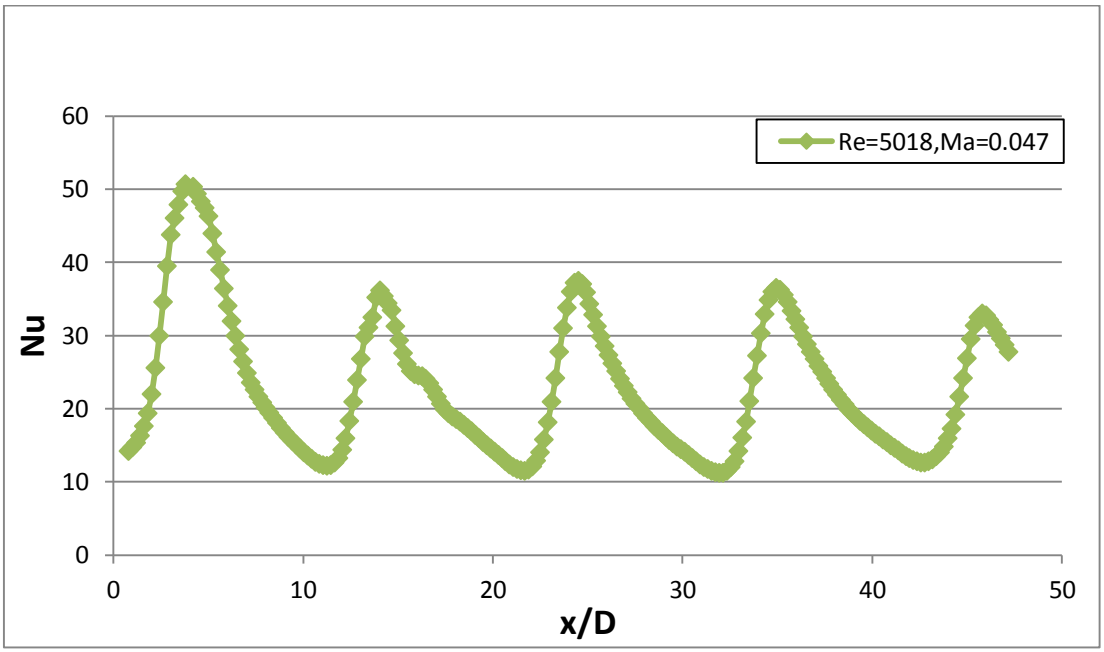

Figure 4.2: Local Nusselt number at y/D=0 for the ProtoCAM baseline plate at Re=5000.

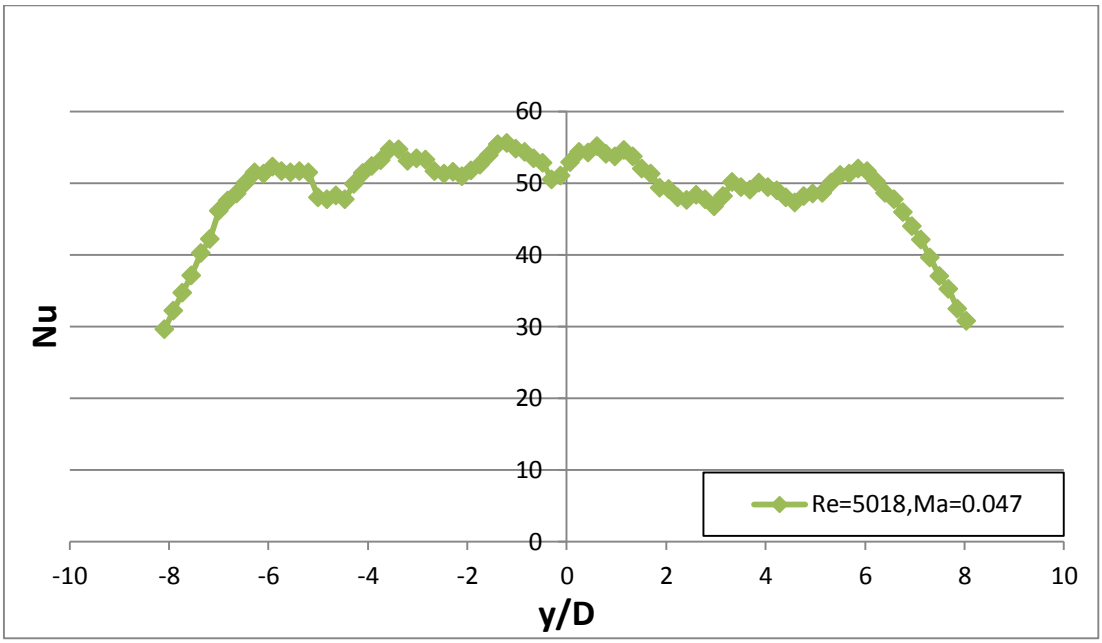

Figure 4.3: Local Nusselt number at x/D=4 for the ProtoCAM baseline plate at Re=5000.

B. Comparison of Rectangle Roughness Arrangements

Figures 4.4 through 4.11 display the results from the experiments with all ProtoCAM rectangle arrangements and the ProtoCAM baseline plate (plates 1-8 as listed in Table 1). Figures 4.4, 4.6, 4.8, and 4.10 show line-averaged Nusselt number results, while Figures 4.5, 4.7, 4.9, and 4.11 show spatially-averaged Nusselt number results. The line-averaged results are averaged over y/D values from -5.4 to 5.4. For the laminar Reynolds number cases, shown in Figures 4.4 through 4.7, the plates with small roughness alone show higher Nusselt numbers than the plates with a combination of small and large roughness. This is because the large roughness is having an insulating effect because of the conduction within, and increases thermal resistance, and reduces heat transfer coefficients along the wetted target surface. Here, thermal transport within the flow is of the same order of magnitude as conduction transport within roughness elements. The turbulent Reynolds number cases, shown in Figures 4.8 through 4.11, give different results. The plates with a combination of large and small roughness give higher Nusselt numbers than the plates with small roughness alone, when compared at the same Re_j and x/D values. This is because the large pins increase the mixing of the flow, increasing turbulent transport and surface convective heat transfer. Here, turbulent transport is significantly greater than conduction transport within roughness elements.

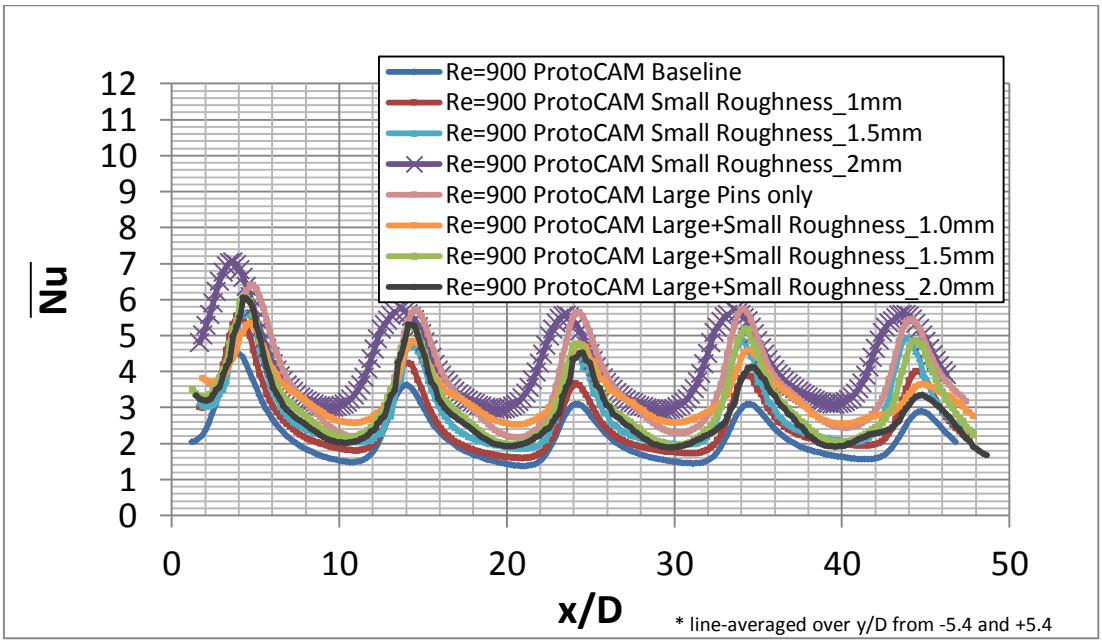

Figure 4.4: Line-averaged Nusselt numbers as dependent upon *x/D*, for all rectangle roughness arrangements for Re=900.

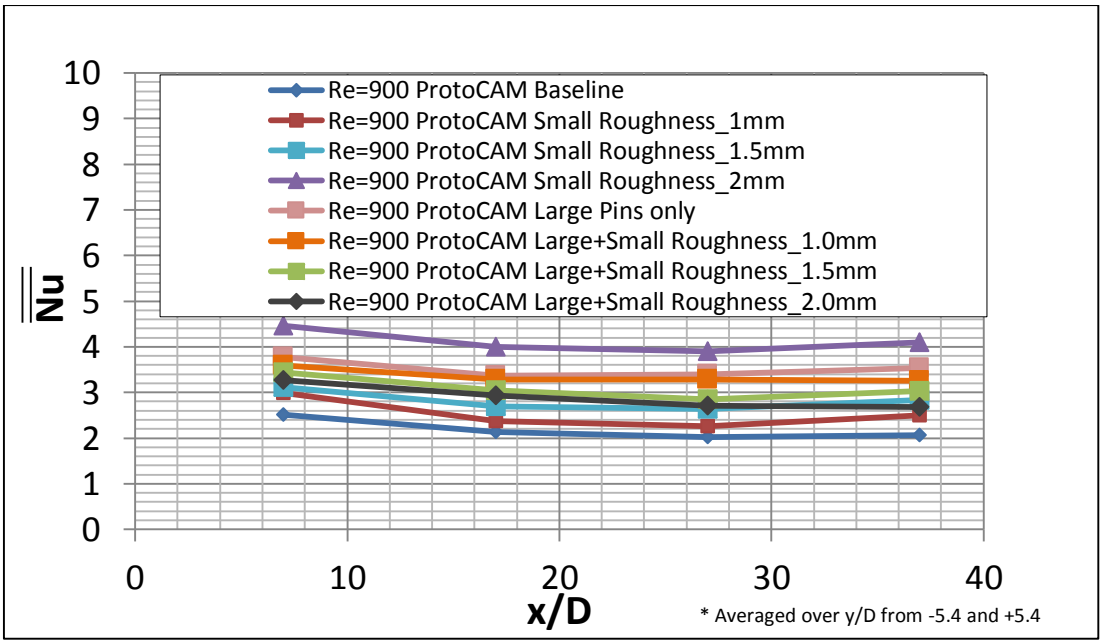

Figure 4.5: Spatially-averaged Nusselt numbers as dependent upon *x/D*, for all rectangle roughness arrangements for Re=900.

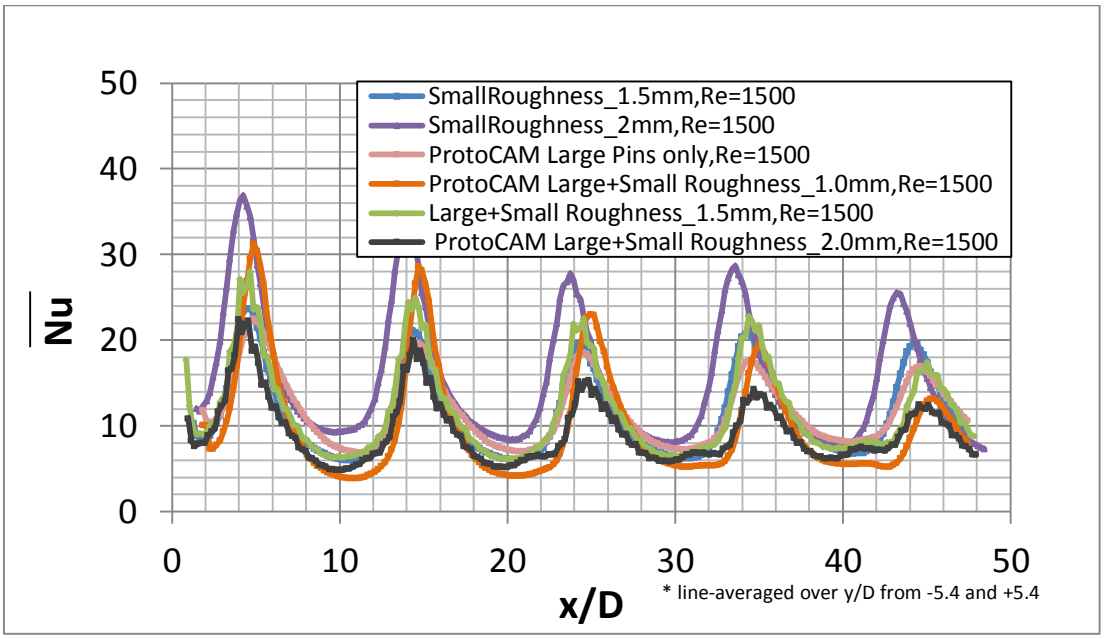

Figure 4.6: Line-averaged Nusselt numbers as dependent upon *x/D*, for all rectangle roughness arrangements for Re=1500.

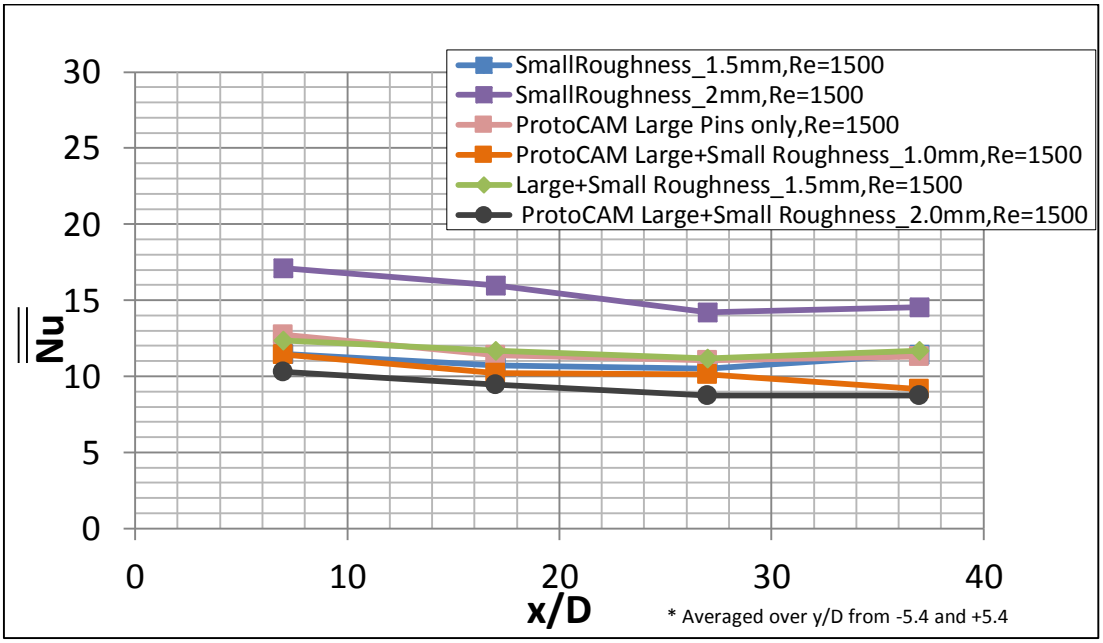

Figure 4.7: Spatially-averaged Nusselt numbers as dependent upon *x/D*, for all rectangle roughness arrangements for Re=1500.

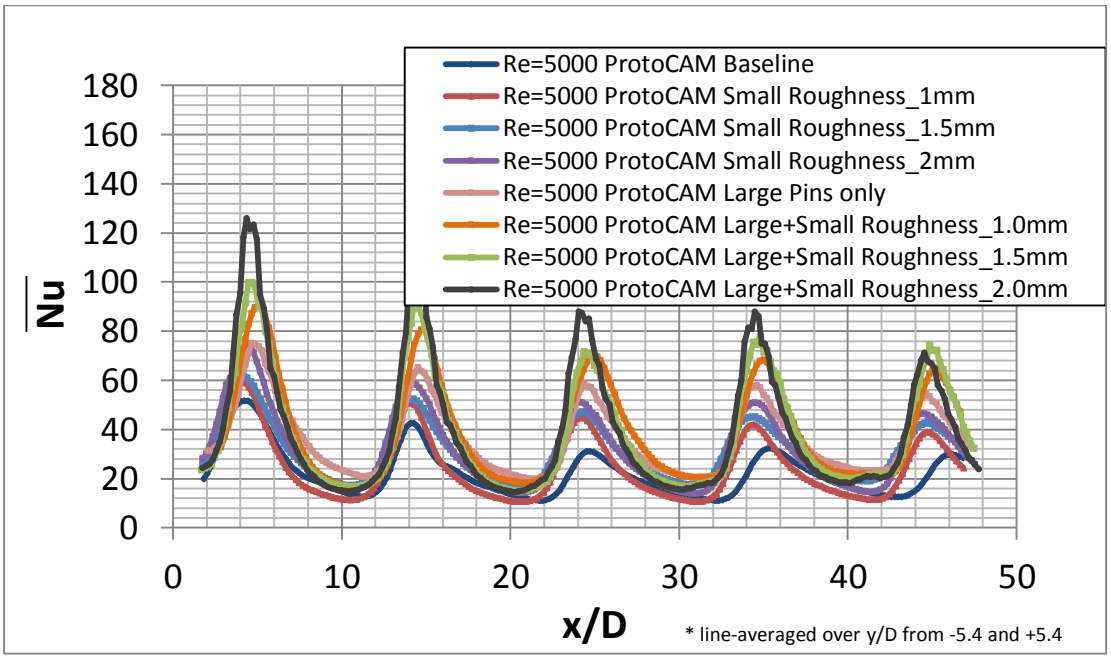

Figure 4.8: Line-averaged Nusselt numbers as dependent upon *x/D*, for all rectangle roughness arrangements for Re=5000.

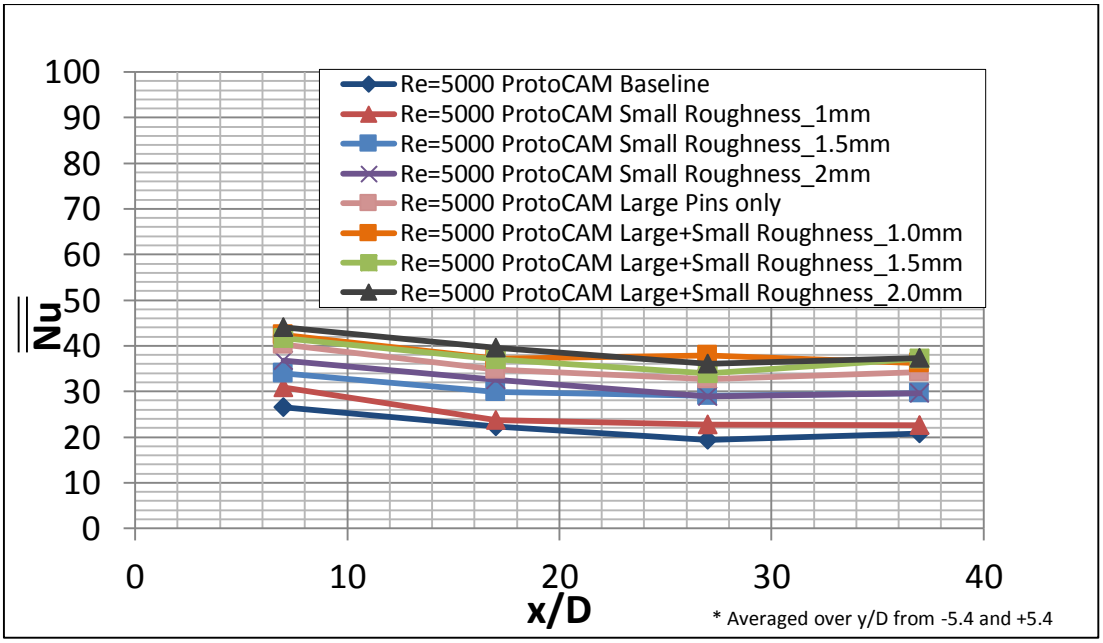

Figure 4.9: Spatially-averaged Nusselt numbers as dependent upon *x/D*, for all rectangle roughness arrangements for Re=5000.

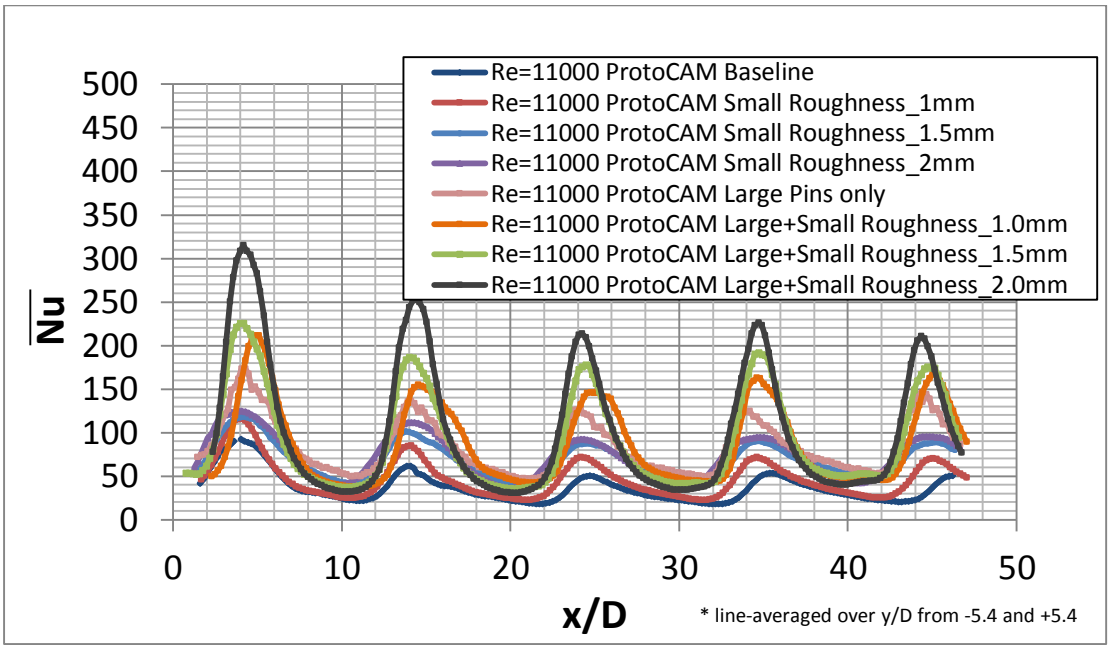

Figure 4.10: Line-averaged Nusselt numbers as dependent upon *x/D*, for all rectangle roughness arrangements for Re=11000.

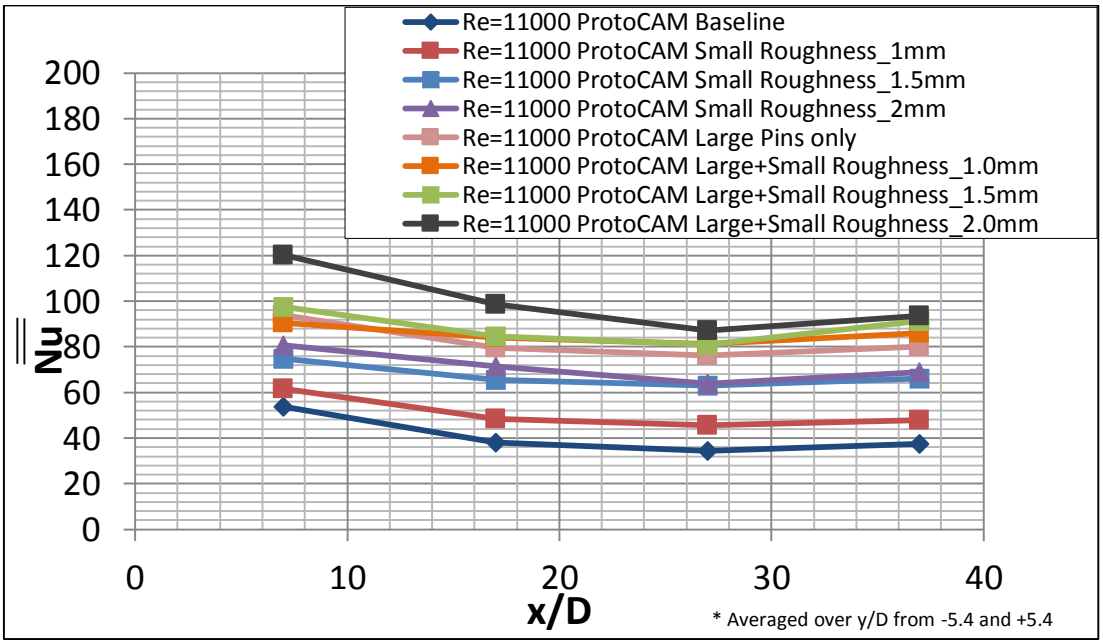

Figure 4.11: Spatially-averaged Nusselt numbers as dependent upon *x/D*, for all rectangle roughness arrangements for Re=11000.

C. Comparison of Triangle Roughness Arrangements

Figures 4.12 through 4.19 display the results from the experiments with all ProtoCAM triangle arrangements (plates 9-14 as listed in Table 2.1). Figures 4.12, 4.14, 4.16, and 4.18 show line-averaged

Nusselt number results, while Figures 4.13, 4.15, 4.17, and 4.19 show spatially-averaged Nusselt number results. The line-averaged results are averaged over y/D values from -5.4 to 5.4. For the laminar Reynolds number cases, shown in Figures 4.12 through 4.15, the plates with small roughness alone show higher Nusselt numbers than the plates with a combination of small and large roughness. This is because the large roughness is having an insulating effect because of the conduction within, and increases thermal resistance, and reduces heat transfer coefficients along he wetted target surface. Here, thermal transport within the flow is of the same order of magnitude as conduction transport within roughness elements. The turbulent Reynolds number cases, shown in Figures 4.16 through 4.19, give mixed results. A Reynolds number of 5000 shows the highest line-averaged Nusselt numbers with the large and small roughness 2.0 mm plate. Despite this, the small roughness of 1.5 mm alone gives higher spatially-averaged results. The large pins are having an insulating effect, similar to the low Reynolds numbers, which lowers the Nusselt number. The tests at a Reynolds number of 11000 also give mixed results. Again, the plate with large pins and 2 mm small roughness gives the highest line-averaged Nusselt numbers. The spatially-averaged results are unclear. The combination plates with 1 mm and 2 mm small roughness give about the same results as the small roughness plates. The large amount of turbulence and mixing at this high Reynolds number reduces the effectiveness of the large pins. Here, turbulent transport is significantly greater than conduction transport within roughness elements.

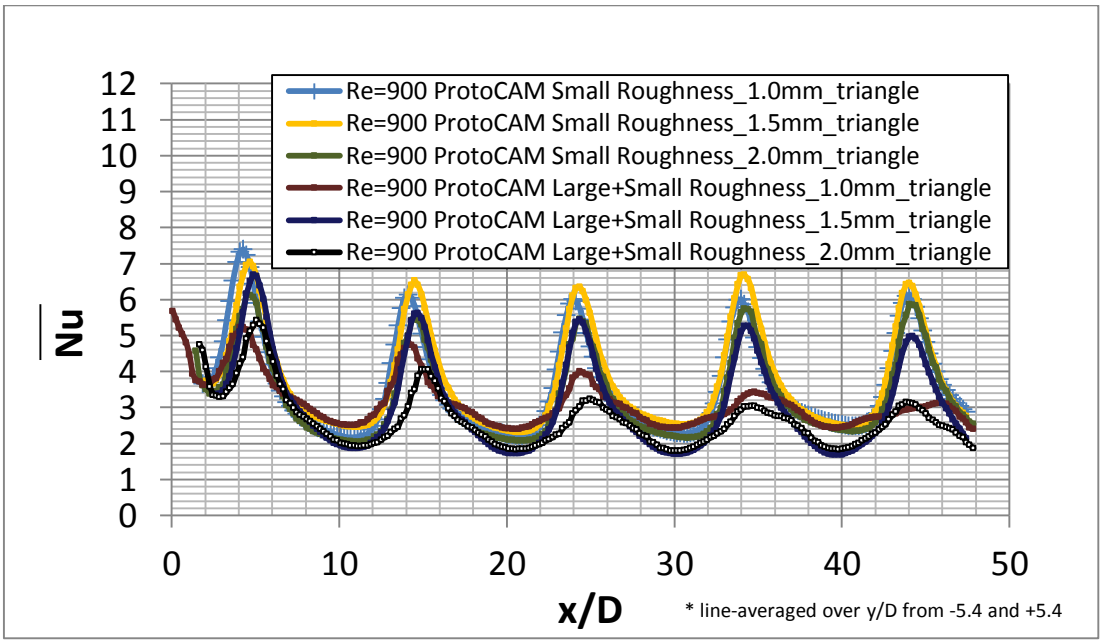

Figure 4.12: Line-averaged Nusselt numbers as dependent upon *x/D*, for all triangle roughness arrangements for Re=900.

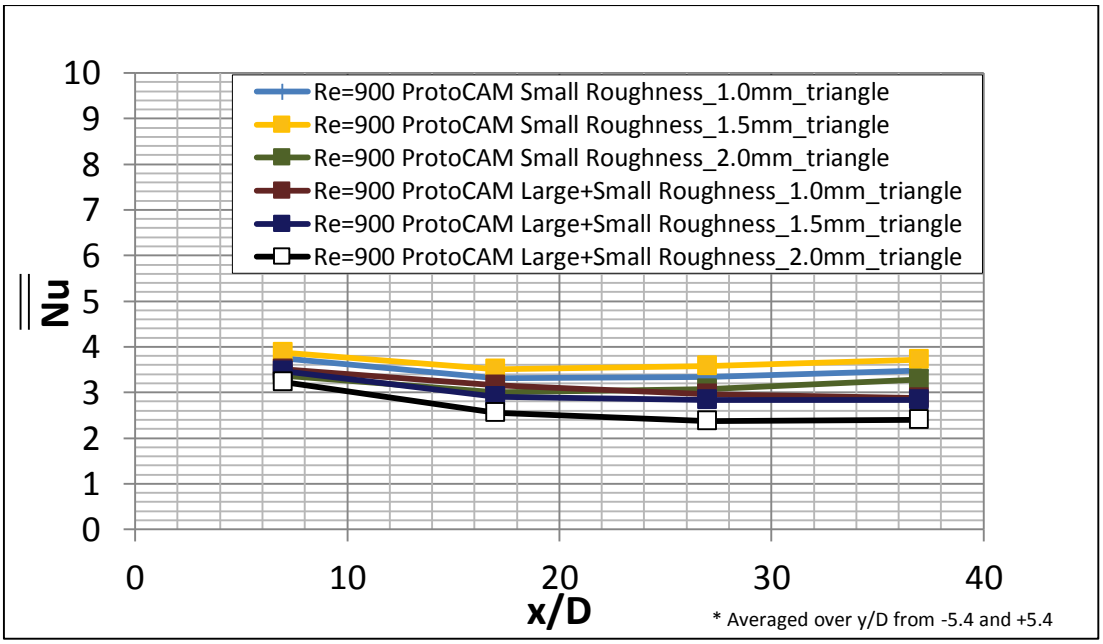

Figure 4.13: Spatially-averaged Nusselt numbers as dependent upon *x/D*, for all triangle roughness arrangements for Re=900.

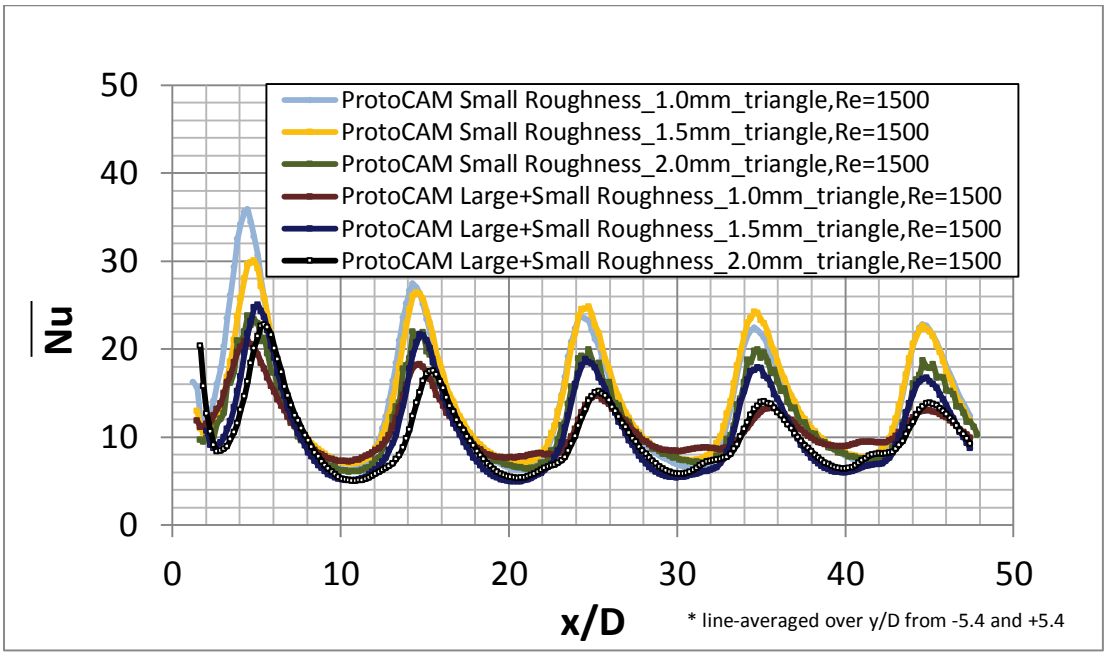

Figure 4.14: Line-averaged Nusselt numbers as dependent upon *x/D*, for all triangle roughness arrangements for Re=1500.

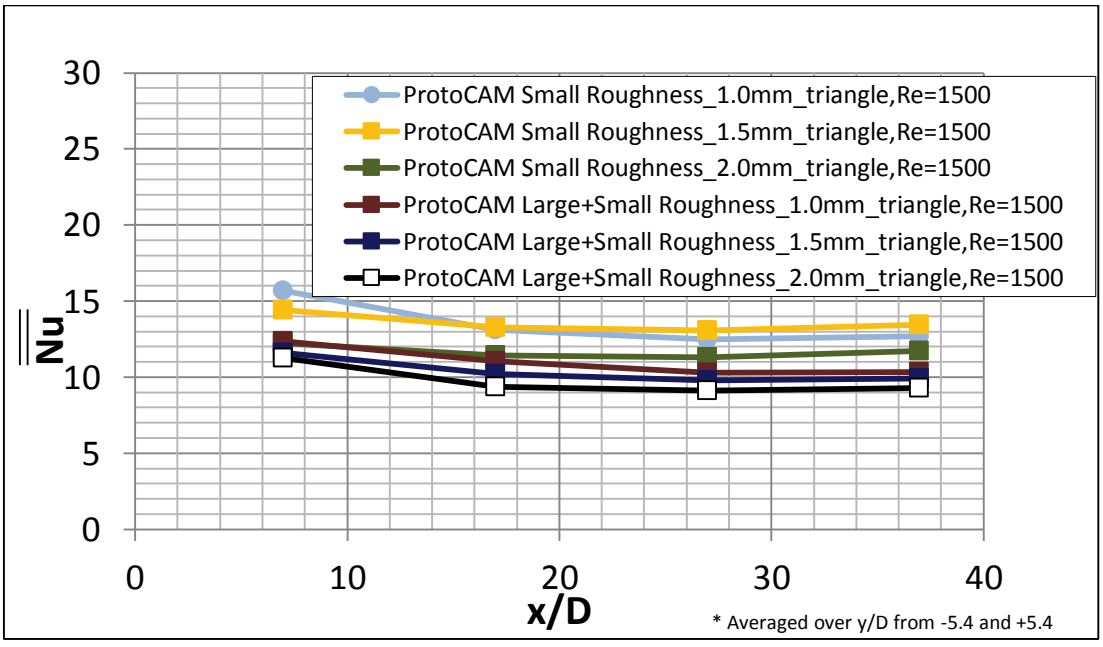

Figure 4.15: Spatially-averaged Nusselt numbers as dependent upon *x/D*, for all triangle roughness arrangements for Re=1500.

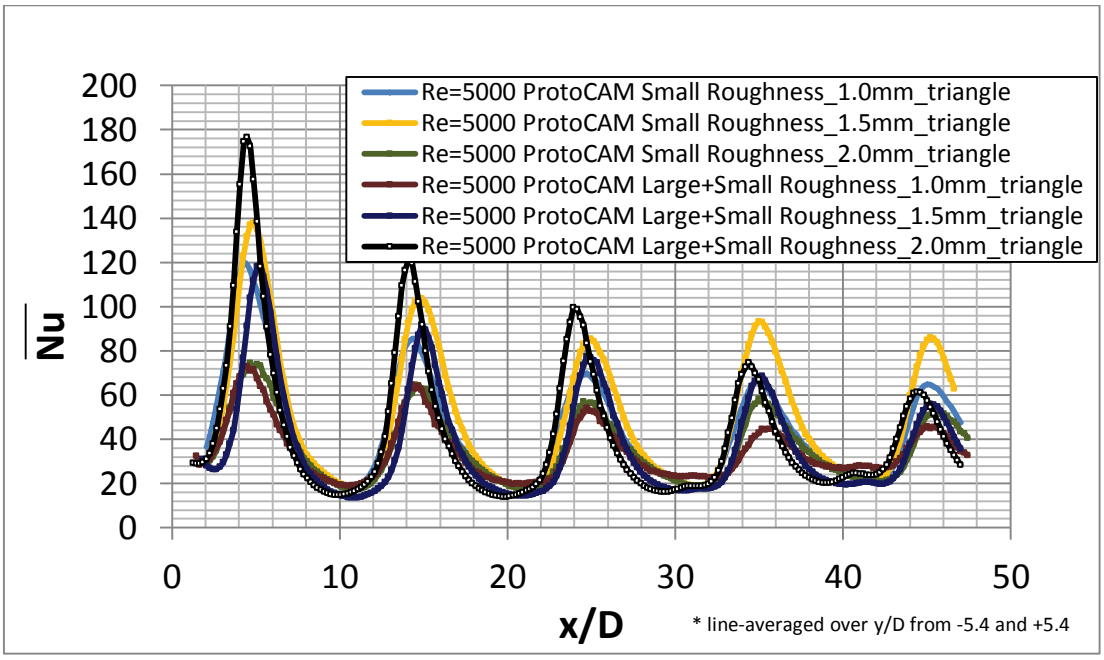

Figure 4.16: Line-averaged Nusselt numbers as dependent upon *x/D*, for all triangle roughness arrangements for Re=5000.

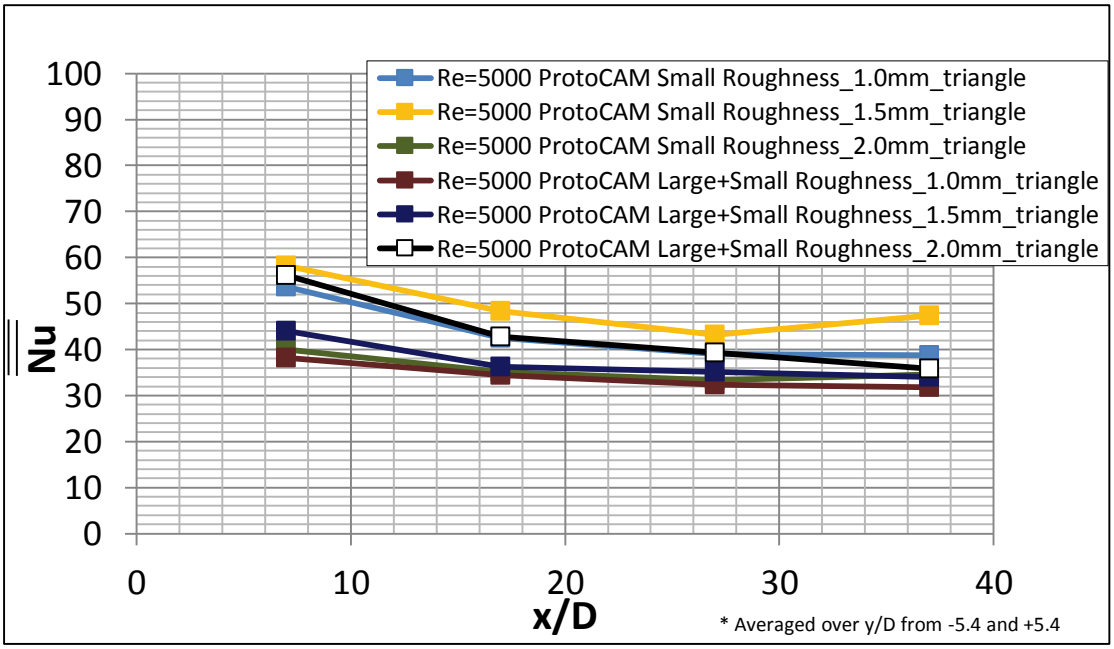

Figure 4.17: Spatially-averaged Nusselt numbers as dependent upon *x/D*, for all triangle roughness arrangements for Re=5000.

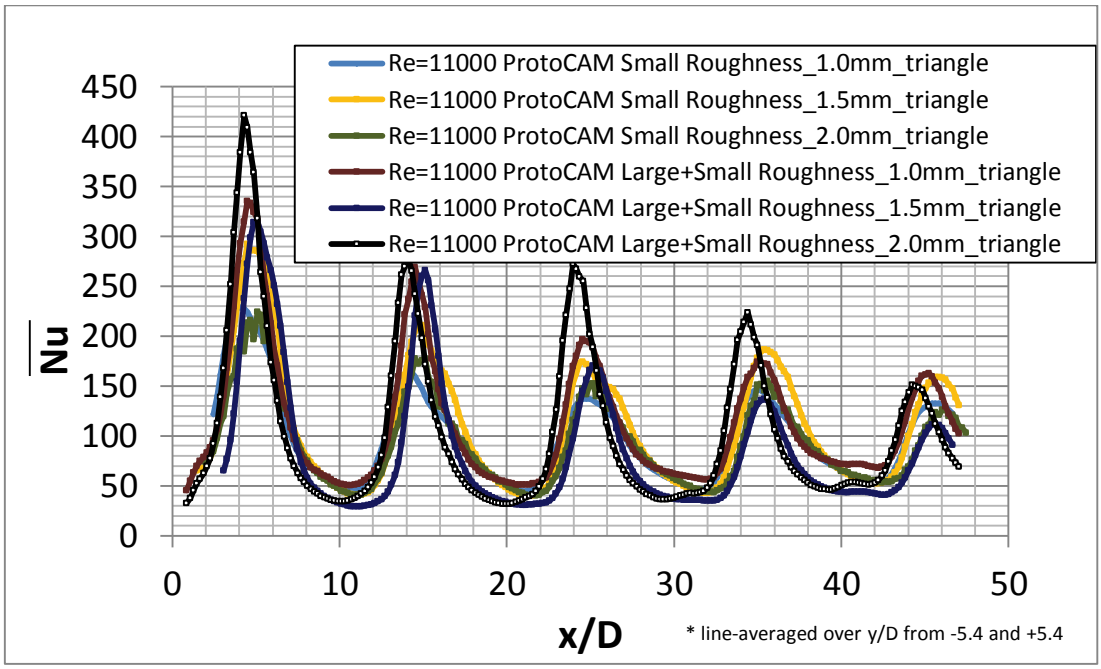

Figure 4.18: Line-averaged Nusselt numbers as dependent upon *x/D*, for all triangle roughness arrangements for Re=11000.

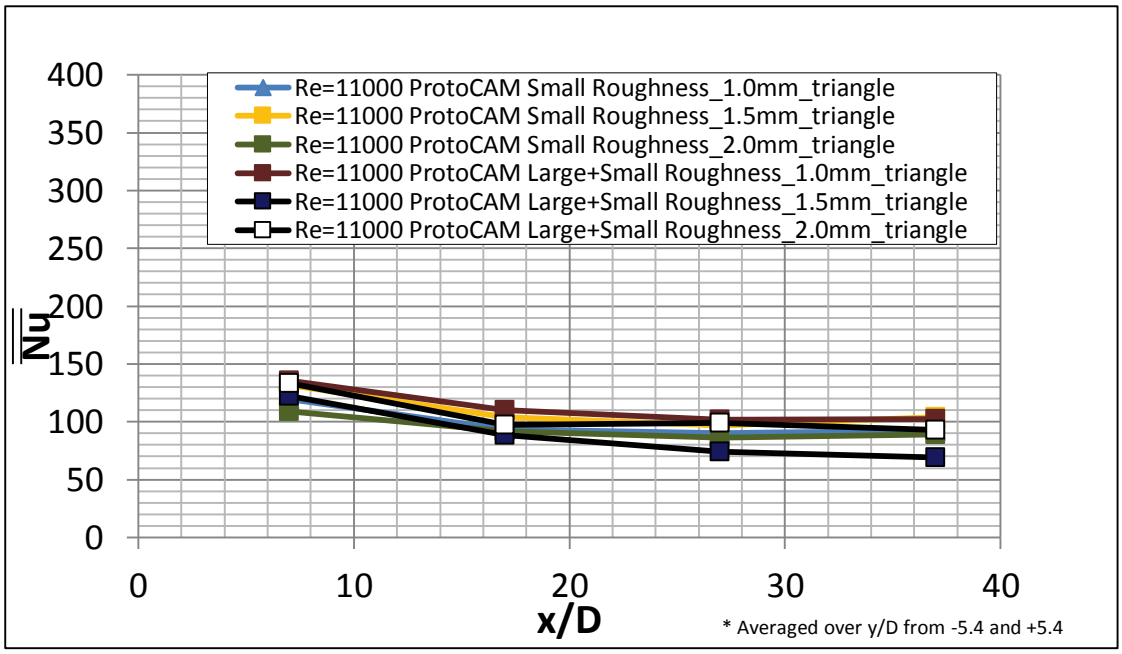

Figure 4.19: Spatially-averaged Nusselt numbers as dependent upon *x/D*, for all triangle roughness arrangements for Re=11000.

D. Comparison of Cylinder Roughness Arrangements

Figures 4.20 through 4.27 display the results from the experiments with all ProtoCAM cylinder arrangements (plates 15-20 as listed in Table 2.1). A scaled result for the ProtoCAM baseline plate is also

shown. Figures 4.20, 4.22, 4.24, and 4.26 show line-averaged Nusselt number results, while Figures 4.21, 4.23, 4.25, and 4.27 show spatially-averaged Nusselt number results. The line-averaged results are averaged over y/D values from -5.0 to 5.0. For the laminar Reynolds number cases, shown in Figures 4.20 through 4.23, the plates with small roughness alone show higher Nusselt numbers than the plates with a combination of small and large roughness. This is because large roughness is having an insulating effect because of the conduction within, and increases thermal resistance, and reduces heat transfer coefficients along the wetted target surface. Here, thermal transport within the flow is of the same order of magnitude as conduction transport within roughness elements. The turbulent Reynolds number cases, shown in Figures4.24 through 4.27, give similar results. The plates with a small roughness of 1.0 mm and 1.5 mm show higher Nusselt numbers than all other cases. The cylinder roughness is allowing the air to pass through smoothly and slowing it down enough so that the high Reynolds number cases act similarly to the low Reynolds number cases. The large pins are insulating the plate because of the conduction within and the increased thermal resistance, which decreases mixing and convective cooling. Despite this, turbulent transport is significantly greater than conduction transport within roughness elements for the turbulent cases.

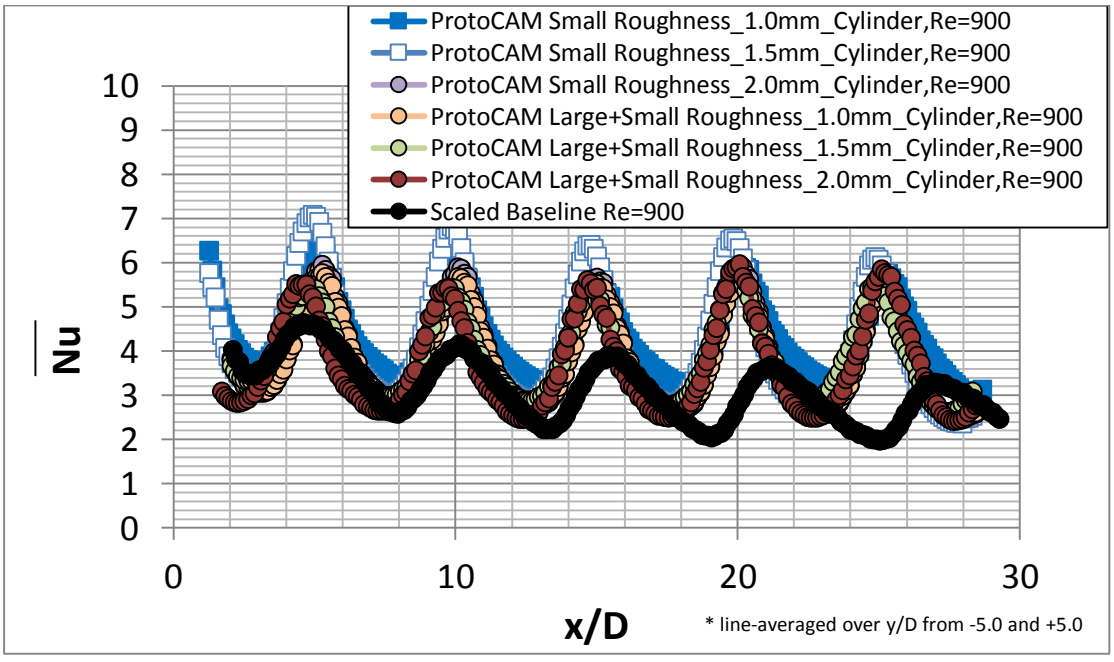

Figure 4.20: Line-averaged Nusselt numbers as dependent upon *x/D*, for all cylinder roughness arrangements for Re=900.

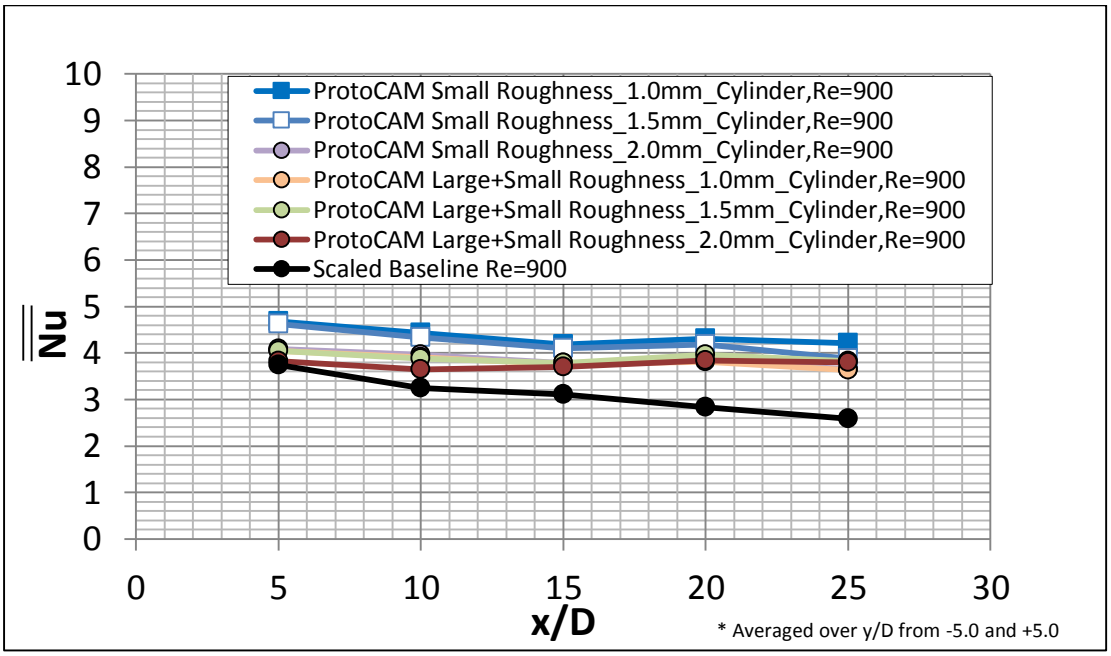

Figure 4.21: Spatially-averaged Nusselt numbers as dependent upon *x/D*, for all cylinder roughness arrangements for Re=900.

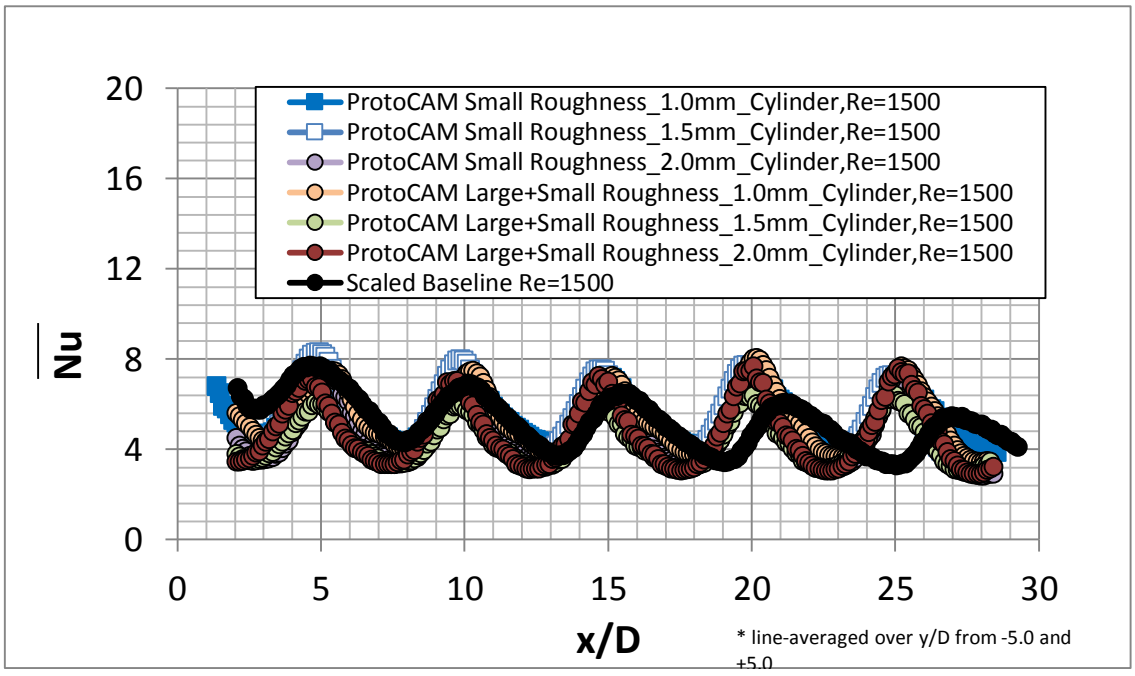

Figure 4.22: Line-averaged Nusselt numbers as dependent upon *x/D*, for all cylinder roughness arrangements for Re=1500.

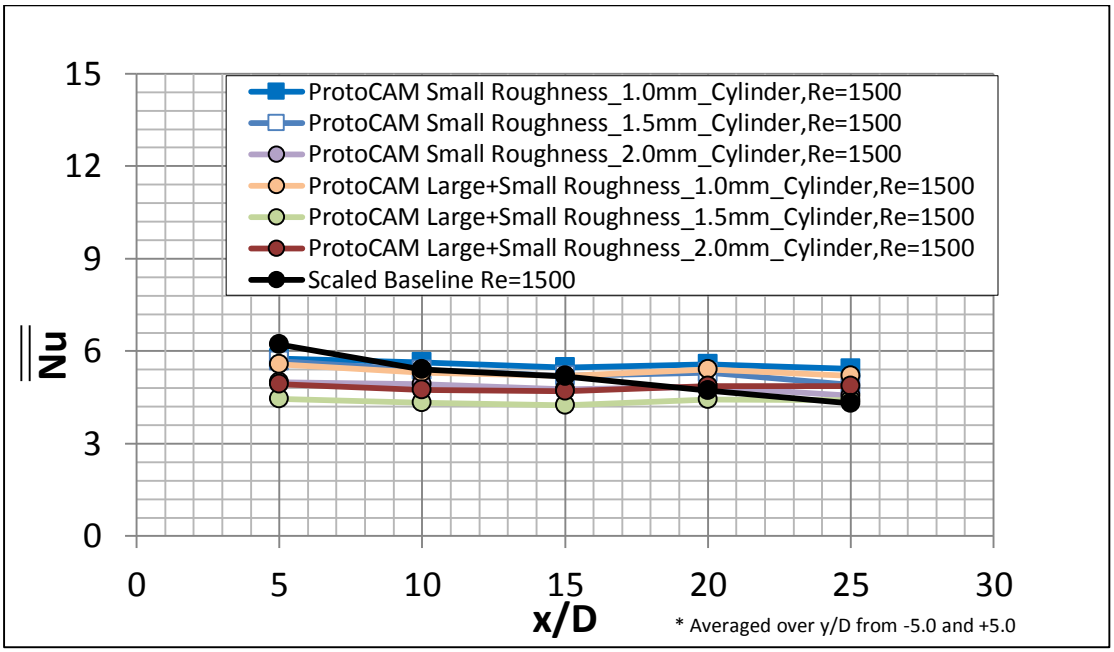

Figure 4.23: Spatially-averaged Nusselt numbers as dependent upon *x/D*, for all cylinder roughness arrangements for Re=1500.

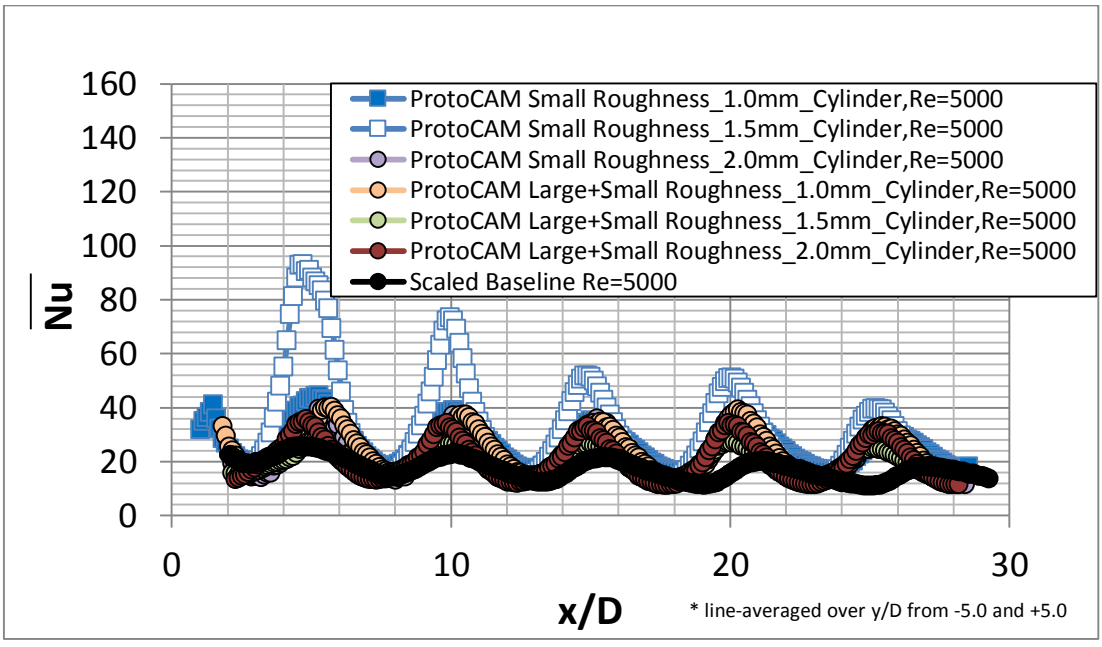

Figure 4.24: Line-averaged Nusselt numbers as dependent upon *x/D*, for all cylinder roughness arrangements for Re=5000.

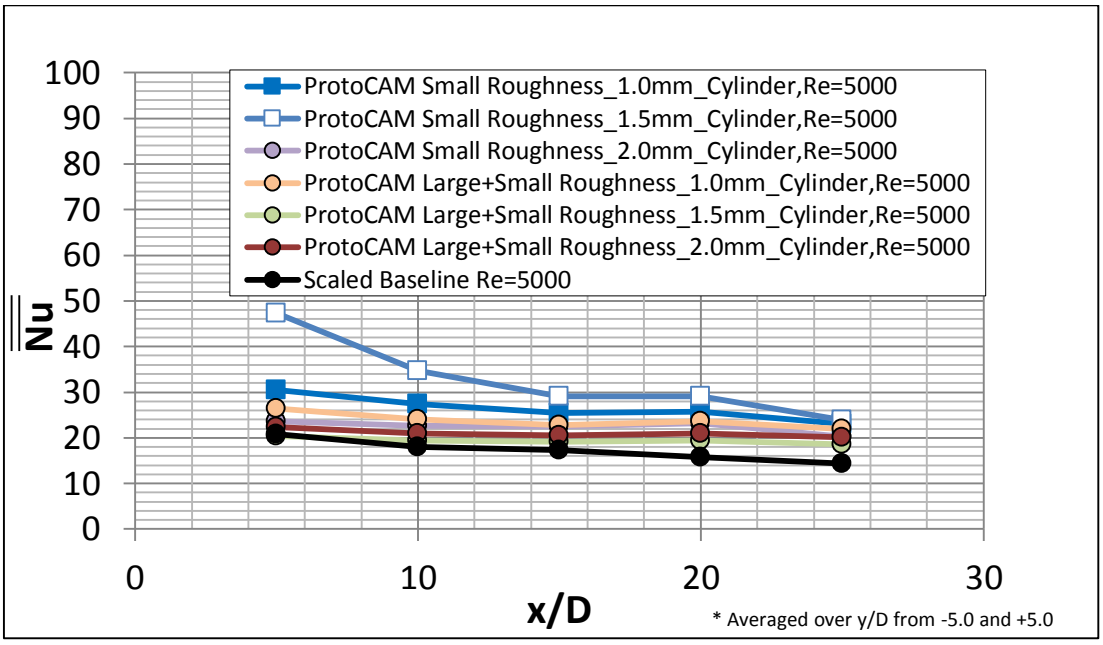

Figure 4.25: Spatially-averaged Nusselt numbers as dependent upon *x/D*, for all cylinder roughness arrangements for Re=5000.

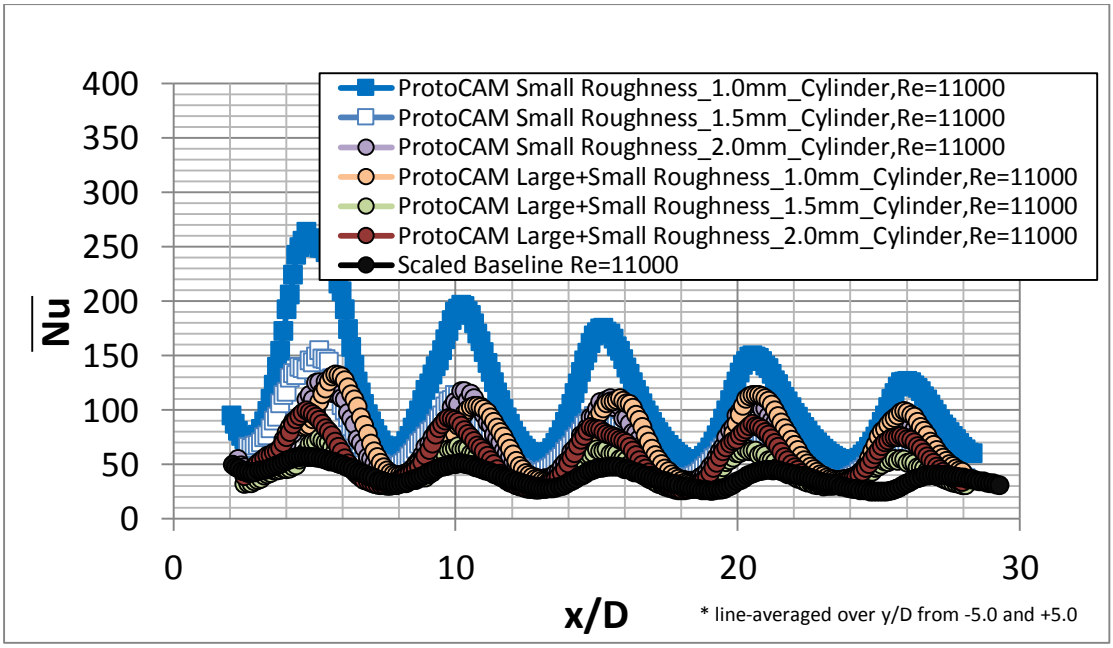

Figure 4.26: Line-averaged Nusselt numbers as dependent upon *x/D*, for all cylinder roughness arrangements for Re=11000.

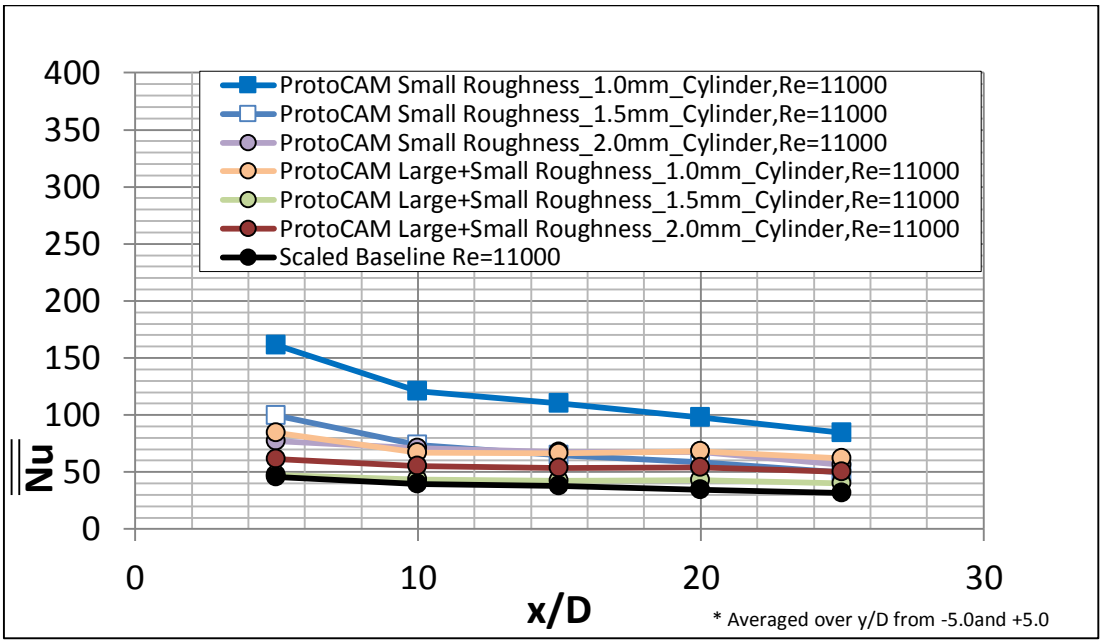

Figure 4.27: Spatially-averaged Nusselt numbers as dependent upon *x/D*, for all cylinder roughness arrangements for Re=11000.

E. Effects of Jet Reynolds Number

Figures 4.28 through 4.32 display the results from the ProtoCAM baseline test, the 2.0 mm small rectangle roughness test, and the 2.0 mm small triangle roughness test. These figures show the effect of jet Reynolds number on Nusselt number variations. For all cases considered, the Nusselt number increases with jet Reynolds number. As the jet Reynolds number increases, the mass flow rate and the airspeed also increase. As a result, advection is increased within thermal boundary layers. This gives increased convective cooling and large surface heat transfer coefficients. The most dramatic increases are evident at the peak value locations where the jets are impinging on the target plate.

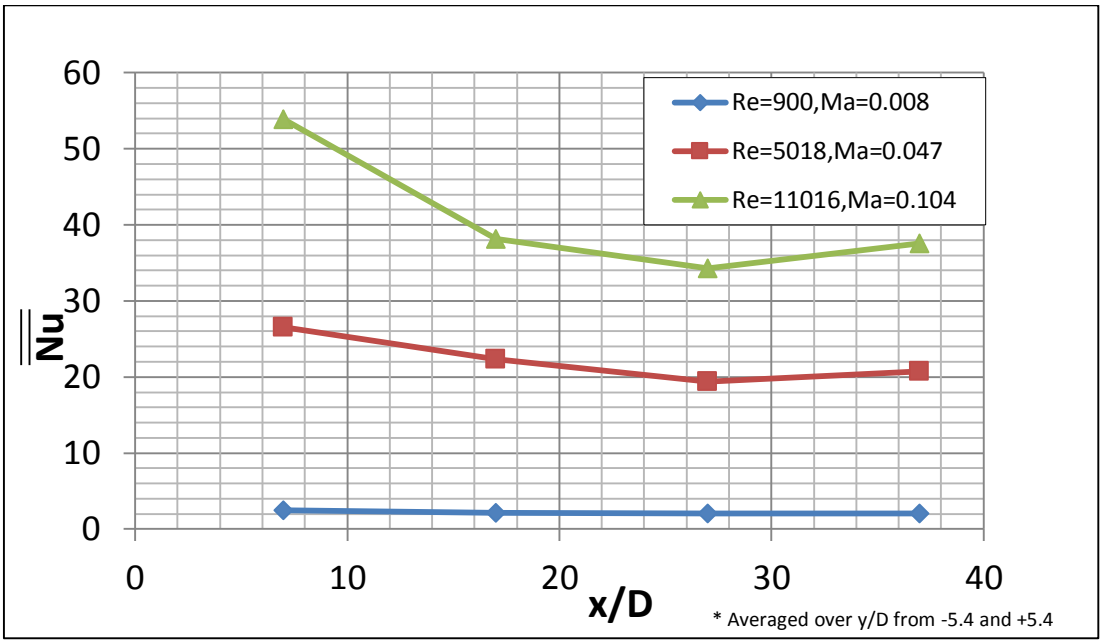

Figure 4.28: Spatially-averaged Nusselt numbers as dependent upon *x/D*, for three different Re_j for the baseline smooth target surface.

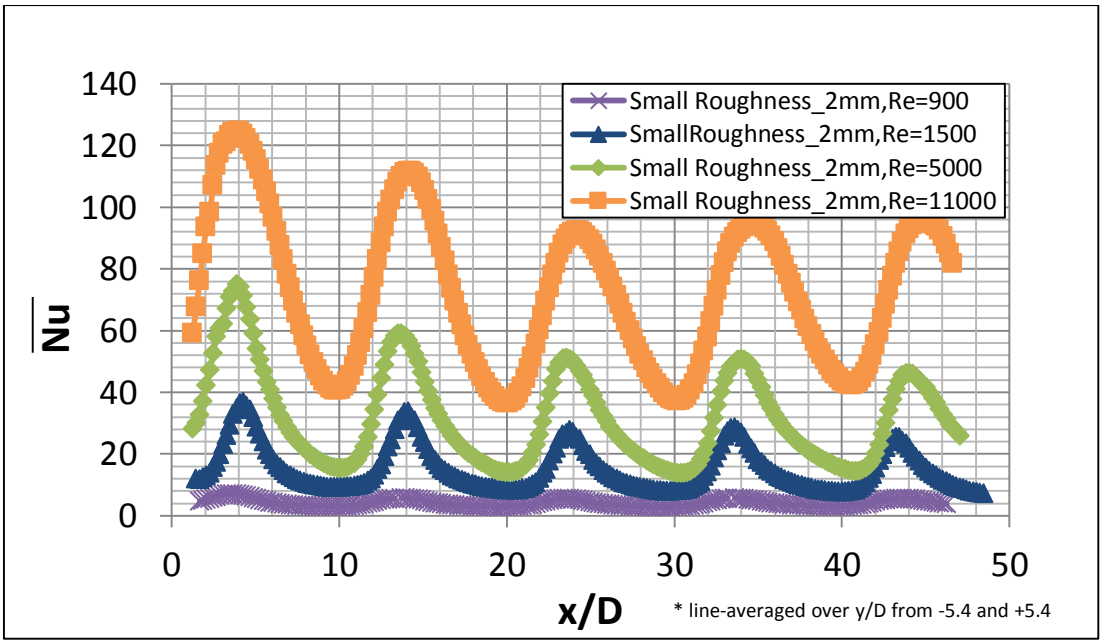

Figure 4.29: Line-averaged Nusselt numbers as dependent upon *x/D*, for four different Re_j for the 2.0 mm small rectangular roughness.

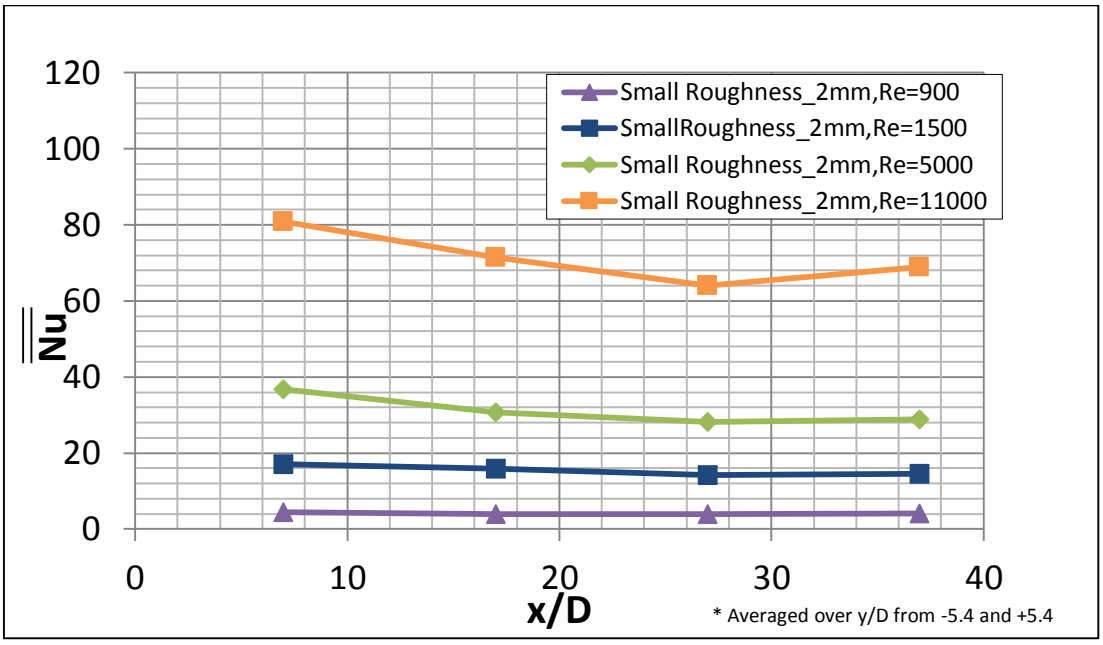

Figure 4.30: Spatially-averaged Nusselt numbers as dependent upon *x/D*, for four different Re_j for the 2.0 mm small rectangular roughness.

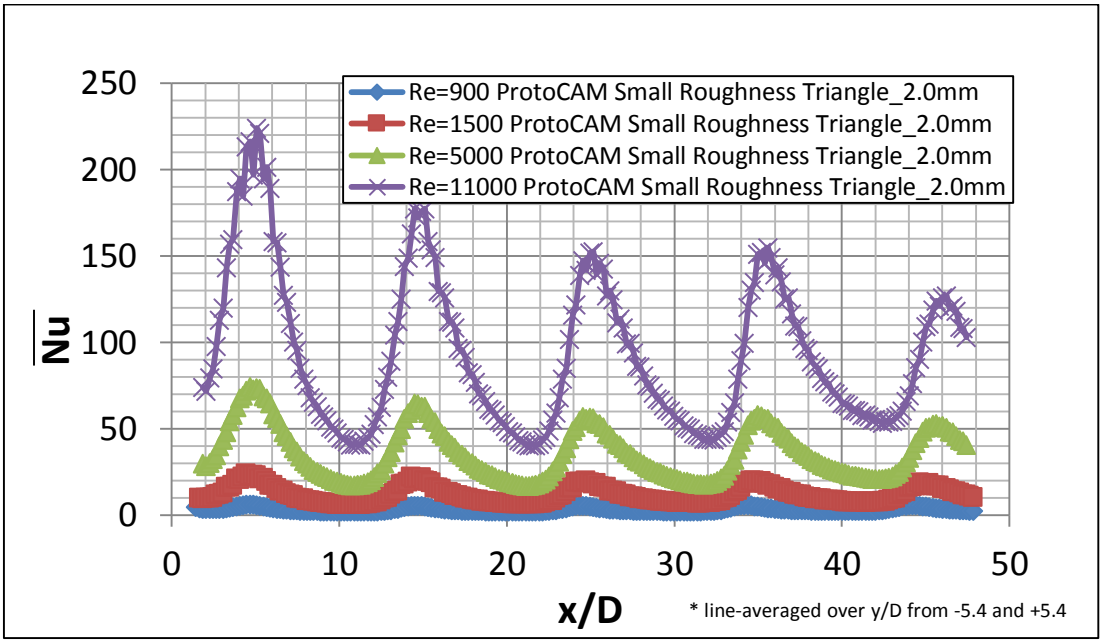

Figure 4.31: Line-averaged Nusselt numbers as dependent upon *x/D*, for four different Re_j for the 2.0 mm small triangle roughness.

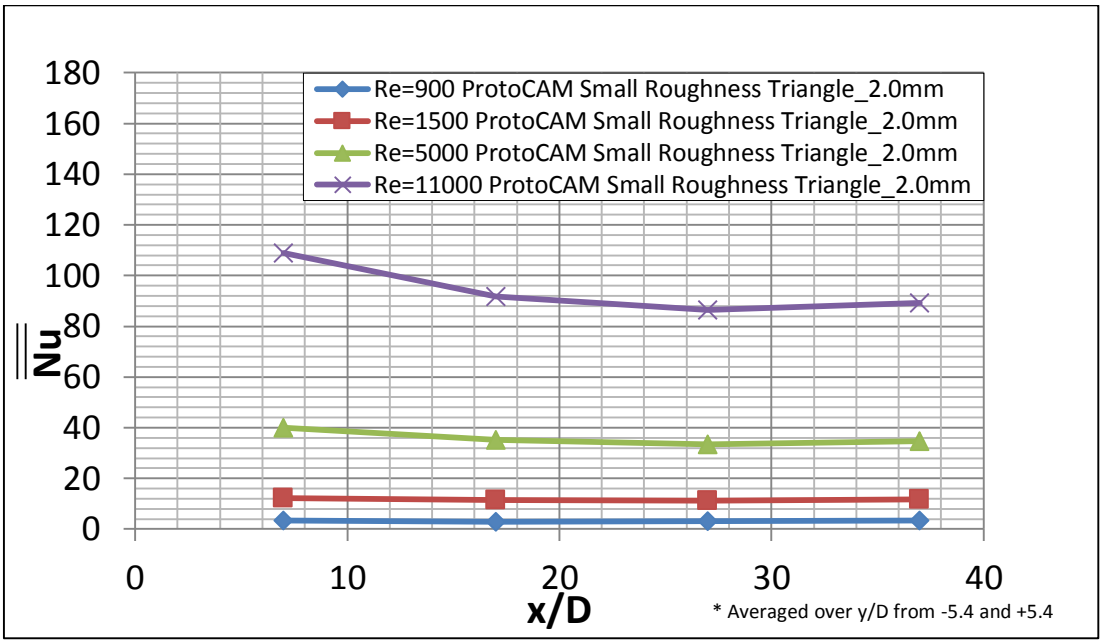

Figure 4.32: Spatially-averaged Nusselt numbers as dependent upon *x/D*, for four different Re_j for the 2.0 mm small triangle roughness.

F. Effects of Small Roughness Height – Rectangle Roughness

Figures 4.33 through 4.36 show results for all three rectangle small roughness cases (plates 3-5 in Table 2.1). Figures 4.33 and 4.34 are for a Reynolds number of 900, while Figures 4.35 and 4.36 are for a Reynolds number of 5000. For both Reynolds numbers, an increase in small roughness height generally leads to higher Nusselt numbers, when compared at the same Re_j and x/D values. The increased height of the small roughness causes more mixing and more vorticity in the flow. Although there is more material in the flow, increased insulating effects are not present as small roughness height increases. Additionally, with increased small roughness height, there is more surface area for convective heat transfer.

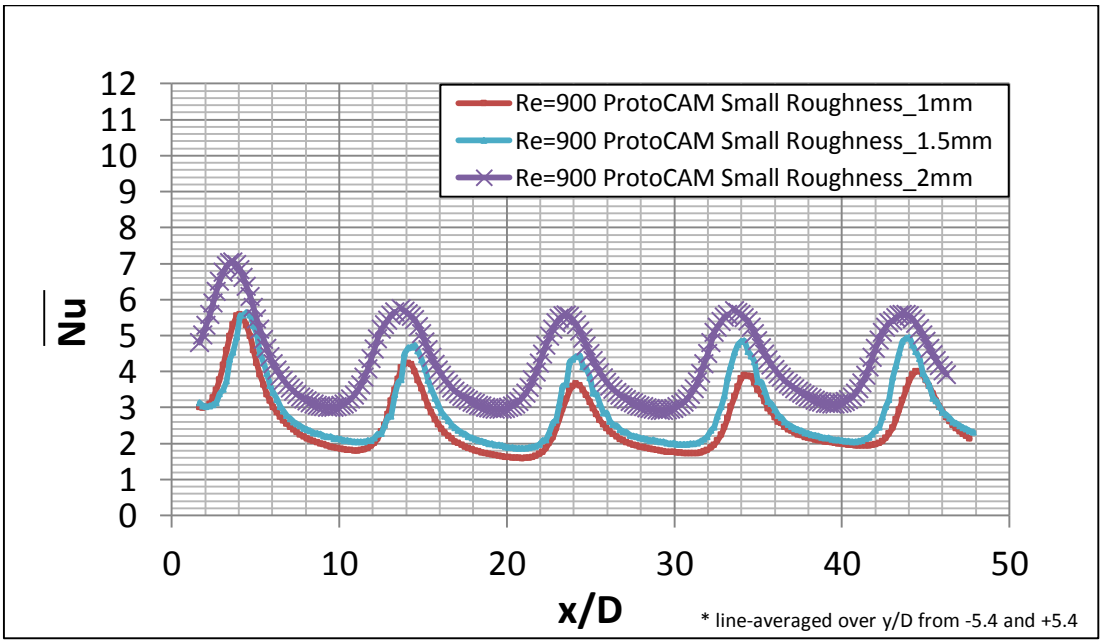

Figure 4.33: Line-averaged Nusselt numbers as dependent upon *x/D*, for three rectangle roughness arrangements for Re=900.

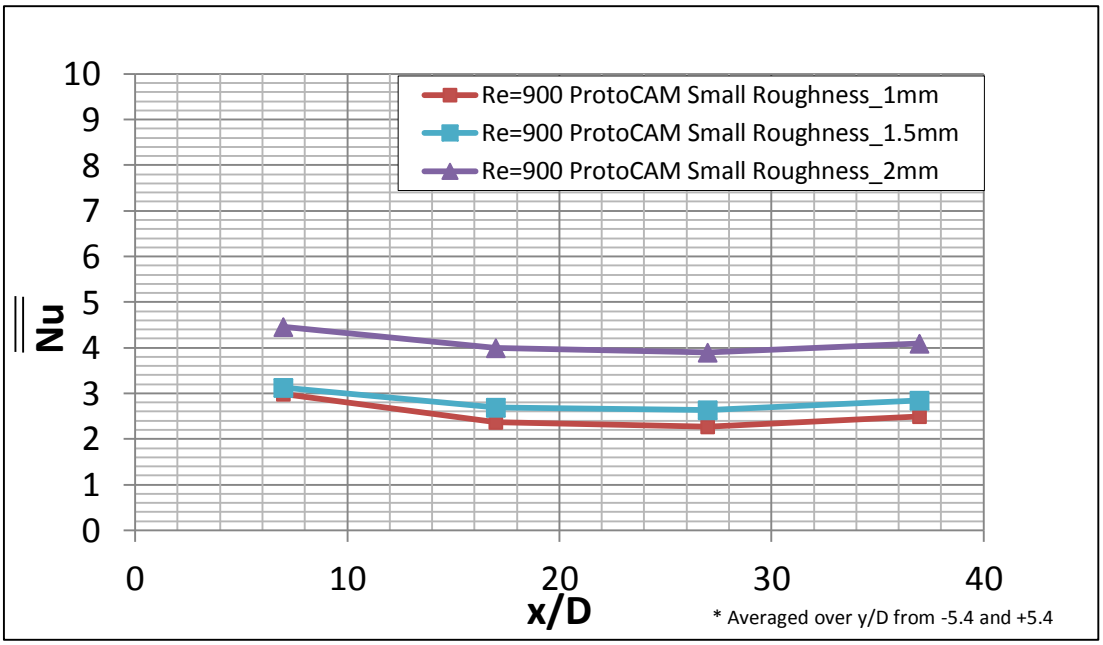

Figure 4.34: Spatially-averaged Nusselt numbers as dependent upon *x/D*, for three rectangle roughness arrangements for Re=900.

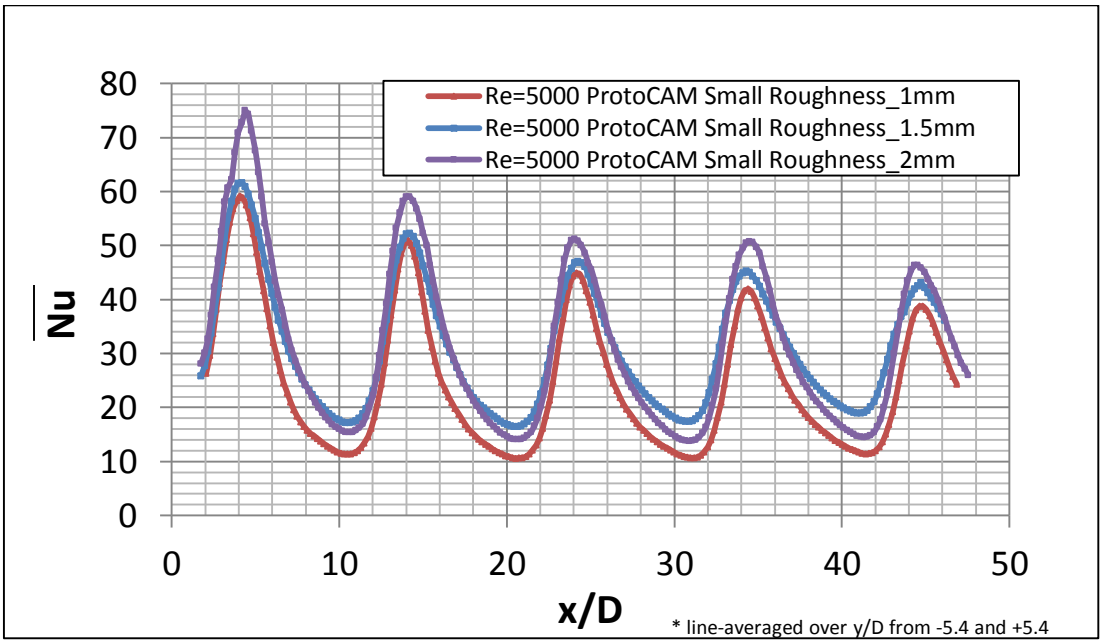

Figure 4.35: Line-averaged Nusselt numbers as dependent upon *x/D*, for three rectangle roughness arrangements for Re=5000.

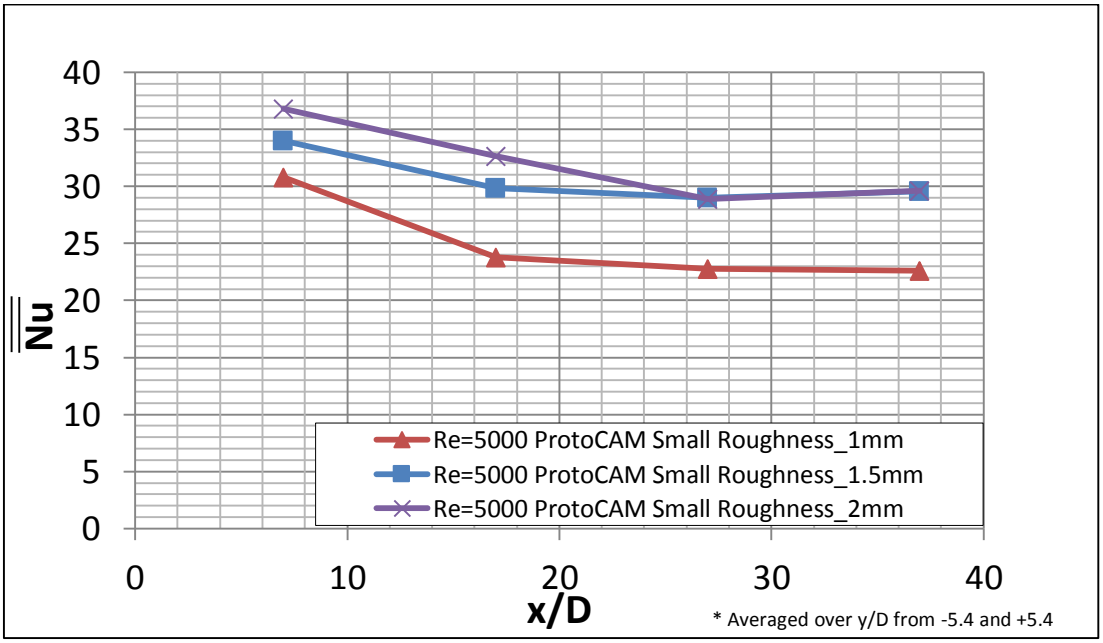

Figure 4.36: Spatially-averaged Nusselt numbers as dependent upon *x/D*, for three rectangle roughness arrangements for Re=5000.

G. Effects of Small Roughness Height – Triangle Roughness

Figures 4.37 through 4.40 show results for all three triangle small roughness cases (plates 9-11 in Table 2.1). Figures 4.37 and 4.38 are for a Reynolds number of 900, while Figures 4.39 and 4.40 are for a

Reynolds number of 5000. For both Reynolds numbers, the 1.5 mm small roughness gives the highest Nusselt numbers, when compared at the same Re_j and x/D values. The increased height of the 1.5 mm small roughness causes more mixing and more vorticity in the flow than in the 1 mm case. The 2 mm case gives lower Nusselt numbers than the other two cases. The added material in the flow with the increased height has an insulating effect because of the conduction within, and increases thermal resistance, and reduces heat transfer coefficients along the wetted target surface.

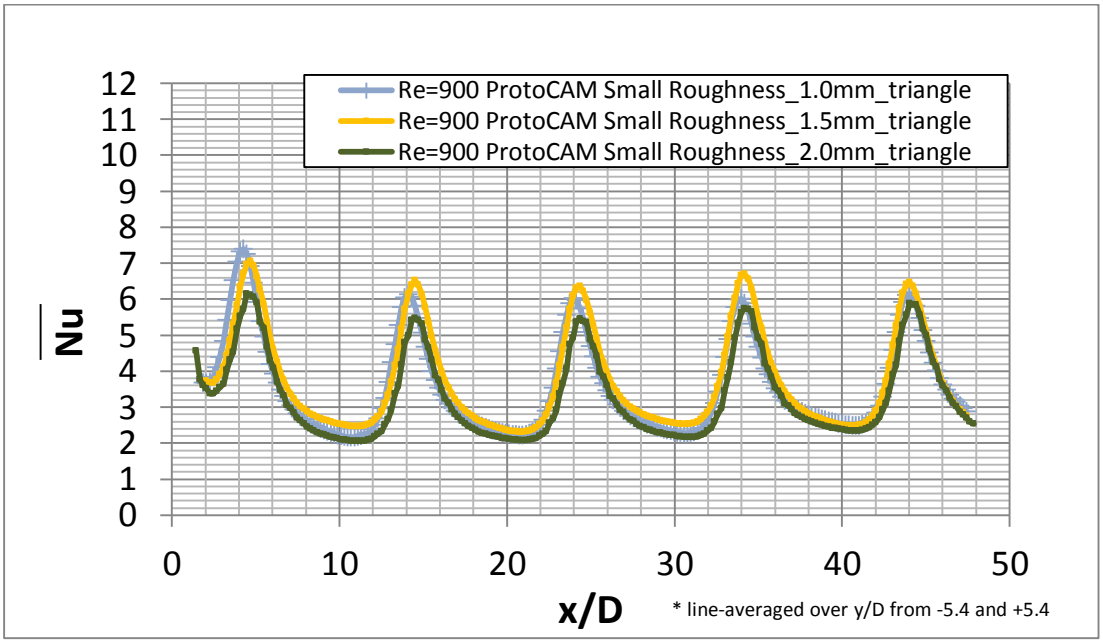

Figure 4.37: Line-averaged Nusselt numbers as dependent upon *x/D*, for three triangle roughness arrangements for Re=900.

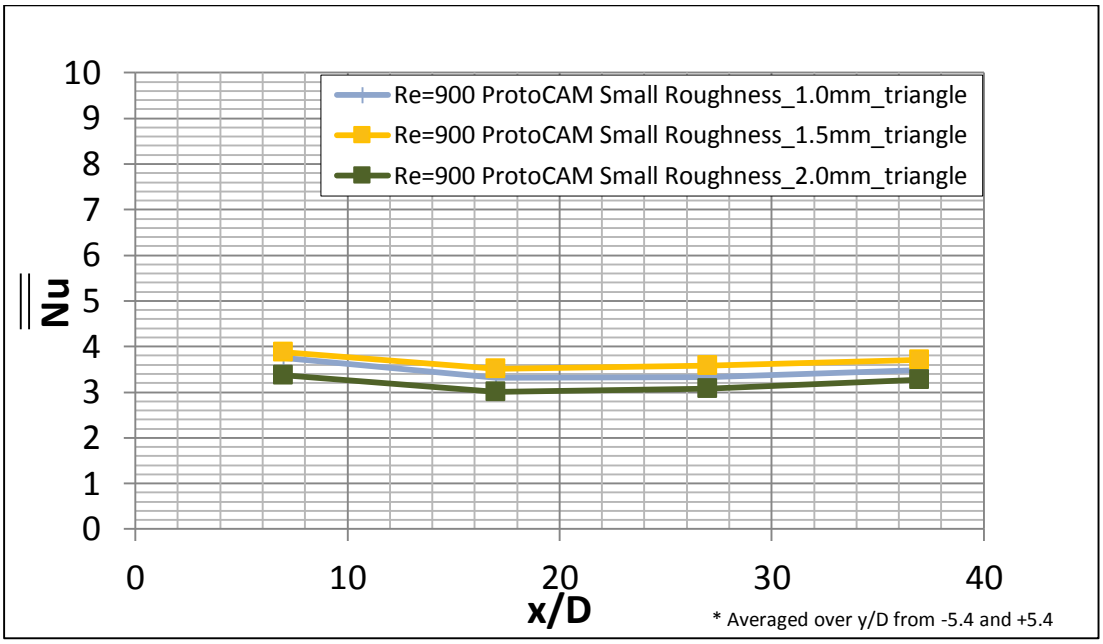

Figure 4.38: Spatially-averaged Nusselt numbers as dependent upon *x/D*, for three triangle roughness arrangements for Re=900.

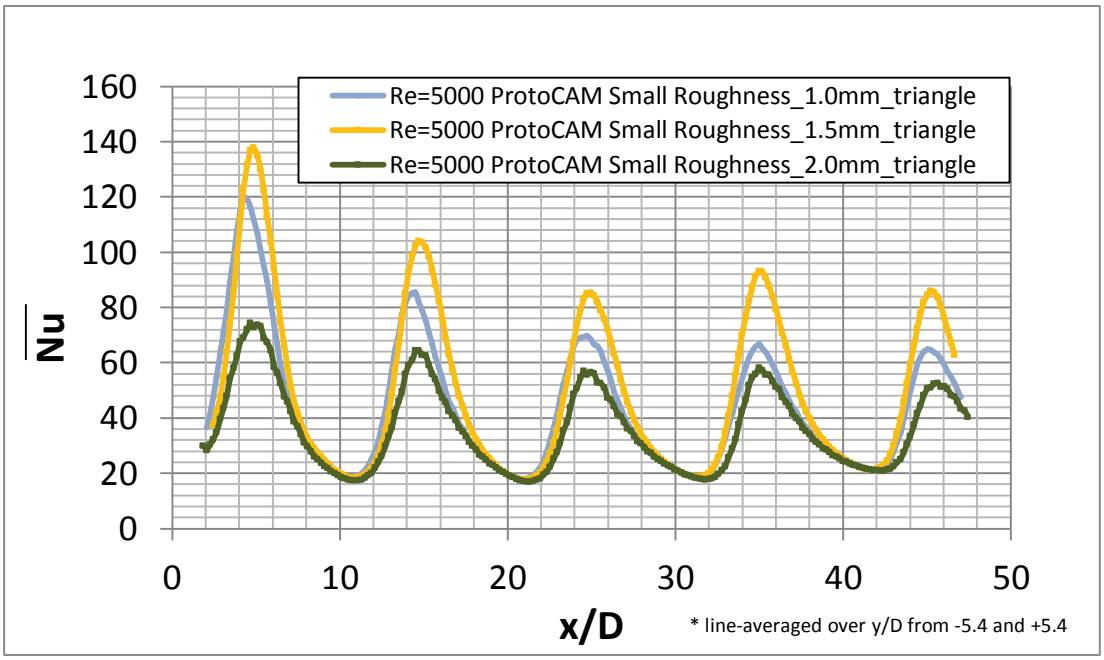

Figure 4.39: Line-averaged Nusselt numbers as dependent upon *x/D*, for three triangle roughness arrangements for Re=5000.

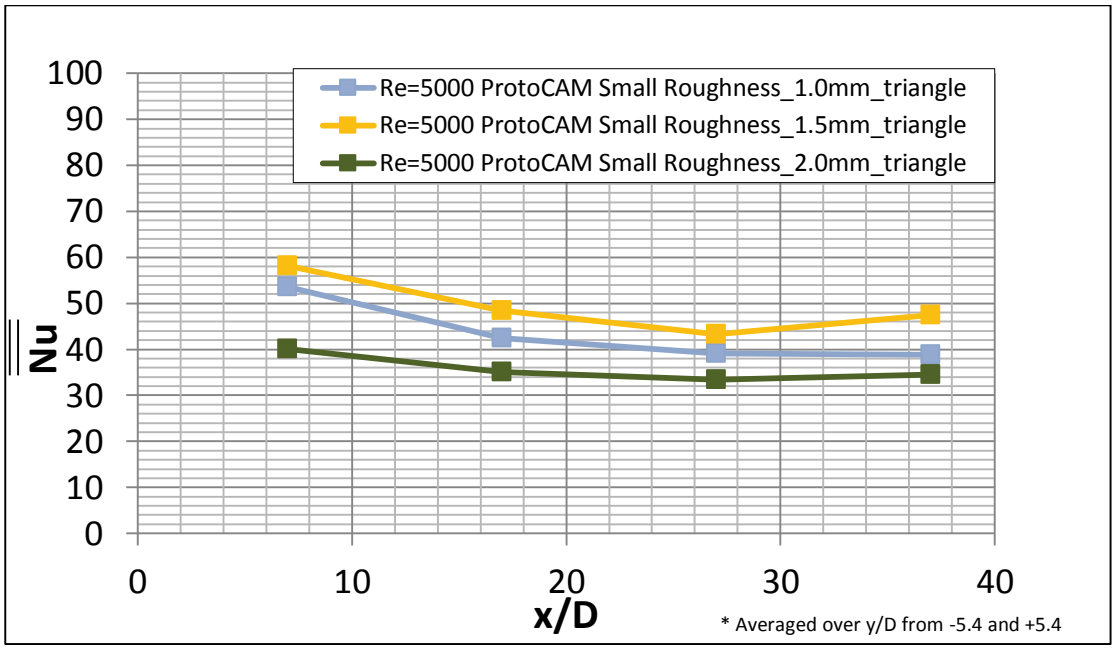

Figure 4.40: Spatially-averaged Nusselt numbers as dependent upon *x/D*, for three triangle roughness arrangements for Re=5000.

H. Effects of Small and Large Roughness

Figures 4.41 through 4.48 display the results from all rectangle and triangle roughness configurations (plates 3-14 as listed in Table 2.1). Figures 4.41 through 4.44 show the results from the rectangle roughness tests, while Figures 4.45 through 4.48 show the results from the triangle roughness tests. In general, the large roughness had an adverse effect on the Nusselt number at laminar Reynolds numbers, but had a positive effect at turbulent Reynolds numbers. The large roughness blocks the flow at low Reynolds numbers and has an insulating effect because of the conduction within, and increases thermal resistance, and reduces heat transfer coefficients along the wetted target surface. Here, thermal transport within the flow is of the same order of magnitude as conduction transport within roughness elements. At turbulent Reynolds numbers, the airflow is strong enough that the large pins increase the amount of turbulence without insulating the plate. The pins increase the vorticity and mixing at these high Reynolds numbers, which increases the Nusselt number, when compared at the same Re_j and x/D values. This increases the turbulent transport and surface convective heat transfer. Here, turbulent transport is significantly higher than conduction transport within roughness elements.

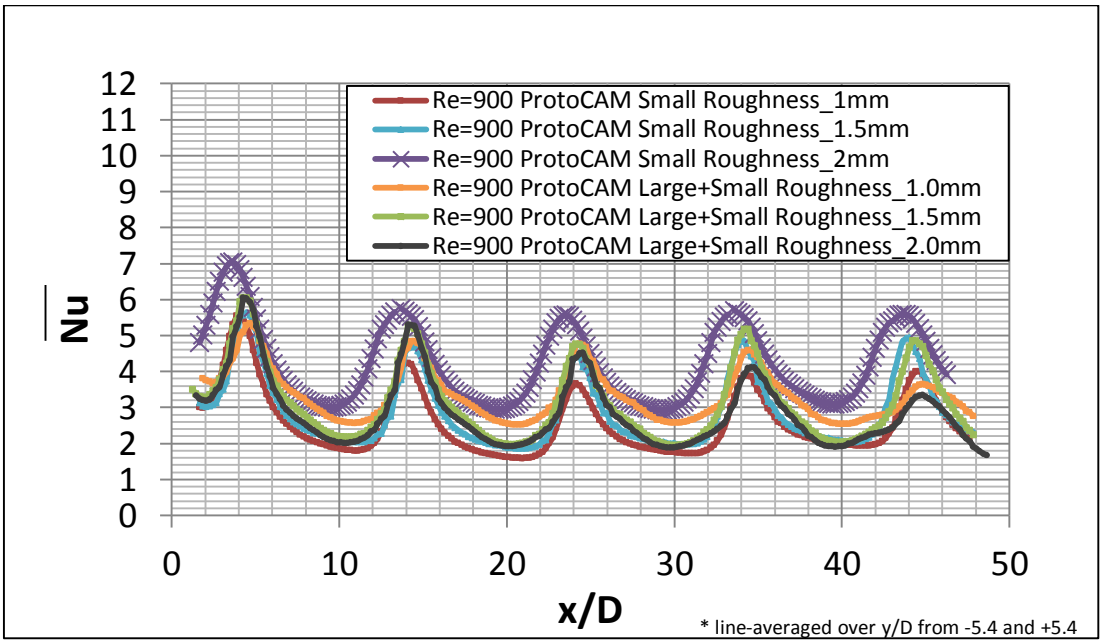

Figure 4.41: Line-averaged Nusselt numbers as dependent upon *x/D*, for six rectangle roughness arrangements for Re=900.

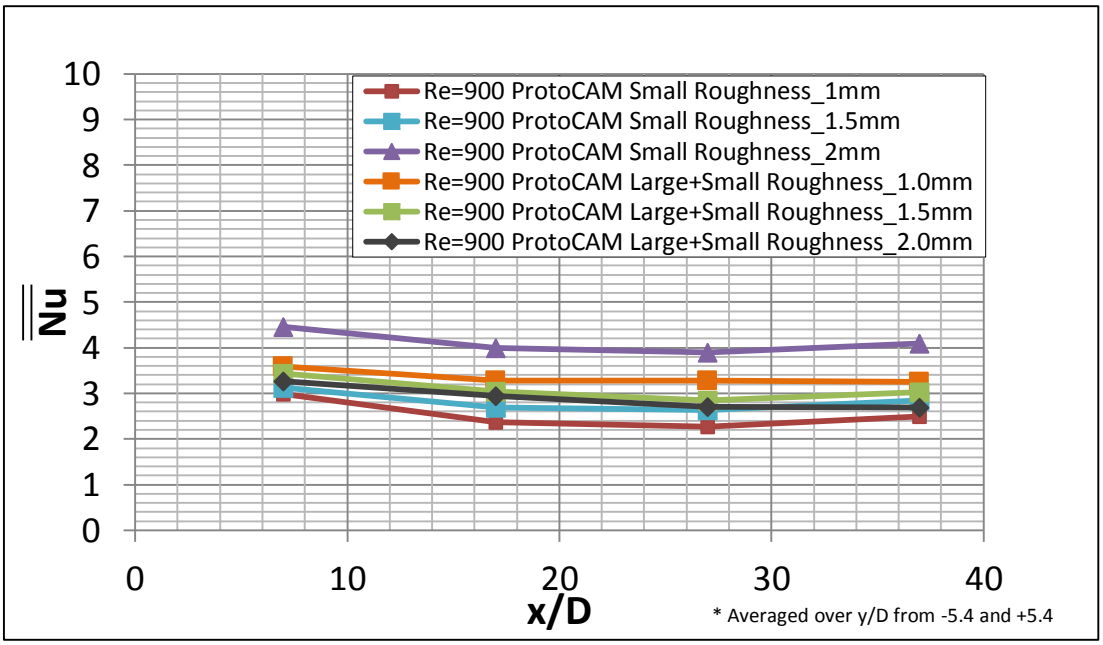

Figure 4.42: Spatially-averaged Nusselt numbers as dependent upon *x/D*, for six rectangle roughness arrangements for Re=900.

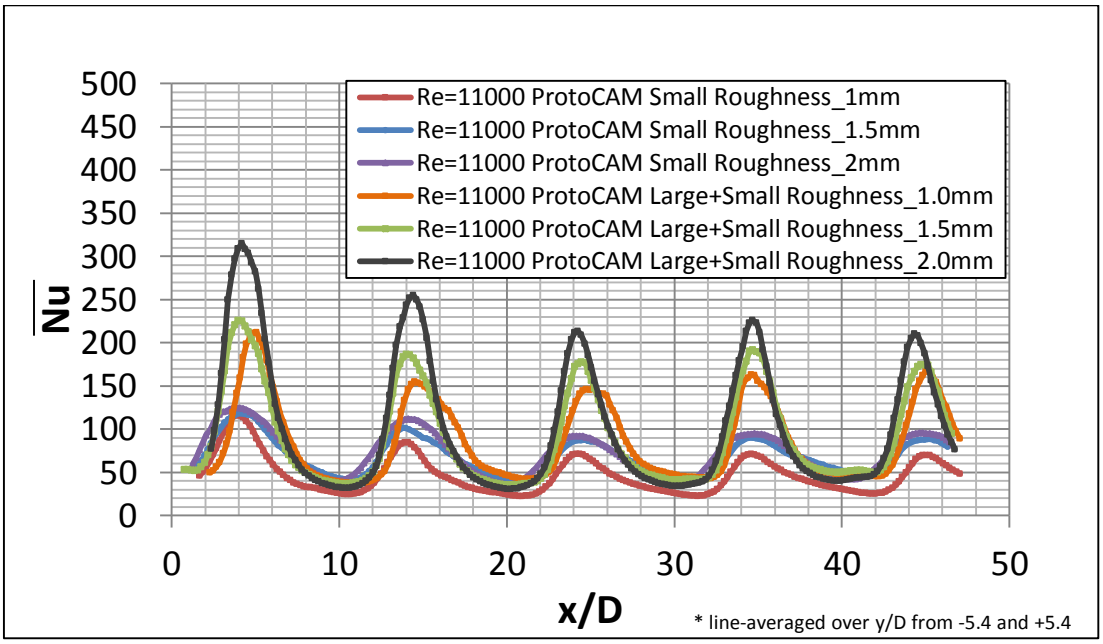

Figure 4.43: Line-averaged Nusselt numbers as dependent upon *x/D*, for six rectangle roughness arrangements for Re=11000.

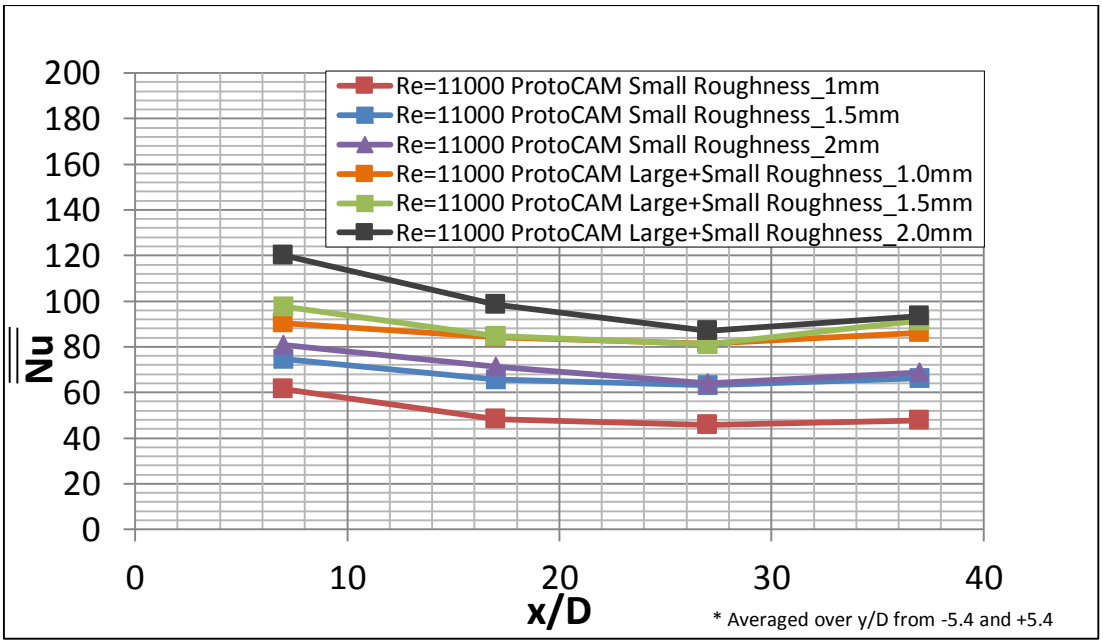

Figure 4.44: Spatially-averaged Nusselt numbers as dependent upon *x/D*, for six rectangle roughness arrangements for Re=11000.

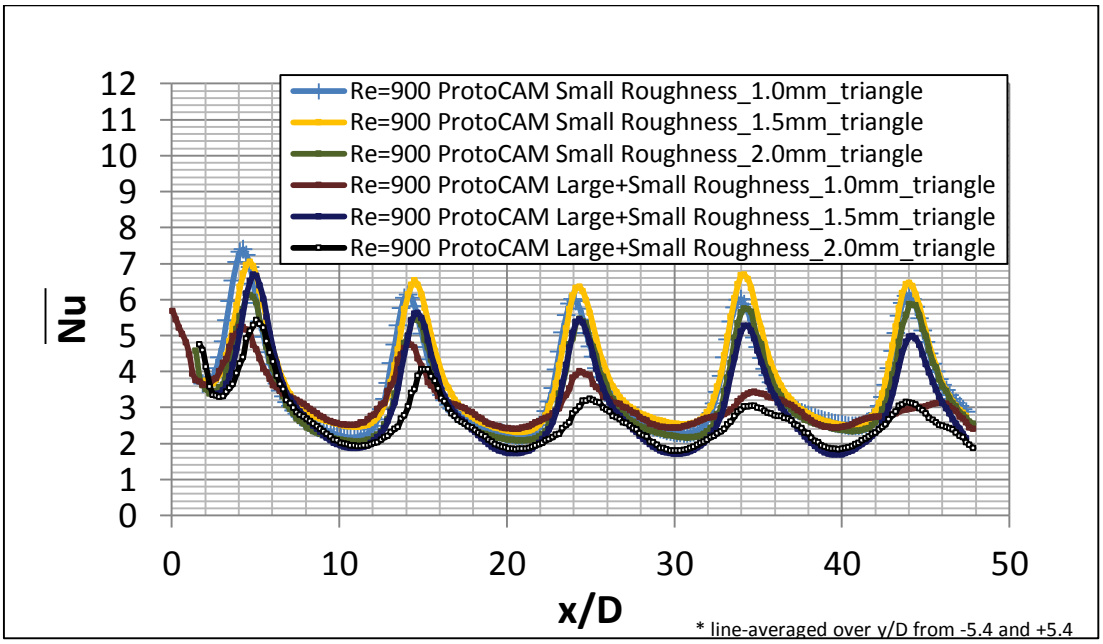

Figure 4.45: Line-averaged Nusselt numbers as dependent upon *x/D*, for six triangle roughness arrangements for Re=900.

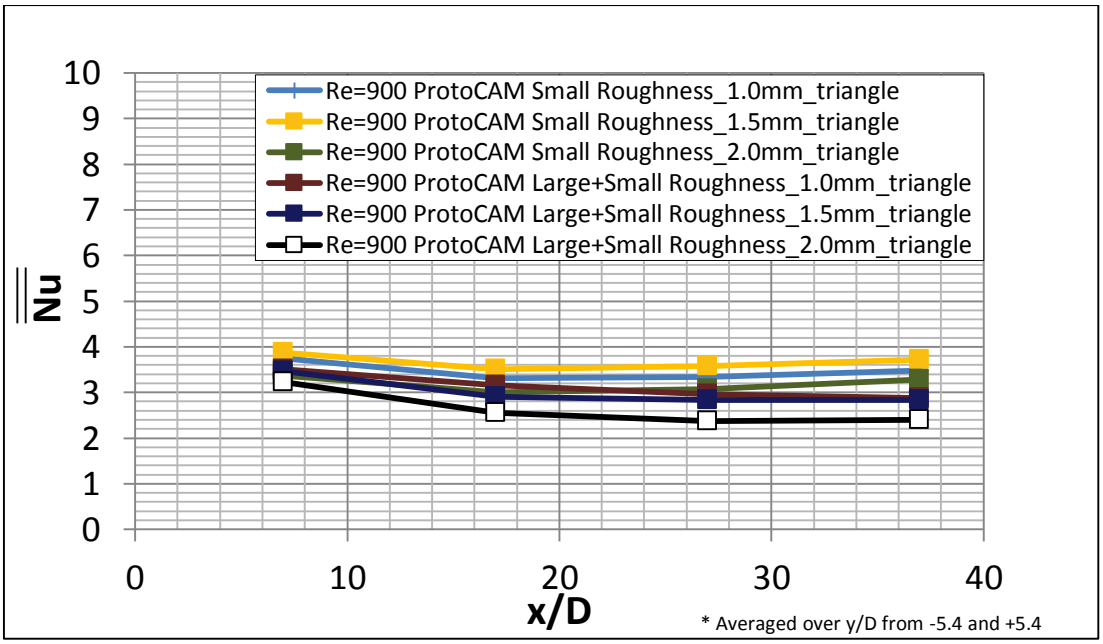

Figure 4.46: Spatially-averaged Nusselt numbers as dependent upon *x/D*, for six triangle roughness arrangements for Re=900.

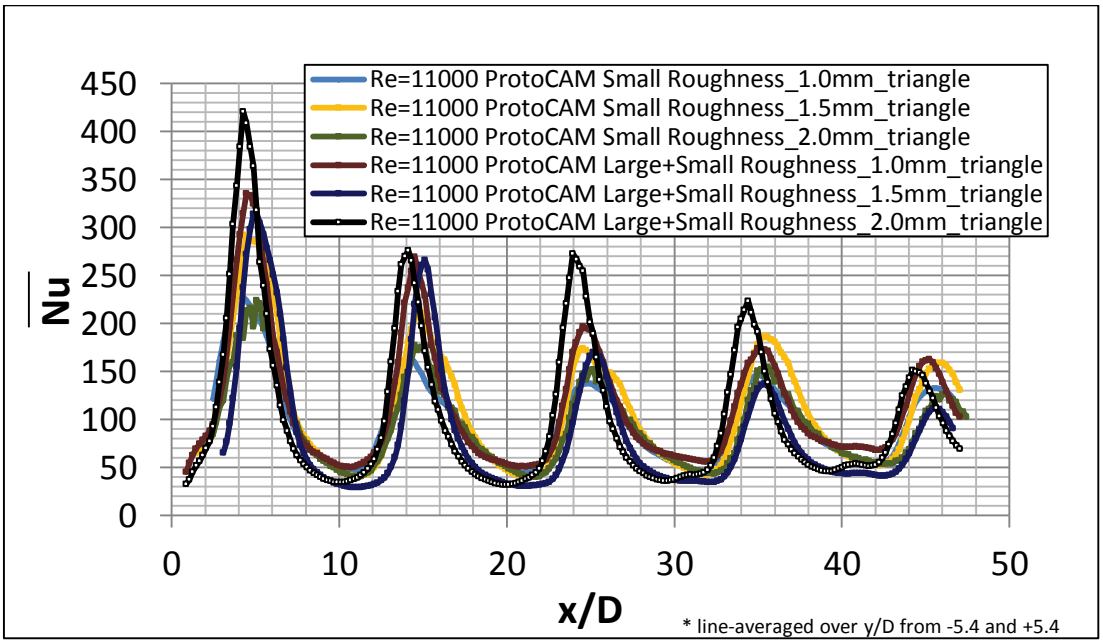

Figure 4.47: Line-averaged Nusselt numbers as dependent upon *x/D*, for six triangle roughness arrangements for Re=11000.

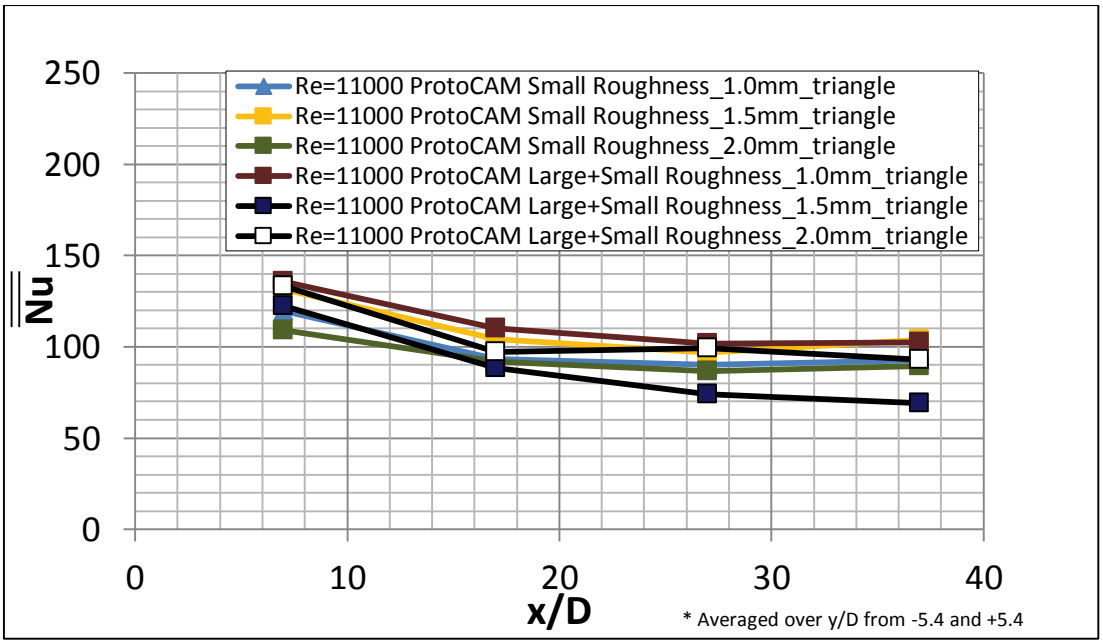

Figure 4.48: Spatially-averaged Nusselt numbers as dependent upon *x/D*, for six triangle roughness arrangements for Re=11000.

I. Comparison Between Rectangle and Triangle Roughness

Figures 4.49 through 4.52 present comparisons between the rectangle roughness configurations (plates 3-8 in Table 2.1) and the triangle roughness configurations (plates 9-14 in Table 2.1). Figures 4.49

and 4.50 display the large and small roughness combinations, while Figures 4.51 and 4.52 display the small roughness alone. All figures are for a Reynolds number of 11000. In general, the triangle roughness configurations give higher Nusselt numbers, when compared at a particular Reynolds number and x/D value. The small roughness configurations in particular show a clear increase from the rectangle roughness to the triangle roughness. This is believed to be due to the sharper corners of the small triangle roughness elements. The sharp angles create more turbulent mixing and increased vorticity in the flow. This leads to higher convective heat transfer. In the small and large roughness configurations, the increase in Nusselt number from rectangle to triangle configurations is less pronounced. Despite this, the combination of large pins and triangle small roughness shows the highest Nusselt numbers, compared with the rectangle roughness configurations at the same x/D location and Reynolds number.

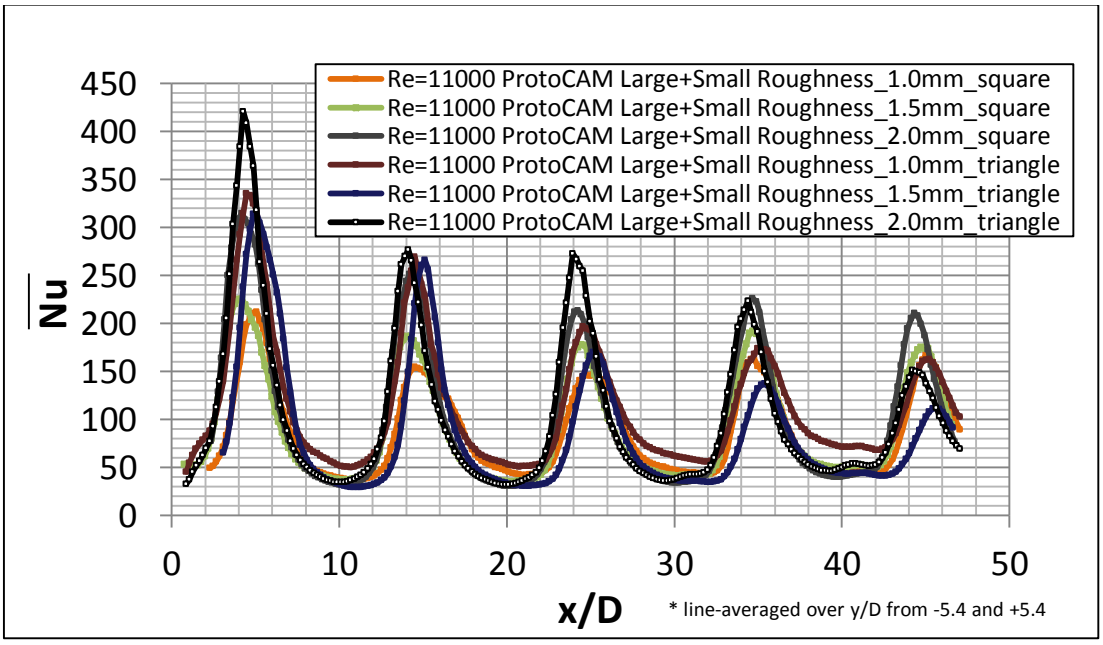

Figure 4.49: Line-Averaged comparison for small and large roughness combinations at Re=11000.

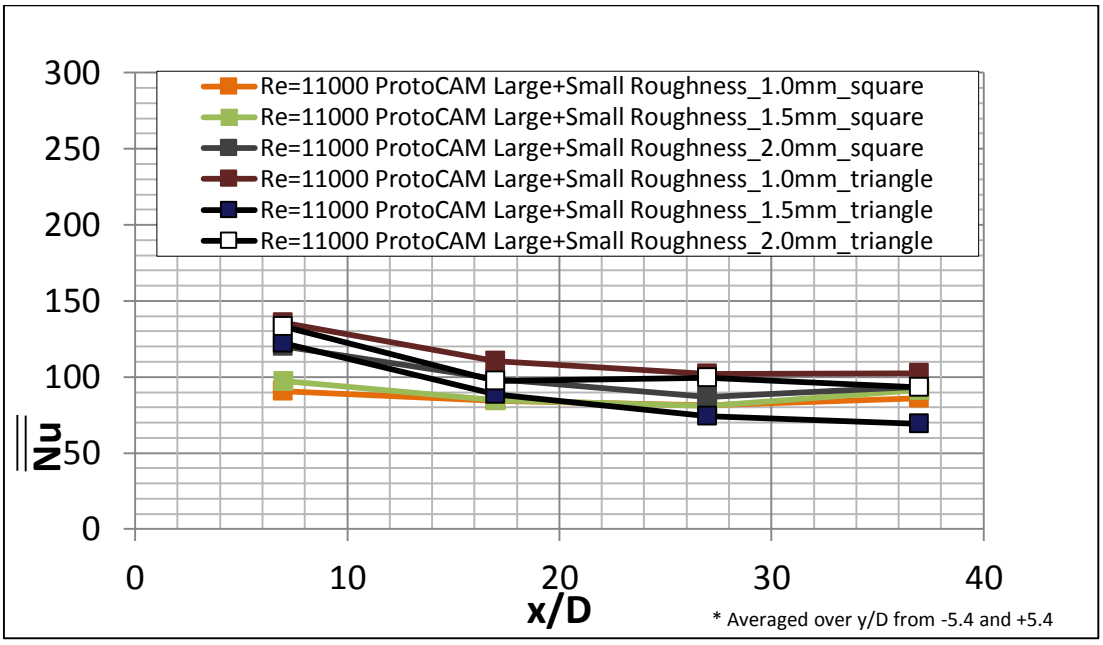

Figure 4.50: Area-Averaged comparison for small and large roughness combinations at Re=11000.

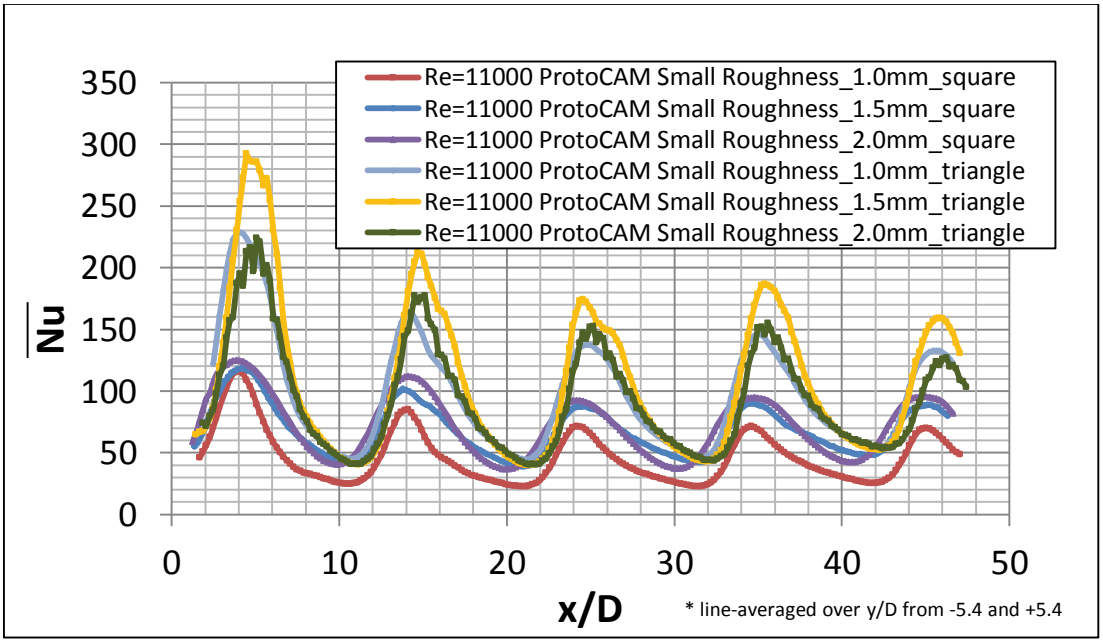

Figure 4.51: Line-Averaged comparison for small roughness at Re=11000.

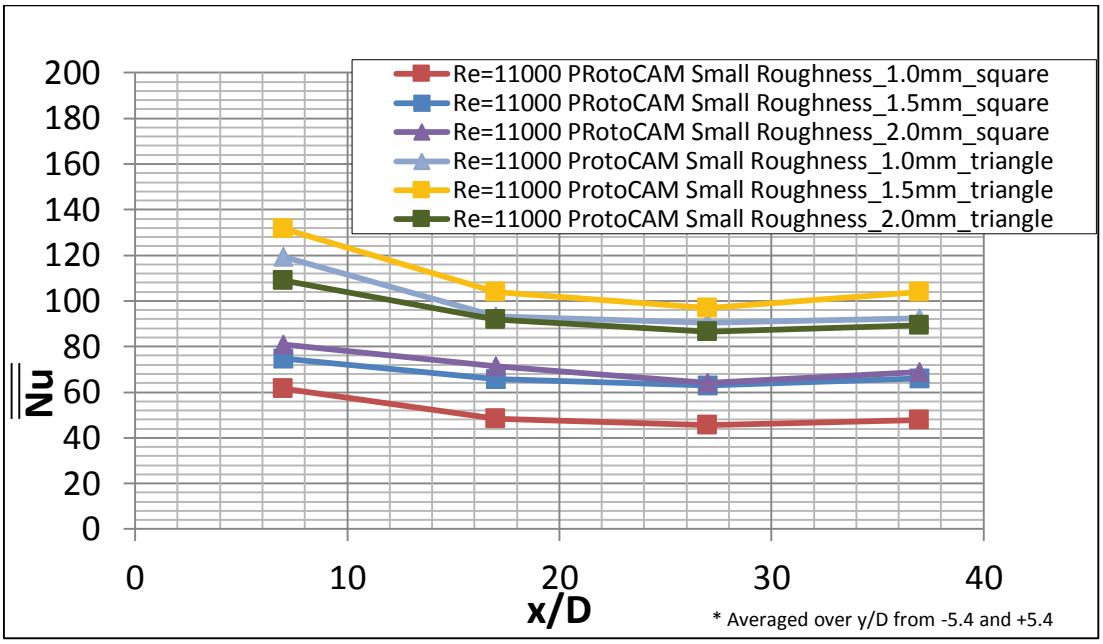

Figure 4.52: Area-Averaged comparison for small roughness at Re=11000.

CHAPTER 5

SUMMARY AND CONCLUSIONS

The present investigation involves testing the addition of special surface roughness patterns to an impingement surface to improve the effectiveness of impingement cooling. This investigation utilizes various sizes, distributions, shapes, and patterns of surface roughness elements for impingement cooling augmentation. Infrared thermography, in addition to thermocouples, is used to measure the surface temperature variations. These temperature variations are analyzed using MATLAB software to calculate surface Nusselt numbers.

An impingement plate with a grid of holes is attached to the end of the final plenum. Air exits the impingement plate and impinges on the test surface. The space between the impingement plate and the test surface is held at 2.5D, where D is the diameter of the impingement holes in the impingement plate. Four jet Reynolds numbers are considered: 900, 1500, 5000, and 11000. Reynolds numbers of 900 and 1500 are believed to be laminar, while Reynolds numbers of 5000 and 11000 are believed to be turbulent. The jet Mach numbers range between 0.01 and 0.2. Twenty test surfaces are considered, with small roughness element shapes of rectangle, triangle, and cylinder. The shapes of the large roughness elements are rectangle and cylinder. In addition to physical tests, numerical conduction analysis software simulations are used to determine variations of temperature and heat flux throughout the target surface. The program, SC/Tetra, is used to verify the assumption of one-dimensional conduction analysis.

Maximum local Nusselt number values are located where jets impinge onto the target plate. Local

maximum Nusselt numbers for the impingement jets become lower as x/D increases due to the cross-flow air moving toward the exit of the test section. The minimum values are present between each row of impingement holes.

In general, the large roughness had an adverse effect on the Nusselt number at laminar Reynolds numbers, but had a positive effect at turbulent Reynolds numbers. The large roughness blocks the flow at low Reynolds numbers and has an insulating effect because of the conduction within, and increases thermal resistance. The result is reduced heat transfer coefficients along the wetted target surface, relative to cases without large roughness. At turbulent Reynolds numbers, the pins increase the vorticity and turbulent mixing, which increases the Nusselt number, when compared at the same Re_j and x/D values. This increases the turbulent transport and surface convective heat transfer rates.

At low Reynolds numbers of 900 and 1500, the rectangle, triangle, and cylinder plates show similar trends. For the laminar Reynolds number cases, the plates with small roughness alone show higher Nusselt numbers than the plates with a combination of small and large roughness. This is because of the physical phenomena described above. The rectangle small roughness cases show an increase in Nusselt number with increasing height. The triangle small roughness cases show that the 1.5 mm height gives higher Nusselt numbers than 1 mm or 2 mm. The cylinder small roughness cases show a decrease in Nusselt number with an increase in small roughness height. These differences can be attributed to differences in flow mixing caused by the varying shapes and conduction within the target plate material. The rectangles and triangles add enough flow mixing to counteract the insulating effect of the added material, while the cylinders do not.

At high Reynolds numbers of 5000 and 11000, the rectangle, triangle, and cylinder plates show different trends. For the rectangle plates, the turbulent Reynolds number cases show that the plates with a combination of large and small roughness give higher Nusselt numbers than the plates with small roughness alone, when compared at the same Re_j and x/D values. This is because the large pins increase the mixing of the flow, increasing turbulent transport, and surface convective heat transfer rates. For the triangle plates, the turbulent Reynolds number cases show very little advantage relative to the small and large roughness combination, relative to the small roughness alone. This same conclusion is evident for the cylinder cases. The large pins are having an insulating effect on these plates, similar to the insulating effect seen for the

laminar case. In comparison, the triangle roughness configurations give higher Nusselt numbers than the rectangle configurations, when compared at a particular Reynolds number and x/D value. This is believed to be due to the sharper corners of the small triangle roughness elements, which create more turbulent mixing and increased vorticity within the flow. This leads to higher convective heat transfer rates.

APPENDIX A: UNCERTAINTY ANALYSIS

The uncertainty analysis for this experiment is described by Lee et al. [5]. This material is included here so that the analysis is shown in great detail.

Table A.1 Experimental uncertainty magnitudes for the local Nusselt number, and quantities employed to determine the local Nusselt number.

Quantity	*Xi*	*δXi*	
A_{ht}	0.03175 m^2	0.0005	
D	0.015 m	0.00025	
T_w	36.35 °C	0.85	
T_{oj}	22.9 °C	0.15	
α	0.0226 W/(m*K)	0.000138	
Total Nusselt Number uncertainty (percent)			8.2

Uncertainty estimates are based on 95 percent confidence levels and are determined using methods described by Kline and McClintock [7] and Moffat [8]. Uncertainty of temperatures measured with thermocouples is ±0.15°C. Spatial and temperature resolutions achieved with infrared imaging are about 0.1 mm to 0.2 mm, and 0.4°C, respectively. This magnitude of temperature resolution is due to temperature resolution is due to uncertainty in determining the exact locations of thermocouples with respect to pixel values used for the *in situ* calibrations. Of the different quantities considered, the uncertainty associated with surface temperature (with a maximum value of approximately ±0.85°C) makes the largest contribution to overall Nusselt number uncertainty. Note that the overall Nusselt number uncertainty also includes possible contributions from lateral conduction within the test plates, although, in general, magnitudes of lateral conduction (in the *x* and *y* directions) are generally insignificant relative to overall convective heat flux levels from impingement.

Numerical predictions of target plate internal conduction, using SC/Tetra Version 11, indicate that Nusselt number variations from lateral conduction within the target plate are less than the overall Nusselt number experimental uncertainty. These predictions also show that lateral conduction magnitudes are very small or negligible for the *X/D*=10, *Y/D*=2.7, $Re_j \approx 5000$, *Z/D*=2.5 test case. As such, no significant alteration

of surface Nusselt number distributions or surface temperature distributions are present from lateral conduction (which occurs in the *x* and *y* directions).

APPENDIX B: DATA FILE DIRECTORY

Appendix B presents a listing and description of the data files containing test data from all tests performed. The first table lists the experimental data files, while the second lists the numerical analysis files from SC/Tetra.

Experimental Data Files				
Plate	**Reynolds Number**	**Folder Name**	**File Name**	**Description**
1 Baseline – SMOOTH	900	Plate 1 Re=900	d_nu1.txt	Raw Nusselt Number data in text file.
			total.bmp	IR camera bitmap image used for camera calibration.
			A.xls	Excel file with grayscale value to temperature camera calibration.
			Summary Output Data.doc	Word file with test conditions.
			Contour Plot.dg7	DeltaGraph Nusselt number contour plot.
			Local Line Spatial.xls	Excel file containing local, line averaged, and spatially averaged Nusselt number data.
1 Baseline – SMOOTH	5000	Plate 1 Re=5000	d_nu1.txt	Raw Nusselt Number data in text file.
			total.bmp	IR camera bitmap image used for camera calibration.
			A.xls	Excel file with grayscale value to temperature camera calibration.
			Summary Output Data.doc	Word file with test conditions.
			Contour Plot.dg7	DeltaGraph Nusselt number contour plot.
			Local Line Spatial.xls	Excel file containing local, line averaged, and spatially averaged Nusselt number data.
1 Baseline – SMOOTH	11000	Plate 1 Re=11000	d_nu1.txt	Raw Nusselt Number data in text file.
			total.bmp	IR camera bitmap image used for camera calibration.
			A.xls	Excel file with grayscale value to temperature camera calibration.
			Summary Output Data.doc	Word file with test conditions.
			Contour Plot.dg7	DeltaGraph Nusselt number contour plot.
			Local Line Spatial.xls	Excel file containing local, line averaged, and spatially averaged Nusselt number data.
2 Large RECTANGLE Roughness	900	Plate 2 Re=900	d_nu1.txt	Raw Nusselt Number data in text file.
			total.bmp	IR camera bitmap image used for camera calibration.
			A.xls	Excel file with grayscale value to temperature camera calibration.
			Summary Output Data.doc	Word file with test conditions.
			Contour Plot.dg7	DeltaGraph Nusselt number contour plot.
			Local Line Spatial.xls	Excel file containing local, line averaged, and spatially averaged Nusselt number data.
	1500	Plate 2 Re=1500	d_nu1.txt	Raw Nusselt Number data in text file.

2 Large RECTANGLE Roughness			total.bmp	IR camera bitmap image used for camera calibration.
			A.xls	Excel file with grayscale value to temperature camera calibration.
			Summary Output Data.doc	Word file with test conditions.
			Contour Plot.dg7	DeltaGraph Nusselt number contour plot.
			Local Line Spatial.xls	Excel file containing local, line averaged, and spatially averaged Nusselt number data.
2 Large RECTANGLE Roughness	5000	Plate 2 Re=5000	d_nu1.txt	Raw Nusselt Number data in text file.
			total.bmp	IR camera bitmap image used for camera calibration.
			A.xls	Excel file with grayscale value to temperature camera calibration.
			Summary Output Data.doc	Word file with test conditions.
			Contour Plot.dg7	DeltaGraph Nusselt number contour plot.
			Local Line Spatial.xls	Excel file containing local, line averaged, and spatially averaged Nusselt number data.
2 Large RECTANGLE Roughness	11000	Plate 2 Re=11000	d_nu1.txt	Raw Nusselt Number data in text file.
			total.bmp	IR camera bitmap image used for camera calibration.
			A.xls	Excel file with grayscale value to temperature camera calibration.
			Summary Output Data.doc	Word file with test conditions.
			Contour Plot.dg7	DeltaGraph Nusselt number contour plot.
			Local Line Spatial.xls	Excel file containing local, line averaged, and spatially averaged Nusselt number data.
3 Small RECTANGLE Roughness – Height = 1.0 mm	900	Plate 3 Re=900	d_nu1.txt	Raw Nusselt Number data in text file.
			total.bmp	IR camera bitmap image used for camera calibration.
			A.xls	Excel file with grayscale value to temperature camera calibration.
			Summary Output Data.doc	Word file with test conditions.
			Contour Plot.dg7	DeltaGraph Nusselt number contour plot.
			Local Line Spatial.xls	Excel file containing local, line averaged, and spatially averaged Nusselt number data.
3 Small RECTANGLE Roughness – Height = 1.0 mm	5000	Plate 3 Re=5000	d_nu1.txt	Raw Nusselt Number data in text file.
			total.bmp	IR camera bitmap image used for camera calibration.
			A.xls	Excel file with grayscale value to temperature camera calibration.
			Summary Output Data.doc	Word file with test conditions.
			Contour Plot.dg7	DeltaGraph Nusselt number contour plot.
			Local Line Spatial.xls	Excel file containing local, line averaged, and spatially averaged Nusselt number data.
3 Small RECTANGLE Roughness – Height = 1.0 mm	11000	Plate 3 Re=11000	d_nu1.txt	Raw Nusselt Number data in text file.
			total.bmp	IR camera bitmap image used for camera calibration.
			A.xls	Excel file with grayscale value to temperature camera calibration.
			Summary Output Data.doc	Word file with test conditions.

			Contour Plot.dg7	DeltaGraph Nusselt number contour plot.
			Local Line Spatial.xls	Excel file containing local, line averaged, and spatially averaged Nusselt number data.
4 Small RECTANGLE Roughness – Height = 1.5 mm	900	Plate 4 Re=900	d_nu1.txt	Raw Nusselt Number data in text file.
			total.bmp	IR camera bitmap image used for camera calibration.
			A.xls	Excel file with grayscale value to temperature camera calibration.
			Summary Output Data.doc	Word file with test conditions.
			Contour Plot.dg7	DeltaGraph Nusselt number contour plot.
			Local Line Spatial.xls	Excel file containing local, line averaged, and spatially averaged Nusselt number data.
4 Small RECTANGLE Roughness – Height = 1.5 mm	1500	Plate 4 Re=1500	d_nu1.txt	Raw Nusselt Number data in text file.
			total.bmp	IR camera bitmap image used for camera calibration.
			A.xls	Excel file with grayscale value to temperature camera calibration.
			Summary Output Data.doc	Word file with test conditions.
			Contour Plot.dg7	DeltaGraph Nusselt number contour plot.
			Local Line Spatial.xls	Excel file containing local, line averaged, and spatially averaged Nusselt number data.
4 Small RECTANGLE Roughness – Height = 1.5 mm	5000	Plate 4 Re=5000	d_nu1.txt	Raw Nusselt Number data in text file.
			total.bmp	IR camera bitmap image used for camera calibration.
			A.xls	Excel file with grayscale value to temperature camera calibration.
			Summary Output Data.doc	Word file with test conditions.
			Contour Plot.dg7	DeltaGraph Nusselt number contour plot.
			Local Line Spatial.xls	Excel file containing local, line averaged, and spatially averaged Nusselt number data.
4 Small RECTANGLE Roughness – Height = 1.5 mm	11000	Plate 4 Re=11000	d_nu1.txt	Raw Nusselt Number data in text file.
			total.bmp	IR camera bitmap image used for camera calibration.
			A.xls	Excel file with grayscale value to temperature camera calibration.
			Summary Output Data.doc	Word file with test conditions.
			Contour Plot.dg7	DeltaGraph Nusselt number contour plot.
			Local Line Spatial.xls	Excel file containing local, line averaged, and spatially averaged Nusselt number data.
5 Small RECTANGLE Roughness – Height = 2.0 mm	900	Plate 5 Re=900	d_nu1.txt	Raw Nusselt Number data in text file.
			total.bmp	IR camera bitmap image used for camera calibration.
			A.xls	Excel file with grayscale value to temperature camera calibration.
			Summary Output Data.doc	Word file with test conditions.
			Contour Plot.dg7	DeltaGraph Nusselt number contour plot.
			Local Line Spatial.xls	Excel file containing local, line averaged, and spatially averaged Nusselt number data.
	1500	Plate 5 Re=1500	d_nu1.txt	Raw Nusselt Number data in text file.

5 Small RECTANGLE Roughness – Height = 2.0 mm			total.bmp	IR camera bitmap image used for camera calibration.
			A.xls	Excel file with grayscale value to temperature camera calibration.
			Summary Output Data.doc	Word file with test conditions.
			Contour Plot.dg7	DeltaGraph Nusselt number contour plot.
			Local Line Spatial.xls	Excel file containing local, line averaged, and spatially averaged Nusselt number data.
5 Small RECTANGLE Roughness – Height = 2.0 mm	5000	Plate 5 Re=5000	d_nu1.txt	Raw Nusselt Number data in text file.
			total.bmp	IR camera bitmap image used for camera calibration.
			A.xls	Excel file with grayscale value to temperature camera calibration.
			Summary Output Data.doc	Word file with test conditions.
			Contour Plot.dg7	DeltaGraph Nusselt number contour plot.
			Local Line Spatial.xls	Excel file containing local, line averaged, and spatially averaged Nusselt number data.
5 Small RECTANGLE Roughness – Height = 2.0 mm	11000	Plate 5 Re=11000	d_nu1.txt	Raw Nusselt Number data in text file.
			total.bmp	IR camera bitmap image used for camera calibration.
			A.xls	Excel file with grayscale value to temperature camera calibration.
			Summary Output Data.doc	Word file with test conditions.
			Contour Plot.dg7	DeltaGraph Nusselt number contour plot.
			Local Line Spatial.xls	Excel file containing local, line averaged, and spatially averaged Nusselt number data.
6 Large RECTANGLE + Small RECTANGLE Roughness – Height = 1.0 mm	900	Plate 6 Re=900	d_nu1.txt	Raw Nusselt Number data in text file.
			total.bmp	IR camera bitmap image used for camera calibration.
			A.xls	Excel file with grayscale value to temperature camera calibration.
			Summary Output Data.doc	Word file with test conditions.
			Contour Plot.dg7	DeltaGraph Nusselt number contour plot.
			Local Line Spatial.xls	Excel file containing local, line averaged, and spatially averaged Nusselt number data.
6 Large RECTANGLE + Small RECTANGLE Roughness – Height = 1.0 mm	1500	Plate 6 Re=1500	d_nu1.txt	Raw Nusselt Number data in text file.
			total.bmp	IR camera bitmap image used for camera calibration.
			A.xls	Excel file with grayscale value to temperature camera calibration.
			Summary Output Data.doc	Word file with test conditions.
			Contour Plot.dg7	DeltaGraph Nusselt number contour plot.
			Local Line Spatial.xls	Excel file containing local, line averaged, and spatially averaged Nusselt number data.
6 Large RECTANGLE + Small RECTANGLE Roughness – Height = 1.0 mm	5000	Plate 6 Re=5000	d_nu1.txt	Raw Nusselt Number data in text file.
			total.bmp	IR camera bitmap image used for camera calibration.
			A.xls	Excel file with grayscale value to temperature camera calibration.
			Summary Output Data.doc	Word file with test conditions.

			Contour Plot.dg7	DeltaGraph Nusselt number contour plot.
			Local Line Spatial.xls	Excel file containing local, line averaged, and spatially averaged Nusselt number data.
6 Large RECTANGLE + Small RECTANGLE Roughness – Height = 1.0 mm	11000	Plate 6 Re=11000	d_nu1.txt	Raw Nusselt Number data in text file.
			total.bmp	IR camera bitmap image used for camera calibration.
			A.xls	Excel file with grayscale value to temperature camera calibration.
			Summary Output Data.doc	Word file with test conditions.
			Contour Plot.dg7	DeltaGraph Nusselt number contour plot.
			Local Line Spatial.xls	Excel file containing local, line averaged, and spatially averaged Nusselt number data.
7 Large RECTANGLE + Small RECTANGLE Roughness – Height = 1.5 mm	900	Plate 7 Re=900	d_nu1.txt	Raw Nusselt Number data in text file.
			total.bmp	IR camera bitmap image used for camera calibration.
			A.xls	Excel file with grayscale value to temperature camera calibration.
			Summary Output Data.doc	Word file with test conditions.
			Contour Plot.dg7	DeltaGraph Nusselt number contour plot.
			Local Line Spatial.xls	Excel file containing local, line averaged, and spatially averaged Nusselt number data.
7 Large RECTANGLE + Small RECTANGLE Roughness – Height = 1.5 mm	1500	Plate 7 Re=1500	d_nu1.txt	Raw Nusselt Number data in text file.
			total.bmp	IR camera bitmap image used for camera calibration.
			A.xls	Excel file with grayscale value to temperature camera calibration.
			Summary Output Data.doc	Word file with test conditions.
			Contour Plot.dg7	DeltaGraph Nusselt number contour plot.
			Local Line Spatial.xls	Excel file containing local, line averaged, and spatially averaged Nusselt number data.
7 Large RECTANGLE + Small RECTANGLE Roughness – Height = 1.5 mm	5000	Plate 7 Re=5000	d_nu1.txt	Raw Nusselt Number data in text file.
			total.bmp	IR camera bitmap image used for camera calibration.
			A.xls	Excel file with grayscale value to temperature camera calibration.
			Summary Output Data.doc	Word file with test conditions.
			Contour Plot.dg7	DeltaGraph Nusselt number contour plot.
			Local Line Spatial.xls	Excel file containing local, line averaged, and spatially averaged Nusselt number data.
7 Large RECTANGLE + Small RECTANGLE Roughness – Height = 1.5 mm	11000	Plate 7 Re=11000	d_nu1.txt	Raw Nusselt Number data in text file.
			total.bmp	IR camera bitmap image used for camera calibration.
			A.xls	Excel file with grayscale value to temperature camera calibration.
			Summary Output Data.doc	Word file with test conditions.
			Contour Plot.dg7	DeltaGraph Nusselt number contour plot.
			Local Line Spatial.xls	Excel file containing local, line averaged, and spatially averaged Nusselt number data.
	900	Plate 8 Re=900	d_nu1.txt	Raw Nusselt Number data in text file.

8 Large RECTANGLE + Small RECTANGLE Roughness – Height = 2.0 mm			total.bmp	IR camera bitmap image used for camera calibration.
			A.xls	Excel file with grayscale value to temperature camera calibration.
			Summary Output Data.doc	Word file with test conditions.
			Contour Plot.dg7	DeltaGraph Nusselt number contour plot.
			Local Line Spatial.xls	Excel file containing local, line averaged, and spatially averaged Nusselt number data.
8 Large RECTANGLE + Small RECTANGLE Roughness – Height = 2.0 mm	1500	Plate 8 Re=1500	d_nu1.txt	Raw Nusselt Number data in text file.
			total.bmp	IR camera bitmap image used for camera calibration.
			A.xls	Excel file with grayscale value to temperature camera calibration.
			Summary Output Data.doc	Word file with test conditions.
			Contour Plot.dg7	DeltaGraph Nusselt number contour plot.
			Local Line Spatial.xls	Excel file containing local, line averaged, and spatially averaged Nusselt number data.
8 Large RECTANGLE + Small RECTANGLE Roughness – Height = 2.0 mm	5000	Plate 8 Re=5000	d_nu1.txt	Raw Nusselt Number data in text file.
			total.bmp	IR camera bitmap image used for camera calibration.
			A.xls	Excel file with grayscale value to temperature camera calibration.
			Summary Output Data.doc	Word file with test conditions.
			Contour Plot.dg7	DeltaGraph Nusselt number contour plot.
			Local Line Spatial.xls	Excel file containing local, line averaged, and spatially averaged Nusselt number data.
8 Large RECTANGLE + Small RECTANGLE Roughness – Height = 2.0 mm	11000	Plate 8 Re=11000	d_nu1.txt	Raw Nusselt Number data in text file.
			total.bmp	IR camera bitmap image used for camera calibration.
			A.xls	Excel file with grayscale value to temperature camera calibration.
			Summary Output Data.doc	Word file with test conditions.
			Contour Plot.dg7	DeltaGraph Nusselt number contour plot.
			Local Line Spatial.xls	Excel file containing local, line averaged, and spatially averaged Nusselt number data.
9 Small TRIANGLE Roughness – Height = 1.0 mm	900	Plate 9 Re=900	d_nu1.txt	Raw Nusselt Number data in text file.
			total.bmp	IR camera bitmap image used for camera calibration.
			A.xls	Excel file with grayscale value to temperature camera calibration.
			Summary Output Data.doc	Word file with test conditions.
			Contour Plot.dg7	DeltaGraph Nusselt number contour plot.
			Local Line Spatial.xls	Excel file containing local, line averaged, and spatially averaged Nusselt number data.
9 Small TRIANGLE Roughness – Height = 1.0 mm	1500	Plate 9 Re=1500	d_nu1.txt	Raw Nusselt Number data in text file.
			total.bmp	IR camera bitmap image used for camera calibration.
			A.xls	Excel file with grayscale value to temperature camera calibration.
			Summary Output Data.doc	Word file with test conditions.

			Contour Plot.dg7	DeltaGraph Nusselt number contour plot.
			Local Line Spatial.xls	Excel file containing local, line averaged, and spatially averaged Nusselt number data.
9 Small TRIANGLE Roughness – Height = 1.0 mm	5000	Plate 9 Re=5000	d_nu1.txt	Raw Nusselt Number data in text file.
			total.bmp	IR camera bitmap image used for camera calibration.
			A.xls	Excel file with grayscale value to temperature camera calibration.
			Summary Output Data.doc	Word file with test conditions.
			Contour Plot.dg7	DeltaGraph Nusselt number contour plot.
			Local Line Spatial.xls	Excel file containing local, line averaged, and spatially averaged Nusselt number data.
9 Small TRIANGLE Roughness – Height = 1.0 mm	11000	Plate 9 Re=11000	d_nu1.txt	Raw Nusselt Number data in text file.
			total.bmp	IR camera bitmap image used for camera calibration.
			A.xls	Excel file with grayscale value to temperature camera calibration.
			Summary Output Data.doc	Word file with test conditions.
			Contour Plot.dg7	DeltaGraph Nusselt number contour plot.
			Local Line Spatial.xls	Excel file containing local, line averaged, and spatially averaged Nusselt number data.
10 Small TRIANGLE Roughness – Height = 1.5 mm	900	Plate 10 Re=900	d_nu1.txt	Raw Nusselt Number data in text file.
			total.bmp	IR camera bitmap image used for camera calibration.
			A.xls	Excel file with grayscale value to temperature camera calibration.
			Summary Output Data.doc	Word file with test conditions.
			Contour Plot.dg7	DeltaGraph Nusselt number contour plot.
			Local Line Spatial.xls	Excel file containing local, line averaged, and spatially averaged Nusselt number data.
10 Small TRIANGLE Roughness – Height = 1.5 mm	1500	Plate 10 Re=1500	d_nu1.txt	Raw Nusselt Number data in text file.
			total.bmp	IR camera bitmap image used for camera calibration.
			A.xls	Excel file with grayscale value to temperature camera calibration.
			Summary Output Data.doc	Word file with test conditions.
			Contour Plot.dg7	DeltaGraph Nusselt number contour plot.
			Local Line Spatial.xls	Excel file containing local, line averaged, and spatially averaged Nusselt number data.
10 Small TRIANGLE Roughness – Height = 1.5 mm	5000	Plate 10 Re=5000	d_nu1.txt	Raw Nusselt Number data in text file.
			total.bmp	IR camera bitmap image used for camera calibration.
			A.xls	Excel file with grayscale value to temperature camera calibration.
			Summary Output Data.doc	Word file with test conditions.
			Contour Plot.dg7	DeltaGraph Nusselt number contour plot.
			Local Line Spatial.xls	Excel file containing local, line averaged, and spatially averaged Nusselt number data.
	11000		d_nu1.txt	Raw Nusselt Number data in text file.

10 Small TRIANGLE Roughness – Height = 1.5 mm		Plate 10 Re=11000	total.bmp	IR camera bitmap image used for camera calibration.
			A.xls	Excel file with grayscale value to temperature camera calibration.
			Summary Output Data.doc	Word file with test conditions.
			Contour Plot.dg7	DeltaGraph Nusselt number contour plot.
			Local Line Spatial.xls	Excel file containing local, line averaged, and spatially averaged Nusselt number data.
11 Small TRIANGLE Roughness – Height = 2.0 mm	900	Plate 11 Re=900	d_nu1.txt	Raw Nusselt Number data in text file.
			total.bmp	IR camera bitmap image used for camera calibration.
			A.xls	Excel file with grayscale value to temperature camera calibration.
			Summary Output Data.doc	Word file with test conditions.
			Contour Plot.dg7	DeltaGraph Nusselt number contour plot.
			Local Line Spatial.xls	Excel file containing local, line averaged, and spatially averaged Nusselt number data.
11 Small TRIANGLE Roughness – Height = 2.0 mm	1500	Plate 11 Re=1500	d_nu1.txt	Raw Nusselt Number data in text file.
			total.bmp	IR camera bitmap image used for camera calibration.
			A.xls	Excel file with grayscale value to temperature camera calibration.
			Summary Output Data.doc	Word file with test conditions.
			Contour Plot.dg7	DeltaGraph Nusselt number contour plot.
			Local Line Spatial.xls	Excel file containing local, line averaged, and spatially averaged Nusselt number data.
11 Small TRIANGLE Roughness – Height = 2.0 mm	5000	Plate 11 Re=5000	d_nu1.txt	Raw Nusselt Number data in text file.
			total.bmp	IR camera bitmap image used for camera calibration.
			A.xls	Excel file with grayscale value to temperature camera calibration.
			Summary Output Data.doc	Word file with test conditions.
			Contour Plot.dg7	DeltaGraph Nusselt number contour plot.
			Local Line Spatial.xls	Excel file containing local, line averaged, and spatially averaged Nusselt number data.
11 Small TRIANGLE Roughness – Height = 2.0 mm	11000	Plate 11 Re=11000	d_nu1.txt	Raw Nusselt Number data in text file.
			total.bmp	IR camera bitmap image used for camera calibration.
			A.xls	Excel file with grayscale value to temperature camera calibration.
			Summary Output Data.doc	Word file with test conditions.
			Contour Plot.dg7	DeltaGraph Nusselt number contour plot.
			Local Line Spatial.xls	Excel file containing local, line averaged, and spatially averaged Nusselt number data.
12 Large RECTANGLE + Small TRIANGLE Roughness – Height = 1.0 mm	900	Plate 12 Re=900	d_nu1.txt	Raw Nusselt Number data in text file.
			total.bmp	IR camera bitmap image used for camera calibration.
			A.xls	Excel file with grayscale value to temperature camera calibration.
			Summary Output Data.doc	Word file with test conditions.

			Contour Plot.dg7	DeltaGraph Nusselt number contour plot.
			Local Line Spatial.xls	Excel file containing local, line averaged, and spatially averaged Nusselt number data.
12 Large RECTANGLE + Small TRIANGLE Roughness – Height = 1.0 mm	1500	Plate 12 Re=1500	d_nu1.txt	Raw Nusselt Number data in text file.
			total.bmp	IR camera bitmap image used for camera calibration.
			A.xls	Excel file with grayscale value to temperature camera calibration.
			Summary Output Data.doc	Word file with test conditions.
			Contour Plot.dg7	DeltaGraph Nusselt number contour plot.
			Local Line Spatial.xls	Excel file containing local, line averaged, and spatially averaged Nusselt number data.
12 Large RECTANGLE + Small TRIANGLE Roughness – Height = 1.0 mm	5000	Plate 12 Re=5000	d_nu1.txt	Raw Nusselt Number data in text file.
			total.bmp	IR camera bitmap image used for camera calibration.
			A.xls	Excel file with grayscale value to temperature camera calibration.
			Summary Output Data.doc	Word file with test conditions.
			Contour Plot.dg7	DeltaGraph Nusselt number contour plot.
			Local Line Spatial.xls	Excel file containing local, line averaged, and spatially averaged Nusselt number data.
12 Large RECTANGLE + Small TRIANGLE Roughness – Height = 1.0 mm	11000	Plate 12 Re=11000	d_nu1.txt	Raw Nusselt Number data in text file.
			total.bmp	IR camera bitmap image used for camera calibration.
			A.xls	Excel file with grayscale value to temperature camera calibration.
			Summary Output Data.doc	Word file with test conditions.
			Contour Plot.dg7	DeltaGraph Nusselt number contour plot.
			Local Line Spatial.xls	Excel file containing local, line averaged, and spatially averaged Nusselt number data.
13 Large RECTANGLE + Small TRIANGLE Roughness – Height = 1.5 mm	900	Plate 13 Re=900	d_nu1.txt	Raw Nusselt Number data in text file.
			total.bmp	IR camera bitmap image used for camera calibration.
			A.xls	Excel file with grayscale value to temperature camera calibration.
			Summary Output Data.doc	Word file with test conditions.
			Contour Plot.dg7	DeltaGraph Nusselt number contour plot.
			Local Line Spatial.xls	Excel file containing local, line averaged, and spatially averaged Nusselt number data.
13 Large RECTANGLE + Small TRIANGLE Roughness – Height = 1.5 mm	1500	Plate 13 Re=1500	d_nu1.txt	Raw Nusselt Number data in text file.
			total.bmp	IR camera bitmap image used for camera calibration.
			A.xls	Excel file with grayscale value to temperature camera calibration.
			Summary Output Data.doc	Word file with test conditions.
			Contour Plot.dg7	DeltaGraph Nusselt number contour plot.
			Local Line Spatial.xls	Excel file containing local, line averaged, and spatially averaged Nusselt number data.
	5000		d_nu1.txt	Raw Nusselt Number data in text file.

13 Large RECTANGLE + Small TRIANGLE Roughness – Height = 1.5 mm		Plate 13 Re=5000	total.bmp	IR camera bitmap image used for camera calibration.
			A.xls	Excel file with grayscale value to temperature camera calibration.
			Summary Output Data.doc	Word file with test conditions.
			Contour Plot.dg7	DeltaGraph Nusselt number contour plot.
			Local Line Spatial.xls	Excel file containing local, line averaged, and spatially averaged Nusselt number data.
13 Large RECTANGLE + Small TRIANGLE Roughness – Height = 1.5 mm	11000	Plate 13 Re=11000	d_nu1.txt	Raw Nusselt Number data in text file.
			total.bmp	IR camera bitmap image used for camera calibration.
			A.xls	Excel file with grayscale value to temperature camera calibration.
			Summary Output Data.doc	Word file with test conditions.
			Contour Plot.dg7	DeltaGraph Nusselt number contour plot.
			Local Line Spatial.xls	Excel file containing local, line averaged, and spatially averaged Nusselt number data.
14 Large RECTANGLE + Small TRIANGLE Roughness – Height = 2.0 mm	900	Plate 14 Re=900	d_nu1.txt	Raw Nusselt Number data in text file.
			total.bmp	IR camera bitmap image used for camera calibration.
			A.xls	Excel file with grayscale value to temperature camera calibration.
			Summary Output Data.doc	Word file with test conditions.
			Contour Plot.dg7	DeltaGraph Nusselt number contour plot.
			Local Line Spatial.xls	Excel file containing local, line averaged, and spatially averaged Nusselt number data.
14 Large RECTANGLE + Small TRIANGLE Roughness – Height = 2.0 mm	1500	Plate 14 Re=1500	d_nu1.txt	Raw Nusselt Number data in text file.
			total.bmp	IR camera bitmap image used for camera calibration.
			A.xls	Excel file with grayscale value to temperature camera calibration.
			Summary Output Data.doc	Word file with test conditions.
			Contour Plot.dg7	DeltaGraph Nusselt number contour plot.
			Local Line Spatial.xls	Excel file containing local, line averaged, and spatially averaged Nusselt number data.
14 Large RECTANGLE + Small TRIANGLE Roughness – Height = 2.0 mm	5000	Plate 14 Re=5000	d_nu1.txt	Raw Nusselt Number data in text file.
			total.bmp	IR camera bitmap image used for camera calibration.
			A.xls	Excel file with grayscale value to temperature camera calibration.
			Summary Output Data.doc	Word file with test conditions.
			Contour Plot.dg7	DeltaGraph Nusselt number contour plot.
			Local Line Spatial.xls	Excel file containing local, line averaged, and spatially averaged Nusselt number data.
14 Large RECTANGLE + Small TRIANGLE Roughness – Height = 2.0 mm	11000	Plate 14 Re=11000	d_nu1.txt	Raw Nusselt Number data in text file.
			total.bmp	IR camera bitmap image used for camera calibration.
			A.xls	Excel file with grayscale value to temperature camera calibration.
			Summary Output Data.doc	Word file with test conditions.

			Contour Plot.dg7	DeltaGraph Nusselt number contour plot.
			Local Line Spatial.xls	Excel file containing local, line averaged, and spatially averaged Nusselt number data.
15 Small CYLINDER Roughness – Height = 1.0 mm	900	Plate 15 Re=900	d_nu1.txt	Raw Nusselt Number data in text file.
			total.bmp	IR camera bitmap image used for camera calibration.
			A.xls	Excel file with grayscale value to temperature camera calibration.
			Summary Output Data.doc	Word file with test conditions.
			Contour Plot.dg7	DeltaGraph Nusselt number contour plot.
			Local Line Spatial.xls	Excel file containing local, line averaged, and spatially averaged Nusselt number data.
15 Small CYLINDER Roughness – Height = 1.0 mm	1500	Plate 15 Re=1500	d_nu1.txt	Raw Nusselt Number data in text file.
			total.bmp	IR camera bitmap image used for camera calibration.
			A.xls	Excel file with grayscale value to temperature camera calibration.
			Summary Output Data.doc	Word file with test conditions.
			Contour Plot.dg7	DeltaGraph Nusselt number contour plot.
			Local Line Spatial.xls	Excel file containing local, line averaged, and spatially averaged Nusselt number data.
15 Small CYLINDER Roughness – Height = 1.0 mm	5000	Plate 15 Re=5000	d_nu1.txt	Raw Nusselt Number data in text file.
			total.bmp	IR camera bitmap image used for camera calibration.
			A.xls	Excel file with grayscale value to temperature camera calibration.
			Summary Output Data.doc	Word file with test conditions.
			Contour Plot.dg7	DeltaGraph Nusselt number contour plot.
			Local Line Spatial.xls	Excel file containing local, line averaged, and spatially averaged Nusselt number data.
15 Small CYLINDER Roughness – Height = 1.0 mm	11000	Plate 15 Re=11000	d_nu1.txt	Raw Nusselt Number data in text file.
			total.bmp	IR camera bitmap image used for camera calibration.
			A.xls	Excel file with grayscale value to temperature camera calibration.
			Summary Output Data.doc	Word file with test conditions.
			Contour Plot.dg7	DeltaGraph Nusselt number contour plot.
			Local Line Spatial.xls	Excel file containing local, line averaged, and spatially averaged Nusselt number data.
16 Small CYLINDER Roughness – Height = 1.5 mm	900	Plate 16 Re=900	d_nu1.txt	Raw Nusselt Number data in text file.
			total.bmp	IR camera bitmap image used for camera calibration.
			A.xls	Excel file with grayscale value to temperature camera calibration.
			Summary Output Data.doc	Word file with test conditions.
			Contour Plot.dg7	DeltaGraph Nusselt number contour plot.
			Local Line Spatial.xls	Excel file containing local, line averaged, and spatially averaged Nusselt number data.
	1500		d_nu1.txt	Raw Nusselt Number data in text file.

16 Small CYLINDER Roughness – Height = 1.5 mm		Plate 16 Re=1500	total.bmp	IR camera bitmap image used for camera calibration.
			A.xls	Excel file with grayscale value to temperature camera calibration.
			Summary Output Data.doc	Word file with test conditions.
			Contour Plot.dg7	DeltaGraph Nusselt number contour plot.
			Local Line Spatial.xls	Excel file containing local, line averaged, and spatially averaged Nusselt number data.
16 Small CYLINDER Roughness – Height = 1.5 mm	5000	Plate 16 Re=5000	d_nu1.txt	Raw Nusselt Number data in text file.
			total.bmp	IR camera bitmap image used for camera calibration.
			A.xls	Excel file with grayscale value to temperature camera calibration.
			Summary Output Data.doc	Word file with test conditions.
			Contour Plot.dg7	DeltaGraph Nusselt number contour plot.
			Local Line Spatial.xls	Excel file containing local, line averaged, and spatially averaged Nusselt number data.
16 Small CYLINDER Roughness – Height = 1.5 mm	11000	Plate 16 Re=11000	d_nu1.txt	Raw Nusselt Number data in text file.
			total.bmp	IR camera bitmap image used for camera calibration.
			A.xls	Excel file with grayscale value to temperature camera calibration.
			Summary Output Data.doc	Word file with test conditions.
			Contour Plot.dg7	DeltaGraph Nusselt number contour plot.
			Local Line Spatial.xls	Excel file containing local, line averaged, and spatially averaged Nusselt number data.
17 Small CYLINDER Roughness – Height = 2.0 mm	900	Plate 17 Re=900	d_nu1.txt	Raw Nusselt Number data in text file.
			total.bmp	IR camera bitmap image used for camera calibration.
			A.xls	Excel file with grayscale value to temperature camera calibration.
			Summary Output Data.doc	Word file with test conditions.
			Contour Plot.dg7	DeltaGraph Nusselt number contour plot.
			Local Line Spatial.xls	Excel file containing local, line averaged, and spatially averaged Nusselt number data.
17 Small CYLINDER Roughness – Height = 2.0 mm	1500	Plate 17 Re=1500	d_nu1.txt	Raw Nusselt Number data in text file.
			total.bmp	IR camera bitmap image used for camera calibration.
			A.xls	Excel file with grayscale value to temperature camera calibration.
			Summary Output Data.doc	Word file with test conditions.
			Contour Plot.dg7	DeltaGraph Nusselt number contour plot.
			Local Line Spatial.xls	Excel file containing local, line averaged, and spatially averaged Nusselt number data.
17 Small CYLINDER Roughness – Height = 2.0 mm	5000	Plate 17 Re=5000	d_nu1.txt	Raw Nusselt Number data in text file.
			total.bmp	IR camera bitmap image used for camera calibration.
			A.xls	Excel file with grayscale value to temperature camera calibration.
			Summary Output Data.doc	Word file with test conditions.

			Contour Plot.dg7	DeltaGraph Nusselt number contour plot.
			Local Line Spatial.xls	Excel file containing local, line averaged, and spatially averaged Nusselt number data.
17 Small CYLINDER Roughness – Height = 2.0 mm	11000	Plate 17 Re=11000	d_nu1.txt	Raw Nusselt Number data in text file.
			total.bmp	IR camera bitmap image used for camera calibration.
			A.xls	Excel file with grayscale value to temperature camera calibration.
			Summary Output Data.doc	Word file with test conditions.
			Contour Plot.dg7	DeltaGraph Nusselt number contour plot.
			Local Line Spatial.xls	Excel file containing local, line averaged, and spatially averaged Nusselt number data.
18 Large CYLINDER + Medium CYLINDER + Small CYLINDER Roughness – Height = 1.0 mm	900	Plate 18 Re=900	d_nu1.txt	Raw Nusselt Number data in text file.
			total.bmp	IR camera bitmap image used for camera calibration.
			A.xls	Excel file with grayscale value to temperature camera calibration.
			Summary Output Data.doc	Word file with test conditions.
			Contour Plot.dg7	DeltaGraph Nusselt number contour plot.
			Local Line Spatial.xls	Excel file containing local, line averaged, and spatially averaged Nusselt number data.
18 Large CYLINDER + Medium CYLINDER + Small CYLINDER Roughness – Height = 1.0 mm	1500	Plate 18 Re=1500	d_nu1.txt	Raw Nusselt Number data in text file.
			total.bmp	IR camera bitmap image used for camera calibration.
			A.xls	Excel file with grayscale value to temperature camera calibration.
			Summary Output Data.doc	Word file with test conditions.
			Contour Plot.dg7	DeltaGraph Nusselt number contour plot.
			Local Line Spatial.xls	Excel file containing local, line averaged, and spatially averaged Nusselt number data.
18 Large CYLINDER + Medium CYLINDER + Small CYLINDER Roughness – Height = 1.0 mm	5000	Plate 18 Re=5000	d_nu1.txt	Raw Nusselt Number data in text file.
			total.bmp	IR camera bitmap image used for camera calibration.
			A.xls	Excel file with grayscale value to temperature camera calibration.
			Summary Output Data.doc	Word file with test conditions.
			Contour Plot.dg7	DeltaGraph Nusselt number contour plot.
			Local Line Spatial.xls	Excel file containing local, line averaged, and spatially averaged Nusselt number data.
18 Large CYLINDER + Medium CYLINDER + Small CYLINDER Roughness – Height = 1.0 mm	11000	Plate 18 Re=11000	d_nu1.txt	Raw Nusselt Number data in text file.
			total.bmp	IR camera bitmap image used for camera calibration.
			A.xls	Excel file with grayscale value to temperature camera calibration.
			Summary Output Data.doc	Word file with test conditions.
			Contour Plot.dg7	DeltaGraph Nusselt number contour plot.
			Local Line Spatial.xls	Excel file containing local, line averaged, and spatially averaged Nusselt number data.
	900	Plate 19 Re=900	d_nu1.txt	Raw Nusselt Number data in text file.

19 Large CYLINDER + Medium CYLINDER + Small CYLINDER Roughness – Height = 1.5 mm			total.bmp	IR camera bitmap image used for camera calibration.
			A.xls	Excel file with grayscale value to temperature camera calibration.
			Summary Output Data.doc	Word file with test conditions.
			Contour Plot.dg7	DeltaGraph Nusselt number contour plot.
			Local Line Spatial.xls	Excel file containing local, line averaged, and spatially averaged Nusselt number data.
19 Large CYLINDER + Medium CYLINDER + Small CYLINDER Roughness – Height = 1.5 mm	1500	Plate 19 Re=1500	d_nu1.txt	Raw Nusselt Number data in text file.
			total.bmp	IR camera bitmap image used for camera calibration.
			A.xls	Excel file with grayscale value to temperature camera calibration.
			Summary Output Data.doc	Word file with test conditions.
			Contour Plot.dg7	DeltaGraph Nusselt number contour plot.
			Local Line Spatial.xls	Excel file containing local, line averaged, and spatially averaged Nusselt number data.
19 Large CYLINDER + Medium CYLINDER + Small CYLINDER Roughness – Height = 1.5 mm	5000	Plate 19 Re=5000	d_nu1.txt	Raw Nusselt Number data in text file.
			total.bmp	IR camera bitmap image used for camera calibration.
			A.xls	Excel file with grayscale value to temperature camera calibration.
			Summary Output Data.doc	Word file with test conditions.
			Contour Plot.dg7	DeltaGraph Nusselt number contour plot.
			Local Line Spatial.xls	Excel file containing local, line averaged, and spatially averaged Nusselt number data.
19 Large CYLINDER + Medium CYLINDER + Small CYLINDER Roughness – Height = 1.5 mm	11000	Plate 19 Re=11000	d_nu1.txt	Raw Nusselt Number data in text file.
			total.bmp	IR camera bitmap image used for camera calibration.
			A.xls	Excel file with grayscale value to temperature camera calibration.
			Summary Output Data.doc	Word file with test conditions.
			Contour Plot.dg7	DeltaGraph Nusselt number contour plot.
			Local Line Spatial.xls	Excel file containing local, line averaged, and spatially averaged Nusselt number data.
20 Large CYLINDER + Medium CYLINDER + Small CYLINDER Roughness – Height = 2.0 mm	900	Plate 20 Re=900	d_nu1.txt	Raw Nusselt Number data in text file.
			total.bmp	IR camera bitmap image used for camera calibration.
			A.xls	Excel file with grayscale value to temperature camera calibration.
			Summary Output Data.doc	Word file with test conditions.
			Contour Plot.dg7	DeltaGraph Nusselt number contour plot.
			Local Line Spatial.xls	Excel file containing local, line averaged, and spatially averaged Nusselt number data.
20 Large CYLINDER + Medium CYLINDER + Small CYLINDER Roughness –	1500	Plate 20 Re=1500	d_nu1.txt	Raw Nusselt Number data in text file.
			total.bmp	IR camera bitmap image used for camera calibration.
			A.xls	Excel file with grayscale value to temperature camera calibration.
			Summary Output Data.doc	Word file with test conditions.

Height = 2.0 mm			Contour Plot.dg7	DeltaGraph Nusselt number contour plot.
			Local Line Spatial.xls	Excel file containing local, line averaged, and spatially averaged Nusselt number data.
20 Large CYLINDER + Medium CYLINDER + Small CYLINDER Roughness – Height = 2.0 mm	5000	Plate 20 Re=5000	d_nu1.txt	Raw Nusselt Number data in text file.
			total.bmp	IR camera bitmap image used for camera calibration.
			A.xls	Excel file with grayscale value to temperature camera calibration.
			Summary Output Data.doc	Word file with test conditions.
			Contour Plot.dg7	DeltaGraph Nusselt number contour plot.
			Local Line Spatial.xls	Excel file containing local, line averaged, and spatially averaged Nusselt number data.
20 Large CYLINDER + Medium CYLINDER + Small CYLINDER Roughness – Height = 2.0 mm	11000	Plate 20 Re=11000	d_nu1.txt	Raw Nusselt Number data in text file.
			total.bmp	IR camera bitmap image used for camera calibration.
			A.xls	Excel file with grayscale value to temperature camera calibration.
			Summary Output Data.doc	Word file with test conditions.
			Contour Plot.dg7	DeltaGraph Nusselt number contour plot.
			Local Line Spatial.xls	Excel file containing local, line averaged, and spatially averaged Nusselt number data.

Numerical Data Files			
Plate	**Folder Name**	**File Name**	**Description**
Polystyrene Baseline	Polystyrene Baseline_Re5000	sctusr_Dx64.dll	Dynamic link library file with initial inputs.
		targetplate.his	History of execution file.
		targetplate.I	User function file created in C++.
		targetplate.mdl	Simulink model with geometry.
		targetplate.mon	Library reference file.
		targetplate.oct	Initial input file.
		targetplate.pre	Initial input file.
		targetplate.r	Initial input file.
		targetplate.s	Sourcing file including boundary conditions.
		targetplate_10.fld	Output file from SC/Tetra with all temperature data.
		test_data.xls	Temperature input file from impingement test.
1 ProtoCAM Baseline	ProtoCAM Baseline Re5000	ProtoCAM_Re5000	Simulation data from SLU.
		ProtoCAM_Re5000_UAH	Simulation data from UAH.
		sctusr_Dx64.dll	Dynamic link library file with initial inputs.
		targetplate.his	History of execution file.
		targetplate.I	User function file created in C++.
		targetplate.mdl	Simulink model with geometry.
		targetplate.mon	Library reference file.
		targetplate.oct	Initial input file.
		targetplate.pre	Initial input file.

		targetplate.r	Initial input file.
		targetplate.s	Sourcing file including boundary conditions.
		targetplate_10.fld	Output file from SC/Tetra with all temperature data.
		test_data.xls	Temperature input file from impingement test.
2 Large RECTANGLE Roughness	Largeonly_Re5000	Nu Comparison Data	Excel file containing the comparison between local experimental results and local numerical results.
		sctusr_Dx64.dll	Dynamic link library file with initial inputs.
		targetplate.his	History of execution file.
		targetplate.I	User function file created in C++.
		targetplate.mdl	Simulink model with geometry.
		targetplate.mon	Library reference file.
		targetplate.oct	Initial input file.
		targetplate.pre	Initial input file.
		targetplate.r	Initial input file.
		targetplate.s	Sourcing file including boundary conditions.
		targetplate_10.fld	Output file from SC/Tetra with all temperature data.
		test_data.xls	Temperature input file from impingement test.
3 Small RECTANGLE Roughness - Height = 1.0 mm	Small Roughness_1mm_Re5000	Nu Comparison Data	Excel file containing the comparison between local experimental results and local numerical results.
		sctusr_Dx64.dll	Dynamic link library file with initial inputs.
		targetplate.his	History of execution file.
		targetplate.I	User function file created in C++.
		targetplate.mdl	Simulink model with geometry.
		targetplate.mon	Library reference file.
		targetplate.oct	Initial input file.
		targetplate.pre	Initial input file.
		targetplate.r	Initial input file.
		targetplate.s	Sourcing file including boundary conditions.
		targetplate_10.fld	Output file from SC/Tetra with all temperature data.
		test_data.xls	Temperature input file from impingement test.
4 Small RECTANGLE Roughness - Height = 1.5 mm	Small Roughness_1.5mm_Re5000	Nu Comparison Data	Excel file containing the comparison between local experimental results and local numerical results.
		sctusr_Dx64.dll	Dynamic link library file with initial inputs.
		targetplate.his	History of execution file.
		targetplate.I	User function file created in C++.
		targetplate.mdl	Simulink model with geometry.
		targetplate.mon	Library reference file.
		targetplate.oct	Initial input file.
		targetplate.pre	Initial input file.

		targetplate.r	Initial input file.
		targetplate.s	Sourcing file including boundary conditions.
		targetplate_10.fld	Output file from SC/Tetra with all temperature data.
		test_data.xls	Temperature input file from impingement test.
5 Small RECTANGLE Roughness - Height = 2.0 mm	Small Roughness_2mm_Re5000	Nu Comparison Data	Excel file containing the comparison between local experimental results and local numerical results.
		sctusr_Dx64.dll	Dynamic link library file with initial inputs.
		targetplate.his	History of execution file.
		targetplate.I	User function file created in C++.
		targetplate.mdl	Simulink model with geometry.
		targetplate.mon	Library reference file.
		targetplate.oct	Initial input file.
		targetplate.pre	Initial input file.
		targetplate.r	Initial input file.
		targetplate.s	Sourcing file including boundary conditions.
		targetplate_10.fld	Output file from SC/Tetra with all temperature data.
		test_data.xls	Temperature input file from impingement test.
6 Large RECTANGLE + Small RECTANGLE Roughness - Height = 1.0 mm	LargeSR_1.0_5000	Nu Comparison Data	Excel file containing the comparison between local experimental results and local numerical results.
		sctusr_Dx64.dll	Dynamic link library file with initial inputs.
		targetplate.his	History of execution file.
		targetplate.I	User function file created in C++.
		targetplate.mdl	Simulink model with geometry.
		targetplate.mon	Library reference file.
		targetplate.oct	Initial input file.
		targetplate.pre	Initial input file.
		targetplate.r	Initial input file.
		targetplate.s	Sourcing file including boundary conditions.
		targetplate_10.fld	Output file from SC/Tetra with all temperature data.
		test_data.xls	Temperature input file from impingement test.
7 Large RECTANGLE + Small RECTANGLE Roughness -	LargeSR_1.5_5000	Nu Comparison Data	Excel file containing the comparison between local experimental results and local numerical results.
		sctusr_Dx64.dll	Dynamic link library file with initial inputs.
		targetplate.his	History of execution file.

Height = 1.5 mm		targetplate.I	User function file created in C++.
		targetplate.mdl	Simulink model with geometry.
		targetplate.mon	Library reference file.
		targetplate.oct	Initial input file.
		targetplate.pre	Initial input file.
		targetplate.r	Initial input file.
		targetplate.s	Sourcing file including boundary conditions.
		targetplate_10.fld	Output file from SC/Tetra with all temperature data.
		test_data.xls	Temperature input file from impingement test.
8 Large RECTANGLE + Small RECTANGLE Roughness - Height = 2.0 mm	LargeSR_2.0_5000	Nu Comparison Data	Excel file containing the comparison between local experimental results and local numerical results.
		sctusr_Dx64.dll	Dynamic link library file with initial inputs.
		targetplate.his	History of execution file.
		targetplate.I	User function file created in C++.
		targetplate.mdl	Simulink model with geometry.
		targetplate.mon	Library reference file.
		targetplate.oct	Initial input file.
		targetplate.pre	Initial input file.
		targetplate.r	Initial input file.
		targetplate.s	Sourcing file including boundary conditions.
		targetplate_10.fld	Output file from SC/Tetra with all temperature data.
		test_data.xls	Temperature input file from impingement test.

APPENDIX C: SOFTWARE DIRECTORY

Appendix C presents a listing and description of the software utilized for collecting and analyzing experimental data.

Program	File Name	Description
Microsoft Excel	A.xls	Creates a calibration equation using infrared camera grayscale values and thermocouple data.
MATLAB	BB.m	Reads infrared camera image data and outputs grayscale values.
MATLAB	CC.m	Calculates the Nusselt number from the grayscale values.
LabView	Flat Plate Impingement_cal.vi	Displays and records pressure and temperature data. Calculates Mach number and Reynolds number. Also used for pressure transducer and thermocouple calibration.
ResearchIR MAX 4.0	total.bmp	Records a series of grayscale images from the FLIR infrared camera.
DeltaGraph 7	Contour Plot	Plots the Nusselt number data as a contour plot.
SC/Tetra 11	SC/Tetra	Numerical conduction analysis software.

REFERENCES

[1] Xing Y., and Weigand B., "Experimental Investigation on Staggered Impingement Heat Trasfer on a Rib Roughened Plate With Different Crossflow Schemes," Paper Number GT2010-22043, ASME Turbo Expo 2010: Power for Land, Sea, and Air, Glasgow, UK, June 14-18, 2010.

[2] Xing Y., Spring S., and Weigand B., "Experimental and Numerical Investigation of Impingement Heat Transfer of a Flat and Micro-Rib Roughened Plate With Different Crossflow Schemes," *International Journal of Thermal Sciences*, Vol. 50, 2011, pp. 1293-1307.

[3] Xing Y., and Weigand B., "Experimental Investigation of Impingement Heat Transfer on a Flat and Dimpled Plate With Different Crossflow Schemes," *International Journal of Heat and Mass Transfer*, Vol. 53, 2010, pp.3874-3886.

[4] Nakamata C., Okita Y., Yamane T., Fukuyama Y., and Yoshida T., "Effect of Roughened Elements on Target Surface and Cooling Hole Shape on Impingement Cooling Effectiveness," Paper Number IGTC2011-0003, 10th International Gas Turbine Congress, Osaka, Japan, November 13-18, 2011.

[5] Lee J., Ren Z., Ligrani P. M., Fox M. D., and Moon H.-K., "Crossflows From Jet Array Impingement Cooling: Hole Spacing, Target Plate Distance, Reynolds Number Effects ," *International Journal of Thermal Sciences*, Vol. 88, 2015, pp. 7-18.

[6] Lee J., Ren Z., Haegele J., Potts G., Jin J.S., Ligrani P. M., Fox M. D., and Moon H.-K., "Effects of Jet-to-Target Plate Distance and Reynolds Number on Jet Array Impingement Heat Transfer ," ASME Turbo Expo 2013: Gas Turbine Technical Congress and Exhibition, San Antonio, Texas, USA, June 3-7, 2013.

[7] Kline S. J., and McClintock F. A., "Describing Uncertainties in Single Sample Experiments," Mechanical Engineering, Vol. 75, 1953, pp. 3–8.

[8] Moffat R. J., "Describing the Uncertainties in Experimental Results," Experimental Thermal and Fluid Science, Vol. 1, No. 1, 1988, pp. 3–17.